Copyright Warning & Restrictions

The copyright law of the United States (Title 17, United States Code) governs the making of photocopies or other reproductions of copyrighted material.

Under certain conditions specified in the law, libraries and archives are authorized to furnish a photocopy or other reproduction. One of these specified conditions is that the photocopy or reproduction is not to be "used for any purpose other than private study, scholarship, or research." If a, user makes a request for, or later uses, a photocopy or reproduction for purposes in excess of "fair use" that user may be liable for copyright infringement,

This institution reserves the right to refuse to accept a copying order if, in its judgment, fulfillment of the order would involve violation of copyright law.

Please Note: The author retains the copyright while the New Jersey Institute of Technology reserves the right to distribute this thesis or dissertation

Printing note: If you do not wish to print this page, then select "Pages from: first page # to: last page #" on the print dialog screen

ABSTRACT

CONTINUOUS POLYMER COATING OF HOST PARTICLES BY HOLLOW FIBER-BASED CRYSTALLIZERS

By

Dengyue Chen

Currently, no technique is available to continuously film coat nano-sized drug particles with a polymer to produce large amounts of free-flowing coated particles. In this work, Eudragit RL 100 and Poly (D, L-lactide-co-glycolide) (PLGA) are chosen as the coating polymers; Cosmo 55 (550 nm silica particles), Aerosil 200 (hydrophilic 12 nm silica), Aerosil R974 (hydrophobic 12 nm silica) and Griseofulvin (10 μm drug particles) are chosen as the host particles. Two novel crystallizers are designed and fabricated to continuously coat the host particles with different polymers: solid hollow fiber cooling crystallizer (SHFCC) and porous hollow fiber antisolvent crystallizer (PHFAC).

In the SHFCC-based crystallization/cooling method, the polymer solution containing a suspension of submicron particles flows in the lumen of a solid non-porous polymeric hollow fiber. Controlled cooling of the polymer solution by a coolant on the shell side of the hollow fibers allows for polymer nucleation on the surface of the particles; the precipitated polymer forms a thin film around the particles, the thickness of which can be varied depending on the operating conditions. In the PHFAC based crystallization method, an acetone solution of the host particles containing the dissolved polymer is passed through the shell side of a membrane module containing many porous hollow fiber membranes. Through the lumen side of the hollow fiber membranes, the anti-solvent water

are passed at a higher pressure to inject water jets through every membrane pore in the fiber wall into the shell-side acetone feed solution creating an extremely high level of supersaturation and immediate crystallization. The host particles get coated by the precipitating polymer in the PHFAC module. For the coating of Griseofulvin (GF) drug particles, GF first precipitates from the solution in the PHFAC module due to the addition of anti-solvent water, subsequently GF crystals get coated by the precipitating polymer.

Scanning electron microscopy (SEM), transmission electron microscopy (TEM), energy dispersive X-ray spectrometry (EDS), laser diffraction spectroscopy (LDS) and thermogravimetric analysis (TGA) are all used to characterize the coatings. To study the properties of the coated drug crystals, X-Ray Diffraction (XRD), Raman spectroscopy, and dissolution tests are implemented. These results indicate that a uniformly coated, free-flowing product is successfully developed under appropriate conditions by both the SHFCC and the PHFAC method; the coated drug particles can be potentially used for controlled release of the drug; such a process may be easily scaled up.

CONTINUOUS POLYMER COATING OF HOST PARTICLES BY HOLLOW FIBER-BASED CRYSTALLIZERS

by
Dengyue Chen

A Dissertation
Submitted to the Faculty of
New Jersey Institute of Technology
in Partial Fulfillment of the Requirements for the Degree of
Doctor of Philosophy in Materials Science and Engineering

Interdisciplinary Program in Materials Science and Engineering

January 2015

.

APPROVAL PAGE

CONTINUOUS POLYMER COATING OF HOST PARTICLES BY HOLLOW FIBER-BASED CRYSTALLIZERS

Dengyue Chen

Dr. Kamalesh K. Sirkar, Dissertation Advisor — Date
Distinguished Professor of Chemical Engineering, NJIT

Dr. Robert Pfeffer, Committee Member — Date
Distinguished Professor of Chemical Engineering, NJIT (Emeritus)
Research Professor of Engineering Matter Transport Energy, ASU

Dr. San Kiang, Committee Member — Date
Director of Process R& D, Bristol-Myers Squibb Company

Dr. Piero M. Armenante, Committee Member — Date
Distinguished Professor of Chemical Engineering, NJIT

Dr. N.M. Ravindra, Committee Member — Date
Professor of Physics, NJIT

BIOGRAPHICAL SKETCH

Author: Dengyue Chen

Degree: Doctor of Philosophy

Date: January, 2015

Undergraduate and Graduate Education:

- Doctor of Philosophy in Materials Science and Engineering,
  New Jersey Institute of Technology, Newark, NJ, 2015
- Master of Engineering in Materials Physics and Chemistry,
  Beijing JiaoTong University, Beijing, China, 2010
- Bachelor of Engineering in Chemical Engineering,
  Tianjin University, Tianjin, China, 2008

Major: Materials Science and Engineering

Publications:

Chen, D.C.; Singh, D.; Sirkar, K.K.; Pfeffer, R. Continuous polymer coating/encapsulation of submicron particles using a solid hollow fiber cooling crystallization method, *I&EC Res*, **2014**, *53* (15), 6388-6400.

Chen, D.C.; Singh, D.; Sirkar, K.K.; Zhu, J.; Pfeffer, R. Continuous polymer nanocoating on silica nanoparticles. *Langmuir*, **2014**, *30*, 7804-7810.

Chen, D.C.; Singh, D.; Sirkar, K.K.; Pfeffer, R. Continuous synthesis of polymer coated drug particles by a porous hollow fiber membrane-based anti-solvent crystallization method. Submitted to Langmuir.

Chen, D.C.; Singh, D.; Sirkar, K.K.; Pfeffer, R. Continuous polymer coating drug particles by a solid hollow fiber cooling crystallization method. Ready to submit.

Chen, D.C.; Singh, D.; Sirkar, K.K.; Pfeffer, R. Continuous polymer coating on micron and nanoparticles by novel approach of porous hollow fiber anti-solvent crystallization method. Ready to submit.

Patents:

Co-inventor of US provisional patent application: US 61/899,692. Title: System and method for continuous polymer coating of particles.

Co-inventor of US provisional patent application submitted. Title: A continuous production method for synthesizing polymer-coated drug crystals by using porous hollow fiber membranes and anti-solvent crystallization.

Presentations

Presenter for the Topic: Nanoparticle Coatings & Nanocoatings on Particles. In Particle Technology Forum for 2014 American Institute of Chemical Engineers Annual Conference (AlChE), Atlanta, USA.

Presenter for the Topic: A Novel Technique for Continuous Production of Polymer-Coated Drug Crystals. In Separations Division for 2014 American Institute of Chemical Engineers Annual Conference (AlChE), Atlanta, USA.

Presenter in the Post Session of 2014 North American Membrane Society Annual Conference (NAMS), Houston, USA.

Presenter for the Topic: Continuous Polymer Coating of Nanoparticles: A Novel Method. In Particle Technology Forum for 2013 American Institute of Chemical Engineers Annual Conference (AlChE), San Francisco, USA.

~To my beloved Parents Chen HaiTao, Chen LiHong and my Dear Wang Bing for their love, support and encouragement~

仅以此书献给我的父母陈海涛，陈立红以及爱人王冰的支持，是你们的鼓励和支持让我顺利完成博士学历！

~没有梦想 何以远方~

ACKNOWLEDGMENTS

I would like to express my deepest gratitude to my Advisor Professor Kamalesh K. Sirkar. Dr. Sirkar introduced me into this fascinating area of drug delivery, provided me with valuable guidance and financial support all through my graduate education. Without his profound knowledge and thorough guidance, I would not have been able to finish this PhD project. His hardworking qualities, professionalism and decency will always serve as an inspiration to me. I will always be deeply grateful to Professor Robert Pfeffer who is the senior consultant for my PhD project. I will always remember his professionalism in particle technology and kindness during this period. He is always willing to help me if I have any problem. I will not forget that he helped me revise the manuscripts even during his vacation.

I would like to thank Professor San Kiang, and Professor Piero M. Armenante who were not only gracious enough to act as my committee members, but also provide valuable guidance all through my PhD research. They have used their professional background and expertise to provide me with great supports. I would also like to thank Professor N.M. Ravindra for being one of my committee members, he is always nice and provided the guidance all throughout my graduate studies at NJIT.

I express my deep gratitude to The Center for Membrane Technologies at NJIT, which provided me with an opportunity and platform to pursue my dreams and carry on my research**.** I would like to thank Dr. Dhananjay Singh, Dr. Gordana Obuskovic, Dr. Xingming Jie, Dr. Tripura Mulukutla, Dr. John Chau and Mr. Jose Sousa, for their help and guidance. I would also like to thank all members of the research group for their help in carrying out the research. Considerable assistance from Dr. Jiangtao Zhu (ASU), Dr.

John Mardinly and the LeRoy Eyring Center for Solid State Science (ASU), Dr. Xueyan Zhang and Dr. Larisa Krishtopa with the characterization instructions are also acknowledged herewith.

Finally, I would like to thank my parents for their constant support and encouragement. At last, I cherish all my friends who stood with me at all times and wish you the best.

TABLE OF CONTENTS

TABLE OF CONTENTS
(Continued)

Chapter **Page**

TABLE OF CONTENTS
(Continued)

TABLE OF CONTENTS
(Continued)

TABLE OF CONTENTS
(Continued)

Chapter **Page**

LIST OF TABLES

LIST OF FIGURES

LIST OF FIGURES
(Continued)

Figure **Page**

LIST OF FIGURES
(Continued)

Figure **Page**

LIST OF FIGURES
(Continued)

Figure **Page**

LIST OF FIGURES
(Continued)

Chapter **Page**

LIST OF SYMBOLS

m_{Silica}	Mass of host silica particles, g
ρ_{Silica}	Density of host silica particles, g/cm^3
$m_{Polymer}$	Mass of polymer that covered the silica particles, g
$\rho_{Polymer}$	Density of polymer used for coating, g/cm^3
r	Radius of single silica ball, nm
h	Polymer coating thickness, nm
C	Concentration of the polymer solution, g solute/g solvent
A	Total surface area of host particles, cm^2
$M_{Solvent}$	Molar mass of the solvent, g/mol
C^*	Solubility of the polymer solution, g solute/g solvent
g	Order of the growth kinetic
k_g	Growth kinetic coefficient
t	Time for the solvent to pass through the module, s
Z	Length of the hollow fiber, cm
v	Axial velocity of the flow in the module, cm/s
A_{Single}	Surface area of single silica spherical particle, cm^2
N_{Silica}	Number of silica particles
V_{Silica}	Volume of single silica particle, cm^3
D	Integration constant (Appendix B.2)

CHAPTER 1

INTRODUCTION

1.1 Drug Delivery Systems in Pharmaceutical Industry

Drug delivery refers to approaches that can transport the drug compound to the human body when it is needed to achieve the therapeutic effect. It is often implemented via an appropriate drug formulation or medical device. In controlled drug delivery systems, well-characterized and reproducible dosage forms are utilized to ensure that the rate and duration of drug delivery achieves the required concentration in the host. Usually there is a concentration range for each drug which provides optimal therapeutic effects: higher concentration may cause toxicity whereas a lower one may be therapeutically ineffective. Controlled delivery is usually achieved by either dispersing the drug in a polymer matrix or encapsulating individual drug particle in a polymeric coating [1]. The polymeric coating can also provide protection for fragile drugs (e.g., proteins and peptides) from hydrolysis and degradation, for example, by providing protection from stomach acids. The latter is a prime example since even small drug molecules such as erythromycin can be irritating to the gastric mucosa.

The size range of drug particles can vary between micron-sized, sub-micron and nanoparticles. Due to their greater solubility, high stability, high carrier capacity, incorporation of biodegradable and hydrophobic/hydrophilic substances and administration by a variety of delivery vehicles, nanoparticle-based systems have attracted considerable attention in controlled release of drugs [2] [3], delivery of anticancer drugs and imaging agents to tumors [4], tuberculosis treatment [5], as non-viral gene delivery

vehicles [6] and delivery of platinum(IV) drug to subcutaneous tumor and lung metastasis [7], Dense polyethylene glycol coating improved penetration of polymeric nanoparticles within brain tissue in cases where the blood-brain barrier is compromised [8]. Polymer-coated nanoparticles are also being utilized in chemical, electronic, optical and physical applications.

Nanoparticle-based drug delivery systems are also of significant interest in controlled release of drugs [9], tumor-targeted triplex therapy [10], anticancer drug delivery [11] and for enhanced cancer therapy [12]. Important advantages of nanoparticles in drug delivery systems also include different ways of administering the drug including oral, injection, and inhalation methods. These desirable properties greatly improve drug bioavailability and patient compliance by reduced drug administration frequency.

Lai et al. [13] recently demonstrated that nanoparticles, if sufficiently coated with a muco-inert polymer such as lower molecular weight PEG, can rapidly traverse physiological human mucus with diffusivities almost as high as those in pure water. This finding suggests that it is possible to engineer (coat) nano-sized drug particles to overcome the mucus barrier, allowing sustained drug delivery to specific cells in the body at mucosal surfaces and provide improved efficacy and reduced side effects for a wide range of therapeutics.

The potential for nanoparticles to revolutionize drug delivery systems is huge. However, a number of problems need to be overcome including continuously layering and coating nanoparticles with polymeric materials to achieve time release, protecting them from stomach acids and being trapped by a mucus barrier, or preventing immune cells (macrophages) from engulfing and eliminating the nanoparticles circulating in the

bloodstream [14]. Nanoparticle surface coating or tailoring can also provide a variety of desirable properties in physical, optical, electronic, and chemical applications.

1.2 Polymer Coating Techniques

A variety of methods have been conventionally employed to coat micron-sized, submicron, and nanoparticles with a polymer. Physical vapor deposition, plasma treatment, chemical vapor deposition, and pyrolysis of polymeric organic materials are examples of dry methods; sol-gel processes, emulsification and solvent evaporation techniques are examples of wet methods [15]. Additional methods for polymer coating or encapsulation of nanoparticles and ultrafine particles employing supercritical CO_2 are: Rapid Expansion of Supercritical Solutions (RESS), Supercritical Anti-Solvent (SAS), and Gas Anti-Solvent (GAS) processes. These processes [16-19] have many shortcomings such as, very high pressures, low solubility of polymers many of which may also lack biodegradability. Furthermore these are batch processes and it would be problematic to develop the needed drug production capacities.

Although fluidized bed-based coating processes can be continuous, there are problems due to scale-up difficulties as well as agglomeration of smaller (submicron and nano) particles resulting from van der Waals and other inter-particle forces; the polymer coating will further enhance the tendency for these particles to agglomerate.

Conventional batch crystallization devices [20][21] if used for coating will suffer from imperfect mixing and non-uniform conditions leading to extreme variability of the product. Conventional crystallization/precipitation relies on processes employing cooling, solvent evaporation, anti-solvent addition and precipitation by reaction. For anti-solvent

addition-based processes, the technique of increasing interest in pharmaceutical processing is the use of an impinging-jet mixer, where two high velocity streams are brought into contact to effect high nucleation rates, followed by growth in a well-mixed vessel or a tubular precipitator (Midler et al., 1994) [22]. However, there are a number of well-known shortcomings of this technique. As mentioned earlier, the SAS, GAS and related supercritical anti-solvent techniques are batch processes which require very demanding experimental conditions.

Two hollow fiber membrane-based crystallization (SHFCC and PHFAC) techniques were developed recently to bypass these problems [23][24]. These two concepts were employed in this thesis to develop two continuous techniques whereby micron-size particles (dugs or otherwise) having a thin polymeric coating are produced continuously from an acetone solution of the drug as well as the polymer used to coat it. Scale-up problems in conventional batch crystallizers which are usually stirred vessels include the problems of imperfect mixing and non-uniform conditions leading to a broad crystal size distribution (CSD). New monitoring techniques [25][26] can lead to better prediction and control of the applied supersaturation in crystallizers. However, well-mixed crystallizers are intrinsically inclined toward a spectrum of local conditions in time and space and consequently a relatively broad CSD. These problems are essentially avoided in the two techniques studied here.

1.3 Characterization Methods

In order to understand the physical or chemical properties of the coated particles, these have to be characterized by various tools for different purposes. A brief introduction to the

characterization tools is listed below.

1.3.1 Scanning Electron Microscope (SEM)

A scanning electron microscope (SEM) is a type of electron microscope which can focus the electron beams to scan and produce image of the sample in a large magnification. The sample was "illuminated" by the electrons. Since the wavelength of the electron is much smaller than light, they can detect much smaller structures. The wavelength of the electrons used in the SEM is usually around 0.5 Å, while the wavelength of visible light is around 4000 Å. The electrons first interact with the sample's atoms, then generate and transfer the signal that contains various information, for example, the composition of the sample or surface morphology.

Figure 1.1 is the schematic of a typical SEM. The electron beam, which has an energy ranging from 0.2 kev to 40 kev, is emitted from the electron gun fitted with a tungsten filament cathode. Subsequently the beam passes through the deflector plates or scanning coils in the electron column. When the sample interacts with the emitting electron beam, the electrons tend to lose energy because of the scattering and absorption of the sample. The detector can explore the energy exchange between the sample and the electron beam resulting in the reflection of high-energy electrons by elastic scattering. The scattered electrons from the sample or secondary electron are collected by the electronic device. Once the targeted region of the sample is scanned over by the electron beams, a complete micrograph is generated and displayed on the computer.

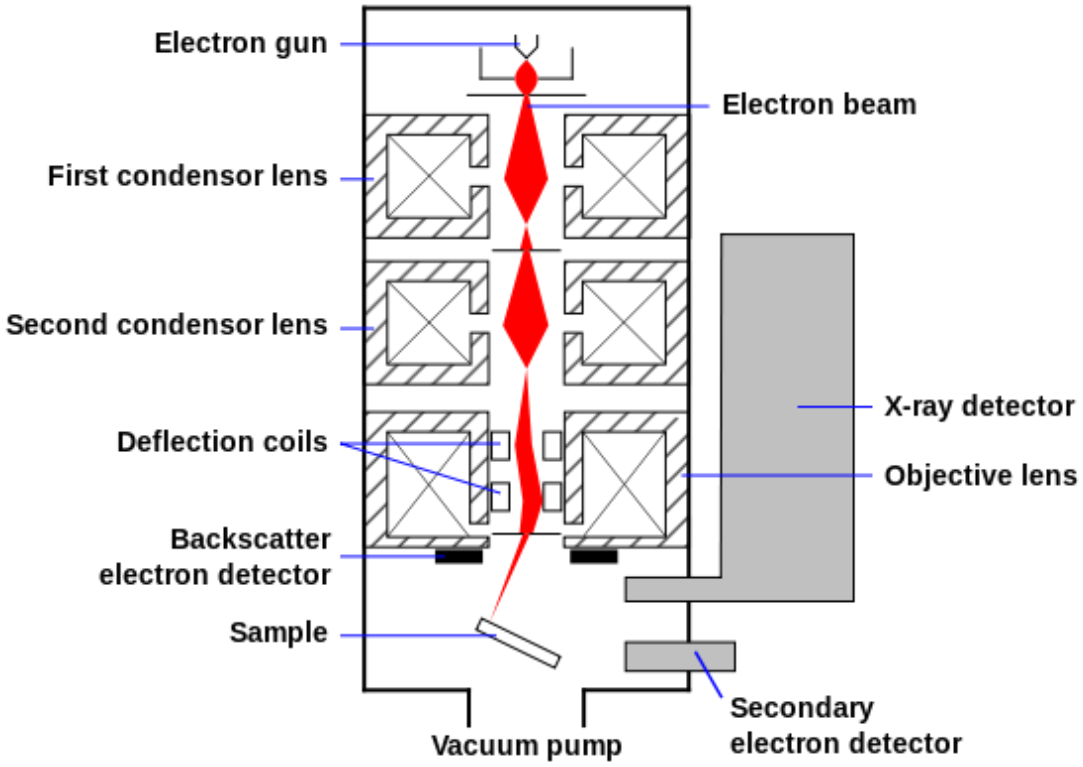

Figure 1.1 Schematic diagram of a typical scanning electron microscope [27].

1.3.2 Scanning Transmission Electron Microscopy (STEM)

Scanning transmission electron microscopy (STEM) is also a microscopy technique similar to SEM. An electron beam is transmitted and interacts with a thin specimen; image of the sample can be detected by the sensor and displayed on the computer. Compared to SEM, normally the STEM can produce images that have higher magnification and greater resolution. Besides, the add-on of Electron energy loss spectroscopy (EELS) and annular dark-field imaging can be used to distinguish the polymer coating and the host particle in order to identify the density of the coating thickness and the topography of the coating covered the particles.

1.3.3 Thermal Gravimetric Analysis (TGA)

Thermal gravimetric analysis (TGA) is a thermal analysis method that can provide the physical or chemical information of the sample that is being heated up as a function of the increasing time or temperature. Normally TGA is used to determine the material properties that exhibit the mass loss due to decomposition of the sample. Figure 1.2 shows the schematic diagram of a thermogravimetric analyzer (Pyris 1, PerkinElmer, Waltham, MA) being used. The purpose is to obtain the weight loss of the polymer coating on the host particles since the polymer will decompose over a contain temperature range when heated up.

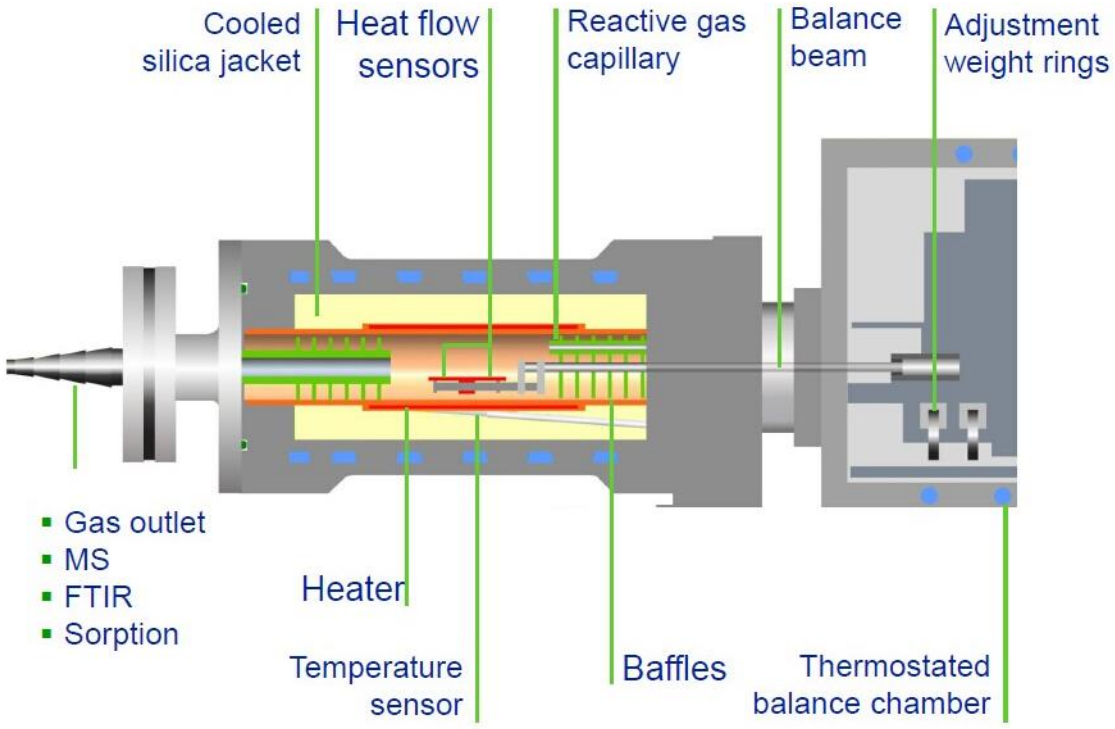

Figure 1.2 Schematic diagram of thermogravimetric analyzer [28].

1.3.4 Dynamic Light Scattering (DLS)

Dynamic light scattering (Figure 1.3) (also known as photon correlation spectroscopy or

quasi-elastic light scattering) is used for the determination of the particle size distribution of small particles suspended in a solution. When light interacts with the small particles in suspension, it is scattered in every direction since the particles normally are smaller than the wavelength of light (less than 250 nm). The intensity of scattering changes all the time because the light source is a laser that is coherent and monochromatic; the fluctuation is due to Brownian motion of the small particles which makes the scattering distance fluctuating with time. The information containing the time scale of movement of the particles will be translated and recorded on the computer. Different types of DLS devices have been used in this project due to the different particle sizes and status of the samples.

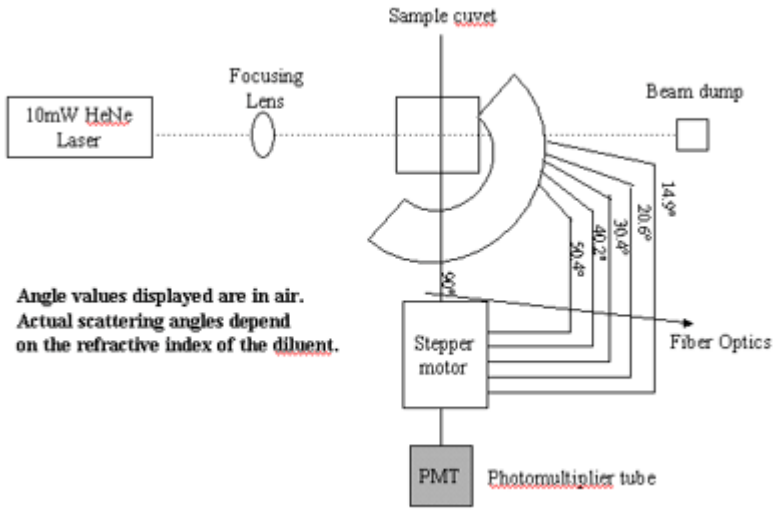

Figure 1.3 Schematic diagram of Beckman Coulter N4 plus analyzer [29].

Beckman Coulter LS230 is an enhanced laser diffraction particle size analyzer which determines the particle size from 0.04 to 2000 µm. Compared to Beckman Coulter N4 plus which is a photon correlation spectroscopy analyzer that can measure the particles size of 3 nm- 3 µm, it is more suitable for submicron particles rather than nanoparticles. Besides, samples for analysis can be either an aqueous suspension or a dry powder that

provides the flexibility to determine the particle size. Figure 1.4 is the schematic of LS230 analyzer that was used in the project to determine the size distribution of polymer coated nanoparticles.

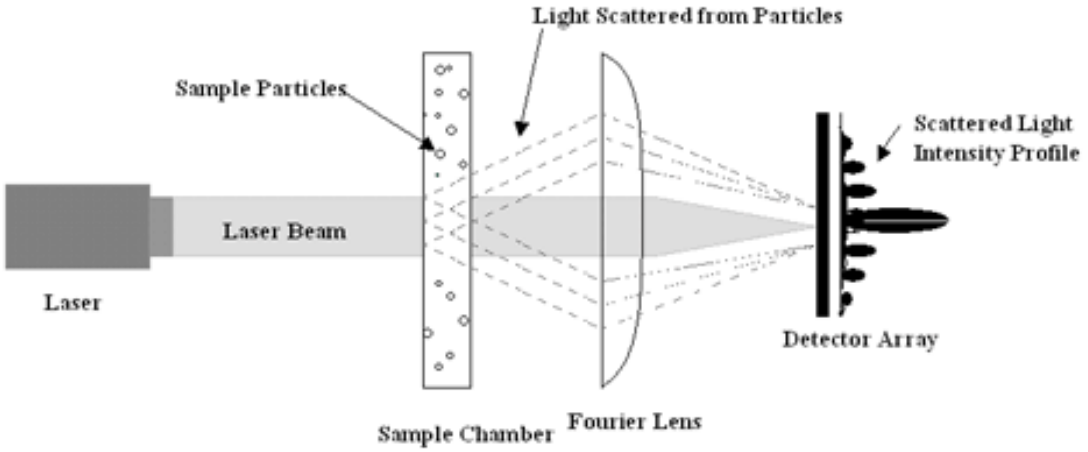

Figure 1.4 Schematic diagram of LS230 analyzer [29].

Sympatec Laser diffraction spectroscope (LDS) coupled with RODOS dry dispersion and R1 lens (0.1-35 μm) was used to identify the particle size distribution (PSD) of the products collected. The main advantage of this technique is the accuracy of determining the real particle size of dry powder sample. RODOS is a universal dry dispersing unit which can combination the feeding and the dispersing to achieve a smooth, complete dispersion of the sample in order to determine the actual particle size of the sample. Figure 1.5 shows a schematic diagram of the Sympatec laser diffraction spectroscope that been used for determining the particle size distribution when the sample is in solid form.

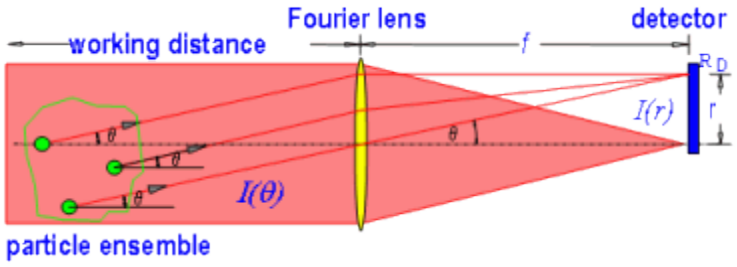

Figure 1.5 Schematic diagram Sympatec laser diffraction spectroscope [30].

1.3.5 X-ray Diffraction (XRD) and Raman Microscope

X-ray Diffraction is a technique to identify the crystalline structure of the material and provide the information on unit cell dimensions. It has three parts: X-ray tube, sample holder and an X-ray detector. A filament is heated in the cathode ray tube to produce electrons. When the energy of electron is strong enough to dislodge the inner shell electrons of the target material, the X-ray spectra which consists typically of K_α and K_β, can be generated. When X-ray interacts with the rotated sample in the chamber, a detector will process and record the X-ray signal if it satisfies Bragg's law. At the end, the converted signal will be the output to a device or computer. Figure 1.6 is the typical diagram of X-ray Diffractometer that is being used in this thesis. The main application of this XRD is to characterize of crystalline materials, determine the unit cell dimensions and measure the sample purity. Polymer coated drug particles were analyzed by XRD to identify whether the characteristic peaks of XRD pattern are in accordance with those of the as-received drug sample.

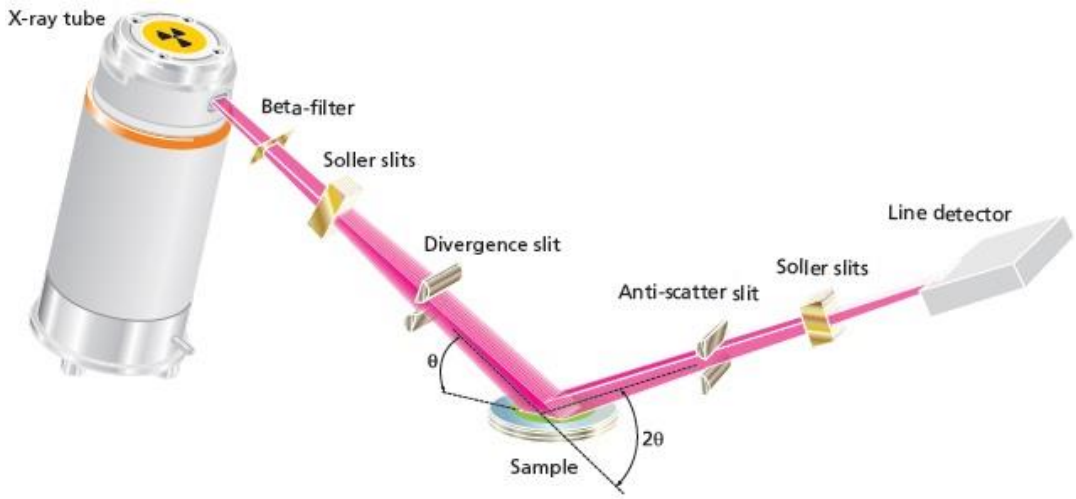

Figure 1.6 Schematic diagram of X-ray diffractometer [31].

Raman Microscope (Figure 1.7) is also an effective tool to analyze the molecular structure of coated and uncoated particles by the characteristic peaks of Raman shift in order to identify whether the coating has damaged the structure of the host crystals. A Raman Microscope (DXR, Thermo scientific, Waltham, MA) was applied to the analysis of coated/uncoated particles in order to identify whether the coating of drug particles affected the drug composition.

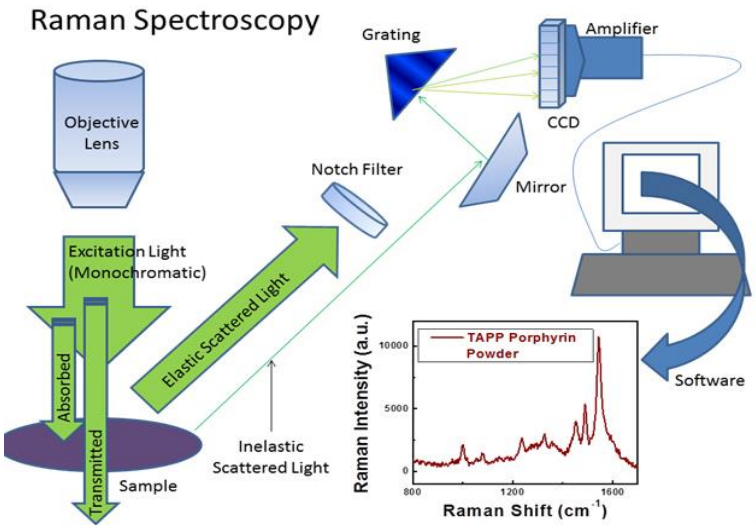

Figure 1.7 Schematic diagram of Raman Microscope [32].

1.3.6 Differential Scanning Calorimetry (DSC)

Differential scanning calorimetry (DSC) is a thermoanalytical technique that is widely used for the determination of fusion, crystallization events as well as glass transition temperatures. Similar to TGA, measurement on a sample is made as a function of temperature over time. The basic principle of DSC is as follows. When the sample undergoes a physical transformation, heat will need to flow to it than the reference to maintain the temperature unchanged. A differential scanning calorimeter shown in Figure 1.8 was used over a temperature range of 30-250 ^{o}C at 10 ^{o}C/min heating rate to measure the heating profile.

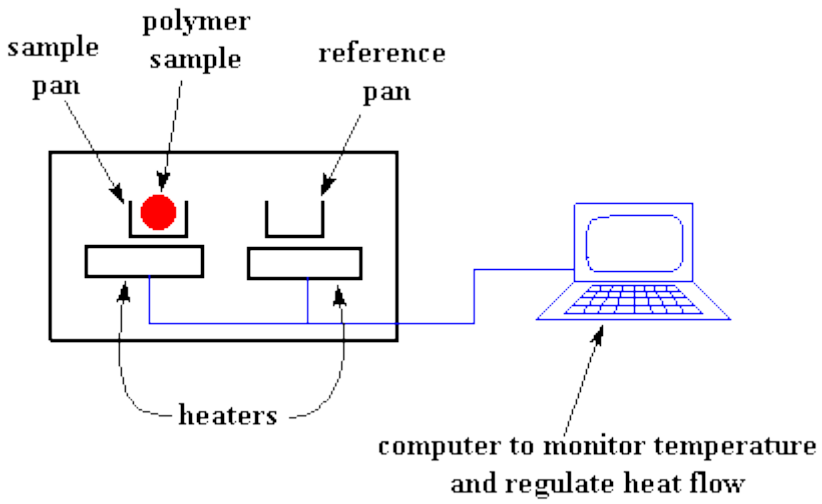

Figure 1.8 Schematic diagram of differential scanning calorimeter [33].

1.3.7 Dissolution Testing

Dissolution testing is widely used in the pharmaceutical industry to determine the drug release information. As a substitute for human studies, well-established dissolution testing information can be very useful for drug formulation and manufacturing changes of the drug. Dissolution testing for uncoated and coated drug particles in this project was determined

via a Distek Dissolution tester (North Brunswick, NJ).

1.4 Objectives of this Thesis

1. Design and build the hollow fiber devices and the experimental setup for both coating techniques: Solid Hollow Fiber Cooling Crystallization (SHFCC) and Porous Hollow Fiber Anti-solvent Crystallization (PHFAC).

2. Select host particles (submicron, nanoparticles and drug particles), polymers, appropriate surfactants, solvent and anti-solvent systems for both of the coating methods.

3. Investigate a continuous process for polymer coating of different host particles via cooling crystallization/precipitation of a polymer solution on submicron and nanoparticles in suspension in a SHFCC exchanger.

4. Investigate a continuous process for polymer coating of different host particles via antisolvent crystallization/precipitation of a polymer on nanoparticles suspended in a polymer solution in a PHFAC device.

5. Characterize the coated host particles collected from SHFCC and PHFAC process.

6. Illustrate the potential for scale-up by operating either one of the two techniques, SHFCC or PHFAC at different rates of operation and larger hollow fiber devices.

1.5 Approach

To overcome the problems of conventional coating methods mentioned in Section 1.2, two novel crystallizer designs based on a hollow fiber device were proposed in the thesis: Solid hollow fiber cooling crystallizer (SHFCC); Porous hollow fiber antisolvent crystallizer (PHFAC). This study has investigated how one can use such devices and techniques to continuously coat host particles such as drug crystals which may be submicron particles or nanoparticles. These devices will be introduced now one by one.

1.5.1 Solid Hollow Fiber Cooling Crystallizer (SHFCC)

Figure 1.9 shows a single polymeric hollow fiber whose wall is solid (nonporous). The internal diameter (I.D.) is 420 μm and the outer diameter (O.D.) 575 μm. The polymeric hollow fiber is of polypropylene (PP) which has a great deal of chemical, pH, and solvent resistance. One could also employ a variety of other polymers, polytetrafluoroethylene (PTFE), polyimide, etc. Polymers PP and PTFE in hollow fiber form are particularly useful since their smooth and non-sticky surfaces do not easily allow accumulation of precipitating crystals as long as the liquid is flowing. The polymer used to make the hollow fiber must be totally inert in the solution environment. Further a smooth surface is necessary to eliminate roughness elements in the wall from acting as possible nucleation sites.

The solution slated for crystallization is made to pass through the bore (or lumen) of the solid hollow fiber while a coolant flows on the outside of this fiber, thereby setting up heat exchange. If one allows the hollow fiber to be part of a cylindrical heat exchange device packed with many such solid wall hollow fibers (Figure 1.10), then many long microfluidic channels have been essentially bundled together in one small device; however, these channels are circular and the channel dimensions are considerably, almost by an order of magnitude, larger than conventional microfluidic channels.

Zarkadas and Sirkar [34] have experimentally demonstrated that such a 30 cm long polymeric hollow fiber heat exchanger (PHFHE) is highly efficient compared to other heat exchangers due to the very large heat exchange surface area/volume (1400 m^{-1}) created by the polymeric hollow fiber surface area. Larger heat exchangers have been successfully tested in systems with precipitating salts of $CaSO_4$, $CaCO_3$[35]. For cooling crystallization

from a solution flowing through the hollow fiber bore with the coolant flowing on the shell side, the SHFCC was highly efficient for both aqueous and organic crystallizing solutions [23]. Examples illustrated include: crystallizing KNO_3 from an aqueous solution, salicyclic acid from ethanol, and paracetamol from an aqueous solution [36]. The number of crystals generated/unit volume was 2-3 orders of magnitude higher, CSDs were much narrower, and the mean crystal sizes were 3-4 times smaller than those from conventional mixed suspension mixed product removal (MSMPR) crystallizers. The very low temperature difference between the SHFCC fiber wall and the crystallizing solution (~1-2 ^{o}C) provided a far greater control over nucleation/crystal growth process compared to that in a MSMPR crystallizer. It is equally valid when one compares the conditions in the bore of a hollow fiber to that in a metallic tube in a conventional shell-and-tube heat exchanger.

In a PHFHE performing as a SHFCC, each hollow fiber acts as a separate crystallizer. It is as if the feed solution has been subdivided into numerous identical fluid packets traveling through each hollow fiber bore with the same velocity and under the same cooling conditions created by the flowing shell side cooling fluid. Therefore, the scale-up problem is minimized which is a major strength of the SHFCC devices. If a few hollow fibers get accidentally blocked, the disturbance to the rest of the fiber assembly is minimal since in a 2.54 cm diameter module, there may be as many as 90 hollow fibers; in a 5.08 cm diameter module, there will be 360 fibers. Note that the fiber bore side flow Reynolds number is quite low (<500) to achieve the type of heat exchange as well as crystallization performances observed.

Therefore, the pressure drops in the PHFHEs are much lower, as low as 1 kPa/NTU (NTU is the number of transfer units) compared to 30 kPa/NTU for conventional metallic

heat exchangers. For the same pumping cost, PHFHEs transfer 5-20 times more heat per unit volume than typical shell-and-tube heat exchangers; this translates immediately into a much more efficient cooling crystallizer. Similar PHFHE devices have been employed here for continuous submicron particle coating.

The hollow fiber I.D. in SHFCC devices studied was 420 μm; therefore a clogging problem with nanoparticles or submicron particles is unlikely in SHFCC devices. Suppose a high level of nanoparticle agglomeration yields particle sizes ~ 1-2 μm; hollow fiber membrane devices routinely handle such particles. Any dissolved polymer in the solution can precipitate onto nanoparticles present if the temperature is reduced appropriately in the SHFCC device. The particle surfaces can also act as nucleation sites for the precipitating polymer. If the submicron particles/nanoparticles are present in a significant volume fraction, it is unlikely that polymer precipitation will create a network spanning the cross section of the tube I.D. Obviously, this has to be studied vis-a-vis the liquid residence time in the fiber bore. Residence time control however has to be balanced against excessive coating of all particles.

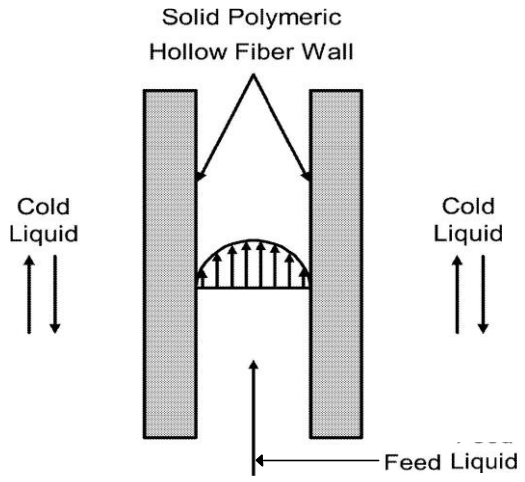

Figure 1.9 Solid hollow fiber cooling crystallizer (SHFCC) [23].

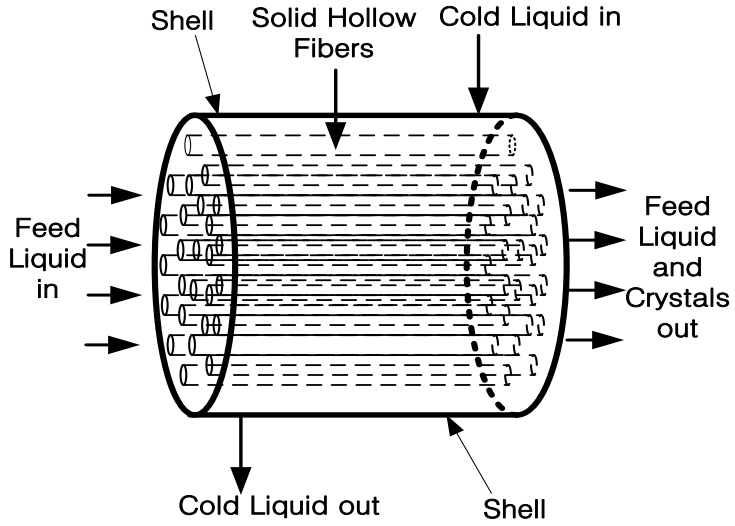

Figure 1.10 Schematic of solid hollow fiber crystallizer/heat exchanger [23].

Figure 1.10 shows solid hollow fibers inside the shell-and-tube SHFCC. The polymeric hollow fiber of polypropylene can resist chemicals such as dioxane and acetone used here; the surface of the nonporous wall of the fiber is smooth and non-sticky so that the precipitating polymers/crystals will not stick to the wall as long as the solution is flowing. The crystallization solution passes through the lumen side of the hollow fiber; the cooling liquid is passed through the shell side extracting heat through the wall so that polymer in the solution precipitates onto the surrogate silica particles present in the solution flowing through the fiber bore. Eventually, the coated particles flow out of the SHFCC along with the solution.

1.5.2 Porous Hollow Fiber Antisolvent Crystallizer (PHFAC)

Figure 1.11 (a) shows a single porous hollow fiber used for anti-solvent crystallization based synthesis of polymer coated host particles. One can use a hydrophilic hollow fiber membrane of Nylon 6; this polymer has considerable pH, chemical and solvent resistance.

The inner diameter (ID) and the outer diameter (OD) for this hollow fiber are 600 μm and 1000 μm, respectively. The fiber wall porosity is 0.75 with pores generally in the range of 0.2 μm; however, there are pores as large as 1.5 μm. Other types of porous hollow fibers may also be used.

Four alternative PHFAC process configurations can be employed. Figure 1.11 (a) shows the feed polymer solution containing the dissolved drug species flowing through the fiber lumen side while the anti-solvent permeates from the shell side through the pores into the lumen. The shell side pressure is kept at a higher level to maintain a certain permeation rate for the anti-solvent. The polymer as well as the drug crystallizes from the solution due to the introduction of the anti-solvent through every membrane pore. As will be shown later, it appears that the drug crystals are formed rapidly; then they get coated by the precipitating/crystallizing polymer molecules in the tube side solution. One can also employ a solution of the polymer containing a suspension of the particles to be coated. As the anti-solvent permeates, the polymer is precipitated on the particles.

Figure 1.11 (b) illustrates an exactly opposite scheme. The anti-solvent flowing in the tube side at a higher pressure flows into the shell side where the acetone solution containing the dissolved drug molecules and the polymer is flowing. Crystallization takes place in the shell side with both the drug and the polymer precipitating; the rapidly crystallizing drug particles get immediately coated by the precipitating polymer. Two other potential operational configurations of the PHFAC technique shown in Figures 1.11 (c) and (d) involve passing the feed solution through the membrane pores. However, in these configurations, there is an undesirable possibility of precipitation occurring in the pores and these configurations should be avoided.

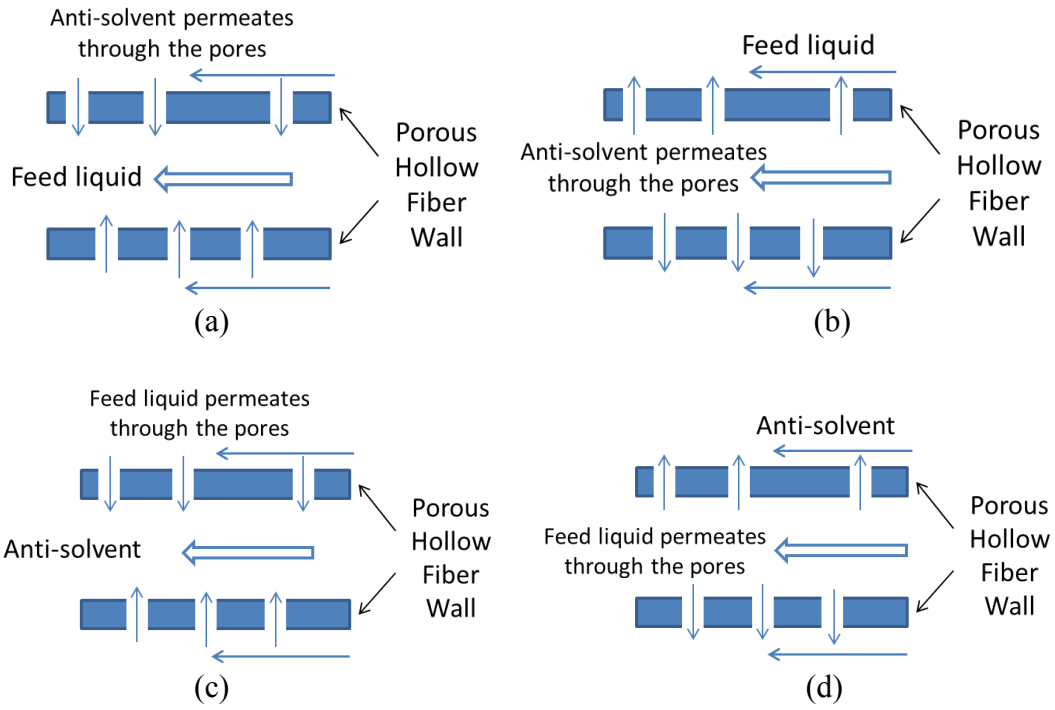

Figure 1.11 Porous hollow fiber anti-solvent crystallization (PHFAC) operating approach for the permeation of anti-solvent through the pores: (a) crystallization in the tube side; (b) crystallization in the shell side. PHFAC operating approach for the permeation of feed liquid through the pores: (c) crystallization in the tube side, (d) crystallization in the shell side.

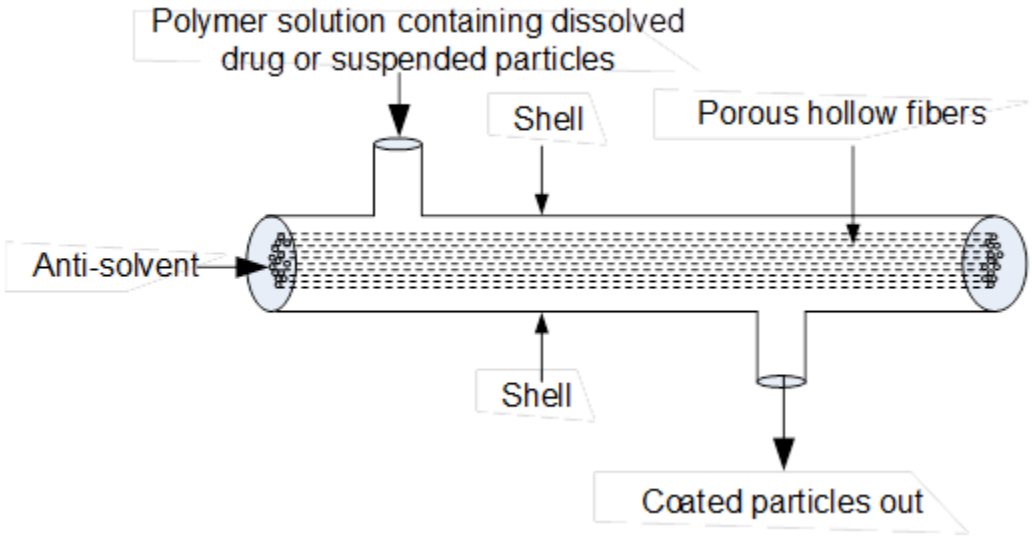

Figure 1.12 Schematic of porous hollow fiber anti-solvent crystallizer (PHFAC).

Figure 1.12 depicts a PHFAC module containing a number of porous hollow fibers for continuous synthesis of polymer-coated drug crystals. The anti-solvent flowing through the hollow fiber tube side at a higher pressure permeates to the shell side where the polymer solution containing the dissolved drug molecules is flowing. Zarkadas and Sirkar (2006) [24] have demonstrated that the mixing efficiency of this process is extraordinary. The rapid local addition of the anti-solvent through every pore mouth drastically decreases the solubility of the drug as well as the polymer in the feed solution; a very high supersaturation is created throughout the shell-side cross section at every axial location in the module causing precipitation of the drug and the polymer resulting in the production of polymer coated drug particles. The suspension of the coated particles along with the excess solution and the anti-solvent are pumped out continuously from an outlet of the shell.

This novel PHFAC device and the process of synthesizing polymer coated drug crystals have certain advantages compared to the other anti-solvent crystallizers. There is an extraordinarily intense contacting of the anti-solvent and the feed solution everywhere in the shell side of the PHFAC module. Since the fractional porosity of the hollow fiber wall is around 0.75, a large number of hollow fibers will result in anti-solvent jets emanating from all of the pores in the membrane module. Therefore, almost the entire shell side will be subjected to an intense contacting due to the very large interfacial area created between the two miscible liquid streams. A very high level of supersaturation is created throughout the shell side resulting in very rapid crystallization of the drug molecules as well as the polymer. The growth of the crystals and the coating thickness will depend on a balance between the rate at which the supersaturation is created locally, the level of

supersaturation created and the time allowed for the growth process to occur which is largely determined by the residence time of the shell-side liquid stream.

Another advantage of the PHFAC device is the high surface area/volume ratio that can be achieved if there is a reasonably high packing density of the hollow fiber membranes. That will lead to maximization of the rate of production of the coated drug particles and achievement of a high product recovery rate. Furthermore, scale-up should be relatively straightforward since the number of hollow fibers in a module can be increased or decreased according to the needs of production; correspondingly, the module shell diameter can be increased or decreased. Theoretically, the larger the number of hollow fibers in the tube side of PHFAC module, the higher the rate of production. The morphology and dimensions of the coated drug particles are likely to remain the same if the flow rates can be increased in proportion to the increase in the number of hollow fibers.

CHAPTER 2

CONTINUOUS POLYMER COATING/ ENCAPSULATION OF SUBMICRON AND NANOPARTICLES OF SILICA USING A SOLID HOLLOW FIBER COOLING CRYSTALLIZATION METHOD

2.1 Introduction

Continuous polymer coating of nanoparticles is of interest in many industries such as, pharmaceuticals, cosmetics, food, and electronics. A polymer coating/precipitation technique is introduced here; the goal is to achieve a uniform and controllable nanosized polymer coating on submicron particles and nanoparticles in a continuous manner. The utility of this technique is demonstrated by coating of 550 nm submicron silica particles as well as 12 nm silica nanoparticles (SNPs) with different polymers. Both hydrophilic and hydrophobic SNPs were successfully coated. First, the cloud point of an acetone solution of the polymer containing a controlled amount of the nonsolvent water was determined by an UV spectrophotometer. Then the solid hollow fiber cooling crystallization (SHFCC) technique was employed to continuously coat particles with the polymer. A suspension of the silica particles in an acetone-water solution of the polymer containing a surfactant was passed through the tube side of solid polypropylene hollow fibers in a SHFCC device while cold liquid was circulated on the shell side. Due to rapid cooling-induced supersaturation and heterogeneous nucleation, precipitated polymers will coat the submicron particles and nanoparticles. The thickness and morphology of the coating and the particle size distribution of the coated host particles were analyzed by scanning transmission electron microscopy (STEM) with electron energy loss spectroscopy (EELS), thermogravimetric analysis (TGA) and dynamic light scattering (DLS).

2.2 Materials and Methods

2.2.1 Materials and SHFCC Module

The coating polymers employed were Eudragit RL 100 (copolymer of ethyl acrylate, methyl methacrylate and a low content of methacrylic acid ester; M_w, 150,000, (Evonik-Degussa, Parsippany, NJ) and PLGA (Poly (D, L-lactide-*co*-glycolide), M_w, 7,000-17,000) (Sigma-Aldrich, St. Louis, MO). The surrogate host particles are: Cosmo 55 non-porous hydrophilic silica nanoparticles, 550 nm, (Presperse, Somerset, NJ); Aerosil 200 (non-porous hydrophilic fumed silica with a diameter of 12 nm) (Evonik-Degussa, Parsippany, NJ) and Aerosil R974 (non-porous hydrophobic fumed silica with a diameter of 12 nm) (Evonik-Degussa, Parsippany, NJ). Acetone, a good solvent for Eudragit RL 100, and dioxane, a good solvent for PLGA, were obtained from Aldrich. Sodium dodecyl sulfate, used as a surfactant, was purchased from Aldrich. All materials were used as received.

Figures 1.9 and 1.10 show respectively a single solid hollow fiber and many hollow fibers inside the shell-and-tube SHFCC. Two sizes of modules were constructed (Table 2.1) to compare the module size effect and number of fibers on the coating capacity, thickness, and scale-up. The shell of both modules was made of fluorinated ethylene propylene (FEP)-based polymer tubing containing 23 or 46 solid PP hollow fibers. Both ends were potted with an epoxy resin to form a tube sheet.

Table 2.1 Specifications of Solid Hollow Fiber Cooling Crystallizer (SHFCC) Modules

	Internal diameter	**Outer diameter**	**Material**	**Number of fibers**	**Length**	**Shell diameter**
Small module	420 μm	575 μm	Polypropylene (PP)	23	47 cm	8 mm
Large module	420 μm	575 μm	Polypropylene (PP)	46	47 cm	14 mm

2.2.2 Experimental Methods

A schematic diagram of the cooling crystallization-based continuous polymer coating setup is shown in Figure 2.1. A certain amount of polymer was introduced into a flask containing acetone under stirring. After the polymer was fully dissolved in acetone, a given amount of DI water, which allows the polymer to precipitate at a predetermined temperature, was decanted into the flask. Then host silica particles and the surfactant SDS were added into the flask. After about 30 min stirring, the flask containing the well-mixed solution-suspension was put in a water bath at a constant temperature (45 ^{o}C). When the experiment was started, the solution-suspension was fed into the lumen side of the SHFCC by a pump (Masterflex, model no.7523-20, Cole-Parmer, Vernon Hills, IL) at a rate of 3.5 ml/min. The temperature indicated by thermocouple T1 was 45 ^{o}C, the inlet temperature of the solution. Experiments were generally run for 10-20 min. In a typical run the distribution of various components will be in the following proportions: Acetone 20 ml, water 4 ml, silica 0.4 g, polymer 2.4 g.

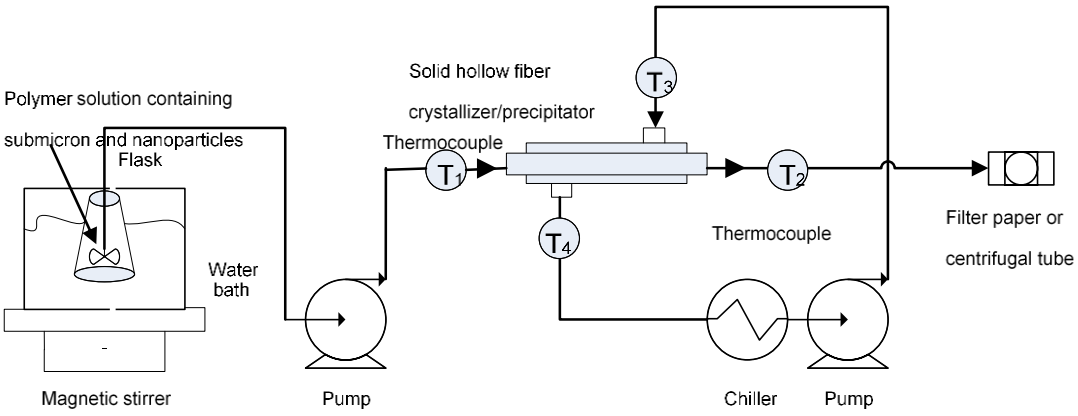

Figure 2.1 Schematic diagram of solid hollow fiber crystallization setup for continuous polymer coating of submicron and nanoparticles.

At the same time an aqueous cooling solution of 50% by volume of ethylene glycol was circulated through the shell side to cool down the solution in the lumen side from 45 ^{o}C to 5 ^{o}C (unless otherwise mentioned) to initiate crystallization in the lumen side of the hollow fibers. A chiller (Polystat CR250WS, Cole-Parmer, Vernon Hills, IL) cooled the glycol solution to -9 ^{o}C in the shell side. The solution containing the coated particles coming out of the hollow fiber module at around 5 ^{o}C (T2) (unless otherwise mentioned) is subjected to two alternative treatments discussed below.

Two methods were used to collect samples of coated particles from the polymer solution leaving the cooling crystallizer/precipitator. Method 1 employing centrifugation involves collecting the solution from the outlet of the crystallizer-precipitator in a centrifuge tube. After 1 min of centrifugation, the supernatant liquid was decanted leaving the product particles coated by polymer. The particles were subjected to vacuum drying and used for further characterization.

The second method employs filtration. After the coated particles and the solution came out of the SHFCC outlet, a vacuum filtration device was employed to collect the sample. This device allowed the solution containing the coated particles to pass through a microfiltration system (Omnipore Membrane, PTFE (Cat.No. JHWP09025), 0.45 μm pore size, 90 mm filter diameter, Millipore, Billerica, MA) and remove most of the solution leaving behind on the filter paper the coated particles; the cake on the filter paper containing the coated particles was collected for post-treatment and further characterization. These two methods, namely, centrifugation and filtration, as well as the various post-treatment approaches used have been summarized in Figure 2.2.

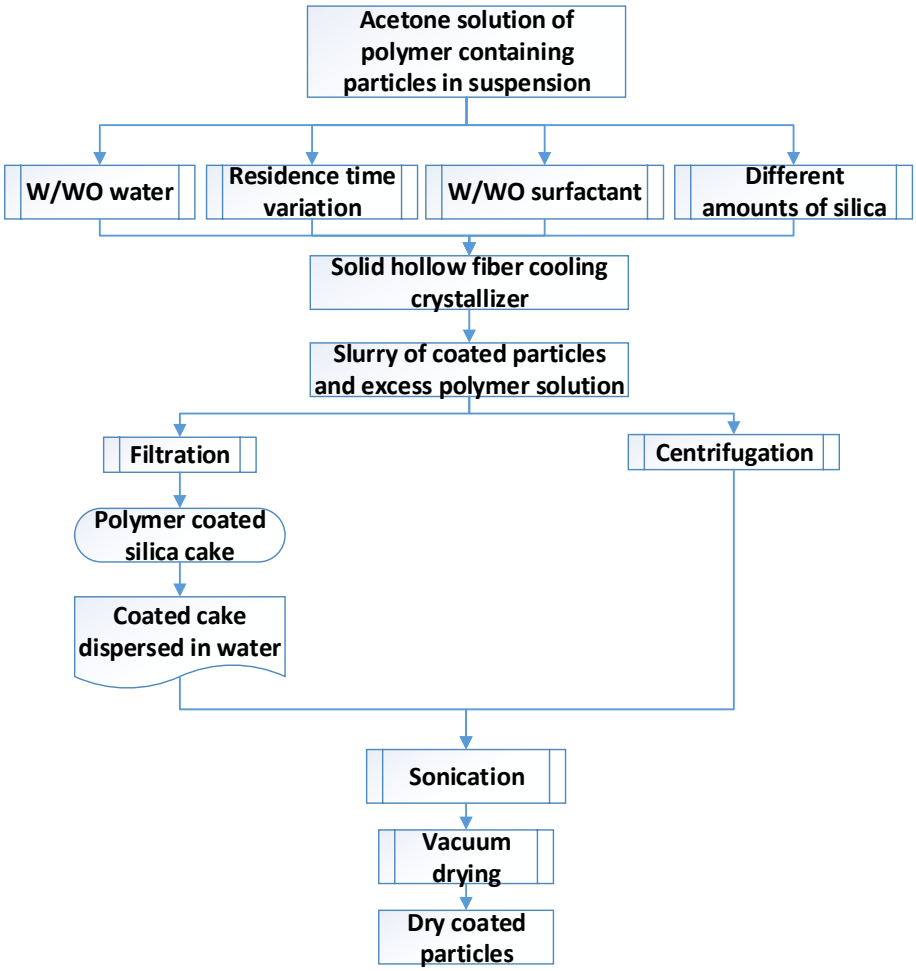

Figure 2.2 Procedure to obtain coated particles from the SHFCC device illustrating various post-treatment methods.

To get free-flowing particles, an additional post-treatment method was developed for both filtration and centrifugation. After filtration, particles remained on the filter paper and formed a "cake." The cake on the filter paper was then placed into DI water under sonication for about 30 s to break-up loose agglomerates. The solution containing the dispersed particles was then decanted onto an aluminum dish and subjected to vacuum drying. Results show that the dry particles are much more free-flowing than before sonication.

Post treatment sonication was also done after centrifugation. After the supernatant liquid was decanted, instead of collecting particles from the residue inside the centrifuge tube some water was added to the tube and the tube was subjected to sonication for about 30s to break-up the agglomerates. The supernatant liquid was poured out and the centrifugation process was repeated once more to remove any excess solution. The particles were then decanted into an aluminum dish and subjected to vacuum drying.

2.2.3 Cloud Point Determination of Various Solutions

Before undertaking coating experiments in the SHFCC, it is necessary to measure the cloud point of the solutions of the polymers Eudragit RL 100 or PLGA. There are two main ways of determining the cloud points of polymeric solutions, either by a UV spectrophotometer or by a refractometer. A Cary 50 UV spectrophotometer (Agilent, Santa Clara, CA) having a temperature controller module was used in the present study. By identifying the absorbance or transmissivity of the solution in the visible wavelength range (550-800 nm), the cloud point can be easily determined.

The procedure followed for determining the cloud point of the binary system of polymer in an organic solvent is as follows:

1. From the specification document in Cole-Parmer[37], the concentration of Eudragit in the solution at the cloud point temperature of 25 ^{o}C should be around 0.2 g/ml. To locate the cloud point concentration accurately, twelve samples of this polymer solution were prepared; the concentrations were 0, 0.14 g/ml, 0.16 g/ml, 0.18 g/ml, 0.20 g/ml, 0.24 g/ml, 0.26 g/ml, 0.28 g/ml, 0.30 g/ml, 0.32 g/ml, 0.34 g/ml and 0.36 g/ml.

2. A baseline correction was run in the UV spectrophotometer in which pure acetone was chosen as the baseline to reduce the impact of acetone; after scanning the peak, the characteristic peak of Eudragit RL 100 was found at a wavelength of 335 nm.

3. A concentration program was then run to obtain a concentration vs. absorbance plot.

4. A concentration of 0.16 g/ml was selected as the cloud point at room temperature since its absorbance is very low and yet from the turbidity of the solution, the sample solution of 0.16 g/ml concentration is at the edge of becoming cloudy.

5. This sample was used to develop temperature vs. absorbance plot and compare with the concentration vs. absorbance plot to get the relationship between temperature and concentration.

The cloud point temperature of the ternary system of polymer/solvent/water was also determined. Eudragit RL 100 was first dissolved in acetone under continuous stirring; then a certain amount of water was added and the solution was heated up to 50 ^{o}C for 30 min. After that, the cuvette containing solution was slowly cooled in steps of 1 ^{o}C per min. The cloud-point temperature was taken as the temperature at which the transmissivity of the solution decreased sharply and the solution changed from clear to turbid. A similar procedure was followed for a solution of PLGA in dioxane and water.

Transmissivity can also be used to determine the cloudiness of solution especially when the characteristic peak for polymer is not obvious or overlapping with the solvent if using an absorbance based determination. The higher the transmissivity % in the spectrophotometer reading for a wavelength ranges from 550 to 800 nm, the clearer the solution. In this case, the solution which has undergone precipitation will have relatively low %T (normally under 20%); so %T < 20% is defined as cloudy and %T > 80% as clear.

2.2.4 Characterization of Submicron Silica Particles

Due to the limitation of resolution of a scanning electron microscope (SEM), relatively large 550 nm diameter COSMO 55 (JGC Catalysts and Chemicals Ltd, Somerset, NJ) nonporous spherical hydrophilic silica submicron particles were employed to act as the initial surrogate drug particles in the experiments reported here.

A scanning electron microscope (LEO 1530 Gemini, Zeiss, Thornwood, NY) was

employed for simple morphological observations. Dry coated particles were attached on the top of the pin stub mount. To examine the coating covering the submicron particles, it is necessary to coat this sample with carbon to make the sample conductive enough to get a clear surface structure picture since charging may occur when the specimen has poor electrical conductivity, causing distorted or deformed pictures.

A 200 kV Schottky field emission (JEOL JEM-2010F, Peabody, MA) analytical transmission electron microscope (TEM) was used for a more thorough analysis of the samples. Z contrast related high angle dark field images of the coated silica spheres were collected under Scanning transmission electron microscopy (STEM) mode to visualize the coating surrounding each individual sphere. The probe size of the electron beam is 1 nm so an accurate thickness can be determined from the STEM image directly. Energy-dispersive X-ray spectroscopy (Model 7246, Oxford Instruments, Concord, MA) provided the distribution of the elements on the surface of the nanoparticles.

A thermogravimetric analyzer (Pyris 1, PerkinElmer, Waltham, MA) was used to determine the amount of coating on the sample particles so that the coating thickness can be calculated by weight loss during heating. Laser diffraction spectroscopy (Vibri, Sympatec, Clausthal-Zellerfeld, Germany) was used to analyze particle size distribution and any agglomeration.

2.3 Results and Discussion for Coating of Submicron Silica Particles

The results of cloud point studies for a number of binary and ternary systems are considered first. Then the various pre-treatments and post-treatments of the particle coating system are considered. Finally the detailed characterizations of the coated particles are provided.

2.3.1 Cloud Point for Polymer/solvent Binary System

The concentration vs. absorbance data for acetone solution of Eudragit RL 100 at 25 C are shown in Figure 2.3 (a). The cloud point data for PLGA/ dioxane are similar to those for Eudragit RL 100/ acetone in that the transmissivity of both solutions is around 100% (Figure 2.3 b and c); the solution remains clear with no precipitation-based particles appearing with a variation in temperature. That is because the cloud point temperature for both of these polymers dissolved in a pure solvent is very low; therefore it is difficult to have precipitation due to a temperature drop under mild conditions (0 ºC to 50 ºC). It has been suggested[38] that when dissolving PLGA/Eudragit RL 100 into dioxane/acetone, addition of a little water decreases the solvation power of the solvent. The solution will turn from clear to cloudy depending on the temperature change. Therefore, one can also adjust the cloud point of the system by adjusting the amount of water added.

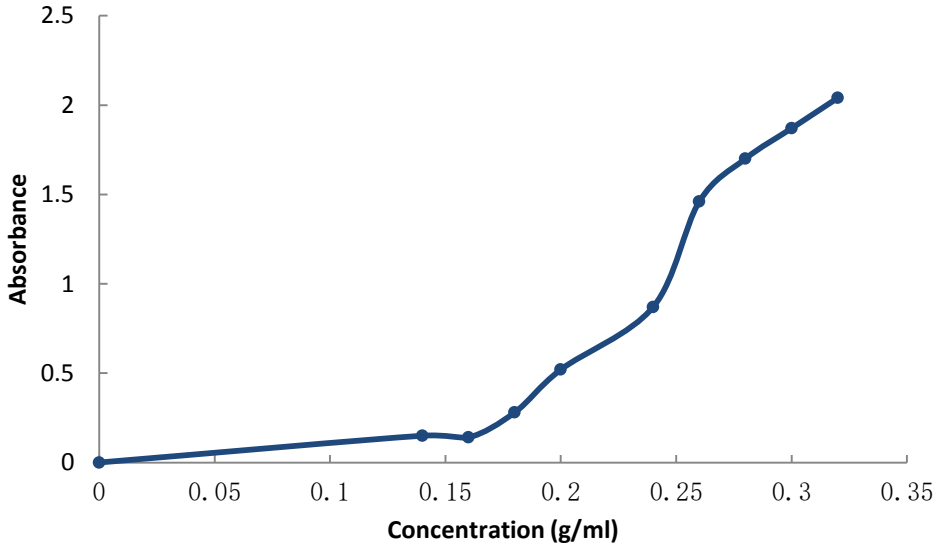

(a)

Figure 2.3 (a) Concentration vs. absorbance for Eudragit RL with acetone at 25 ºC;

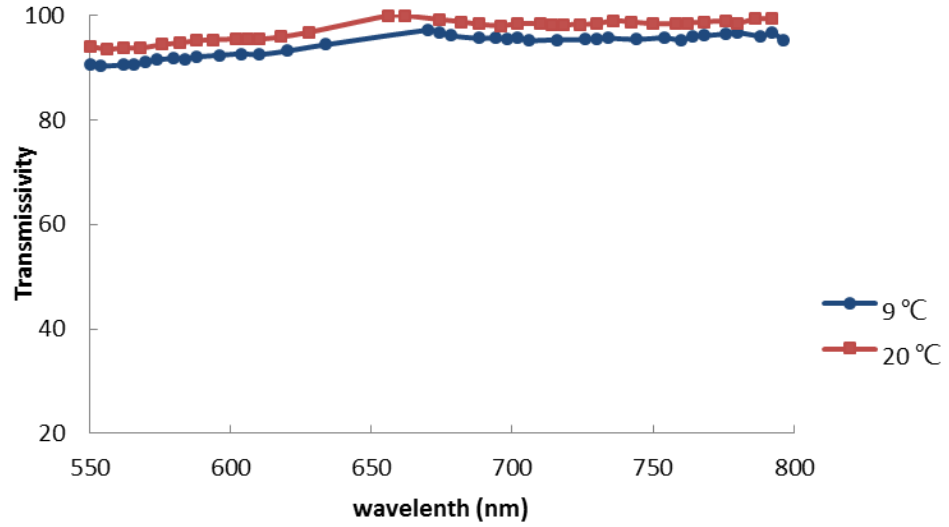

(b)

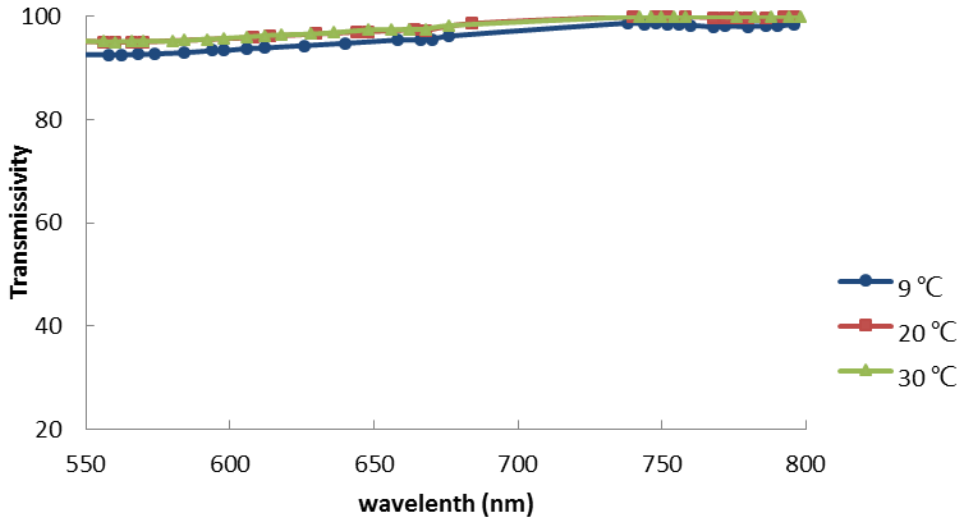

(c)

Figure 2.3 (b) Transmissivity at different temperatures of 10 wt% Eudragit RL 100/2.5 ml acetone solution; **(c)** Transmissivity at different temperatures of 10 wt% PLGA/2.5 ml dioxane solution. (Continued)

2.3.2 Cloud Point for Polymer/solvent/water Ternary System

A limited amount of antisolvent such as DI water was added to the solution containing Eudragit RL 100 to increase the cloud point temperature at the same polymer concentration. At the same cloud point temperature compared to the solution without addition of water,

less polymer will be in solution if a little DI water was added; further the solution viscosity will be lower making it easier to flow. A few different concentrations of water in the ternary system of polymer/solvent/water have been tested under different temperatures. The results are provided below for the two polymers studied.

2.3.3 Eudragit RL 100

Different concentrations of Eudragit and the amount of water added in a Eudragit/acetone/water ternary system have been studied under different temperatures. Figures 2.4 and 2.5 illustrate the behavior of one such solution; Table 2.2 provides a summary of the cloud point temperatures observed for three different compositions of acetone/water. Since 15 ^{o}C is a modest temperature and was easy to achieve, a volume ratio of 2.5/0.5 for acetone/water was selected to obtain the transmissivity vs. wavelength plot at a few temperatures as shown in Figure 2.4; Figure 2.5 illustrates how transmissivity decreases with temperature for a few wavelengths.

Table 2.2 Cloud Point Temperatures vs. Different Ratios of Acetone/water in Eudragit RL100 Solution

Ratio of acetone/water(ml/ml)	**Cloud point temperature of 10 wt% Eudragit RL100 (C)**
2.5/0.5	15
2.5/0.52	20
2.5/0.54	30

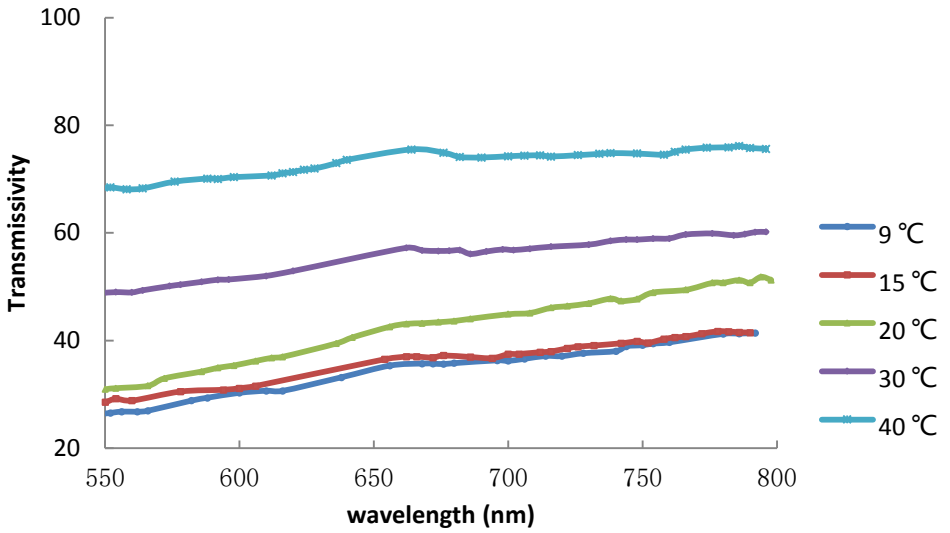

Figure 2.4 Transmissivity of 10 wt% Eudragit RL100 /2.5 ml acetone/0.5 ml water solution vs. wavelength at different temperatures.

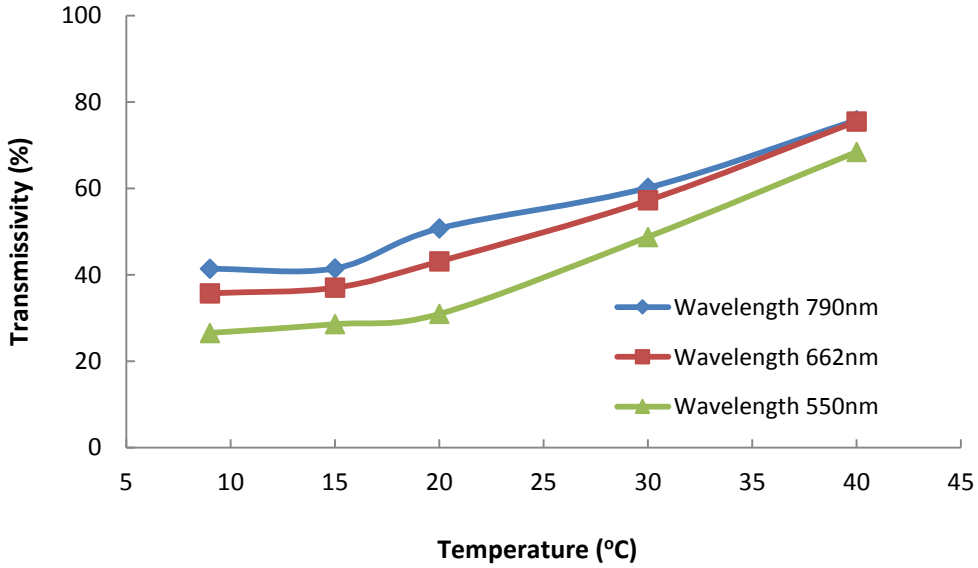

Figure 2.5 Transmissivity of 10 wt% Eudragit RL100 /2.5 ml acetone/0.5 ml water solution vs. temperature for a few wave lengths.

2.3.4 PLGA

Different concentrations of PLGA and the amount of water added in the ternary system of PLGA/dioxane/water have also been tested under different temperatures. Compared to

experiments with Eudragit, the change from clear to cloudy status is easier to see through visual observations or transmissivity in UV.

Figure 2.6 provides a graphical summary of cloud point temperature vs. ratio of dioxane/water for PLGA. A ratio of 2.5/0.5 (dioxane/water) for 10 wt% PLGA solution or 2.5/0.56 for 5 wt% PLGA solution can be chosen for these experiments since a temperature around 20 ^{o}C is a modest temperature and easy to achieve.

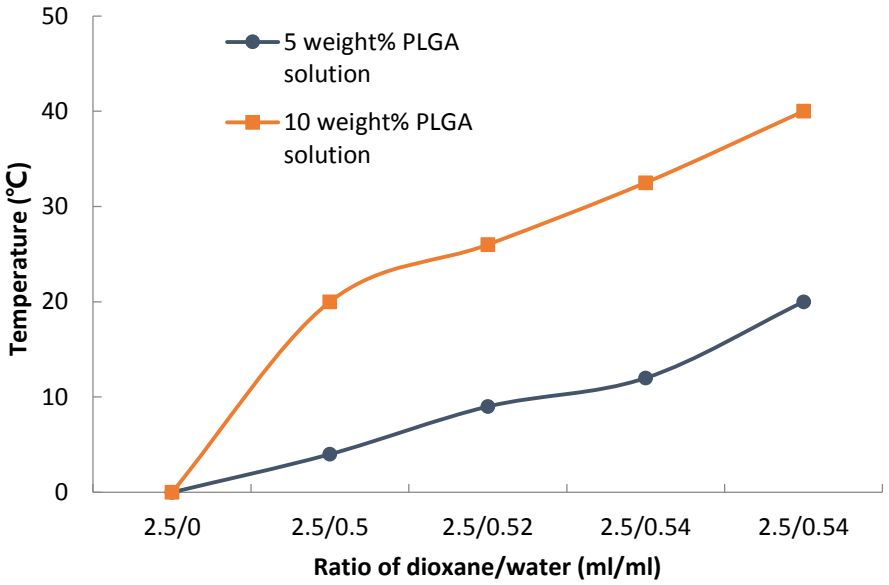

Figure 2.6 Cloud point temperatures vs. different ratios of dioxane/water in PLGA solutions.

2.3.5 Variations in Feed Solution Conditions (Pre-treatments)

By adjusting the feed solution conditions, such as adding different amounts of water, different amounts of silica, adding a surfactant, and changing the residence time, the coating results are seen to be very different. As already pointed out, the cloud point temperature of the two polymer solutions will change from clear to cloudy at higher (therefore more easily realizable) temperatures when adding different amounts of water. Therefore for both polymer solutions, a small amount of nonsolvent (water) was added.

Particle agglomeration can be reduced by the addition of a surfactant, sodium dodecyl sulfate, to the polymer solution. SEM photographs of coated particles with or without the addition of surfactant are shown in Figure 2.7. With the addition of a surfactant (Figure 2.7 (b)), the dispersion of the coated particles is much better as compared to those without the surfactant (Figure 2.7 (a)). The critical micelle concentration (CMC) of sodium dodecyl sulfate in pure water at 25 ^{o}C is 0.0082 M; therefore the concentration of SDS cannot be too high to prevent formation of micelles which can accelerate agglomeration.

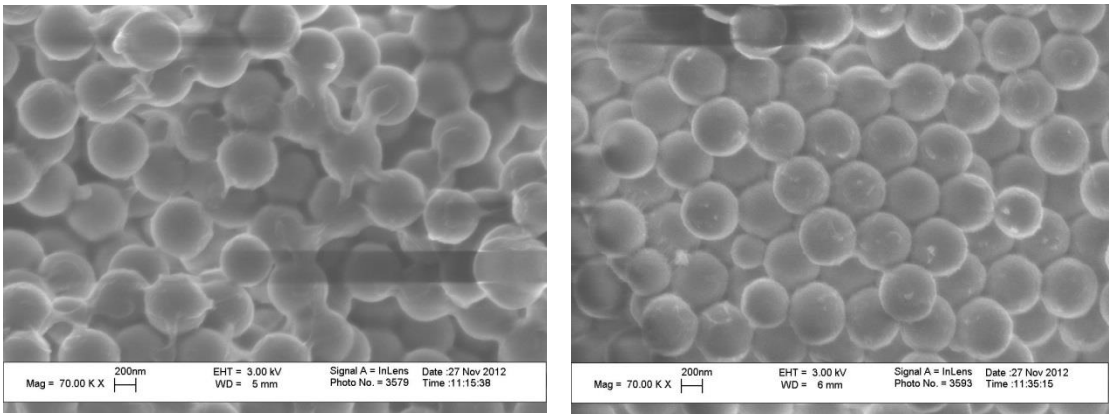

(a) (b)

Figure 2.7 SEM photographs of coated particles: (a) without surfactant; (b) with surfactant (surfactant concentration 0.0035 M).

Figure 2.8 shows the weight loss (percentage) of the coated particles obtained from TGA experiments using different amounts of silica added to Eudragit RL 100 solution. This figure also shows EDS results based on the % carbon which was present on the coatings.

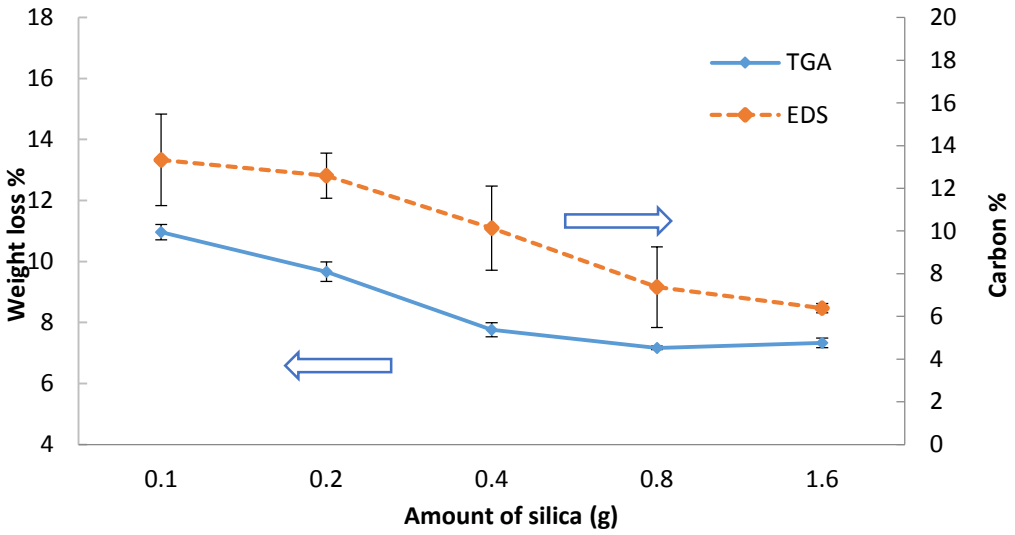

Figure 2.8 TGA and EDS results for different amounts of silica addition.

The TGA results indicate that with more silica added to the solution, the weight loss % is less which implies that the coating thickness around the particles is lower. When the amount of silica added exceeds a certain level (over 0.8 g), the coating thickness no longer decreases and remains relatively constant. Thus, both a too low or too high a silica concentration is undesirable.

Too low a silica concentration will make the coating thickness on individual particles larger; too high a concentration will have little effect on the coating thickness, increase the pressure drop, and could result in the possibility of clogging of the lumen of hollow fibers. As seen in Figure 2.8, the EDS results reinforce those obtained from the TGA. In these experiments when the amount of silica particles added was over 1.6 g per 20 ml of acetone there was a tendency for clogging.

The residence time is also critical for submicron particle coating; a longer residence time will lead to more polymer precipitation and a thicker coating. Variation of residence time can be achieved by changing the feed solution flow rate into the SHFCC. Figure 2.9

shows TGA and EDS results corresponding to suspension flow rates of 1, 5, and 10 ml/min, respectively; these flow rates correspond to residence times of 76.2, 15.2 and 7.62 s respectively. The TGA results show that as the flow rate increases, the weight loss % decreases which indicates that the coating thickness decreases when the residence time decreases. EDS results support the same conclusion.

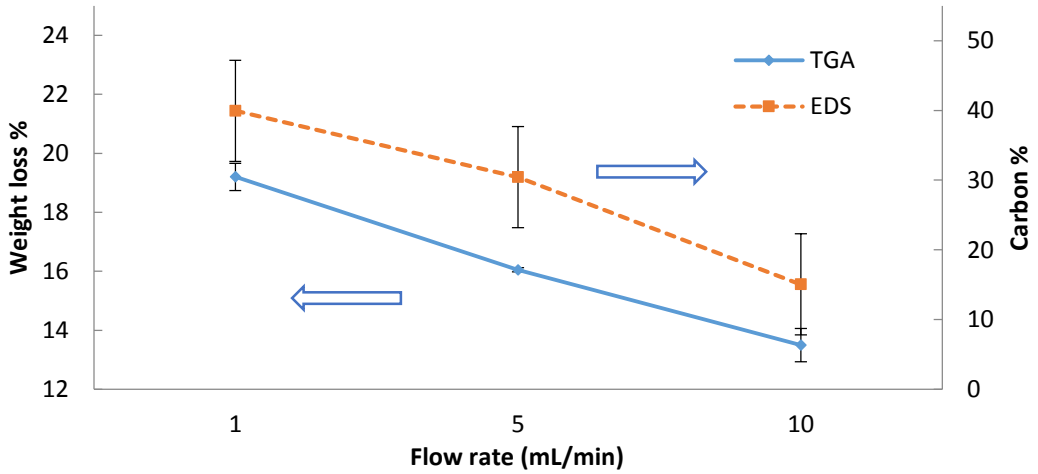

Figure 2.9 TGA and EDS results for coated submicron particles for different residence times.

Figure 2.10 shows SEM micrographs of coated particles for two different feed flow rates employed for Figure 2.9. Polymer coating on the submicron particles is seen to be less thick when the flow rate is increased, i.e., residence time is lowered; agglomeration between the particles also appears to decrease as the feed solution flow rate increases. It is worth noting that the outlet temperatures for the different flow rates studied were only slightly different. It is not expected that there would be a substantial effect of the very minor difference in outlet temperature on the coating since the temperature is very low around 4 ^{o}C.

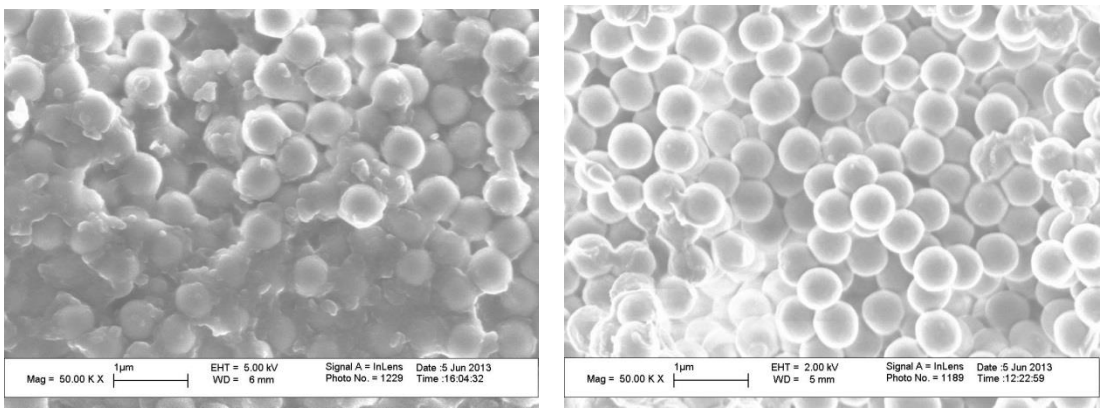

(a) (b)

Figure 2.10 SEM photographs of coated particles for different feed flow rates: (a) 1 ml/min and (b) 10 ml/min.

2.3.6 Methods for Recovering Particles (Post-treatments)

A number of post-treatment strategies were explored including improved vacuum filtration speed, sonication after filtration and centrifugation. These are considered one by one below.

The thickness of the coating on the particles was reduced by incorporating a vacuum filtration device that can increase the filtration rate. Using this filtration device, the filtration rate was increased substantially by enhancing the vacuum level from 1 in Hg to 5 in HG and up to 16 in Hg so that the excess polymer solution would not stay in contact with the particles to form a thicker coating. This is significant since in these experiments the duration of vacuum-driven filtration for example at 1 in Hg was 8 min whereas that for 16 in Hg was 5 min. The results of the enhanced vacuum filtration are shown in Figure 2.11 and Table 2.3. The SEM, TGA, and EDS studies all indicate that the faster the filtration rate, the thinner the coating. Particle agglomeration is also much less because the polymer solution remaining on the filter paper is extracted before it can form an additional coating on the surface of the particles or liquid bridges between the particles which will

lead to agglomeration. Since the filtration rate was found to be critical, all subsequent experiments were run at the highest filtration rate (16 in Hg).

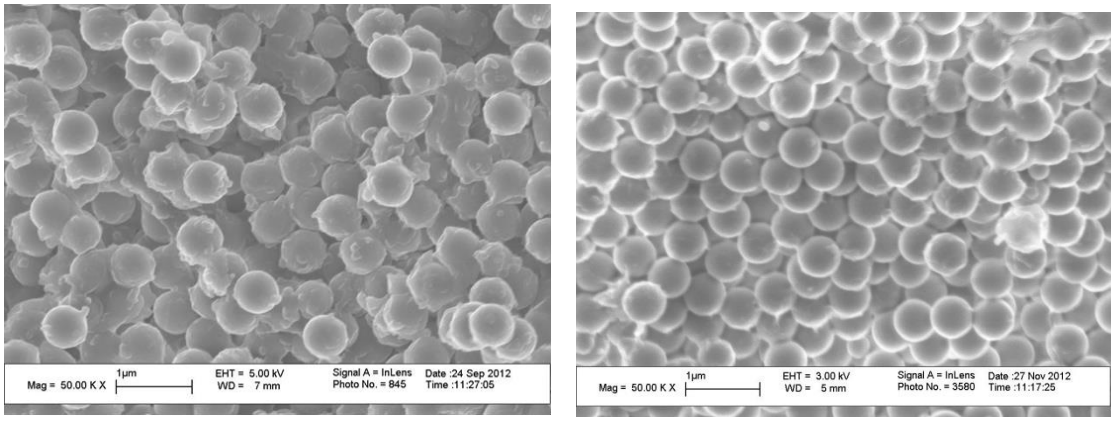

(a) (b)

Figure 2.11 SEM photographs of coated particles at different filtration rates: (a) slow--1 in Hg; (b) fast--16 in Hg.

Table 2.3 TGA and EDS Results for Coated Submicron Particles Under Slow and Fast Filtration Conditions

Vacuum Level	1 in Hg	16 in Hg
TGA Weight loss %	44.9	17.8
EDS Carbon %	37.0	31.2

Previous experimental methods discussed the use of post-treatment sonication after both filtration and centrifugation as a means of producing free-flowing particles. Experimental results of Eudragit RL 100 coated particles obtained using sonication after fast filtration are shown in Figure 2.12 and compared to those without the sonication post-treatment. There is almost no excess polymer on the particles in Figure 2.12 (b) compared with those in Figure 2.12 (a) and agglomeration between particles is less than that in Figure 2.12 (a). By using this post treatment method, the products were free-flowing rather than cohesive due to particles sticking together.

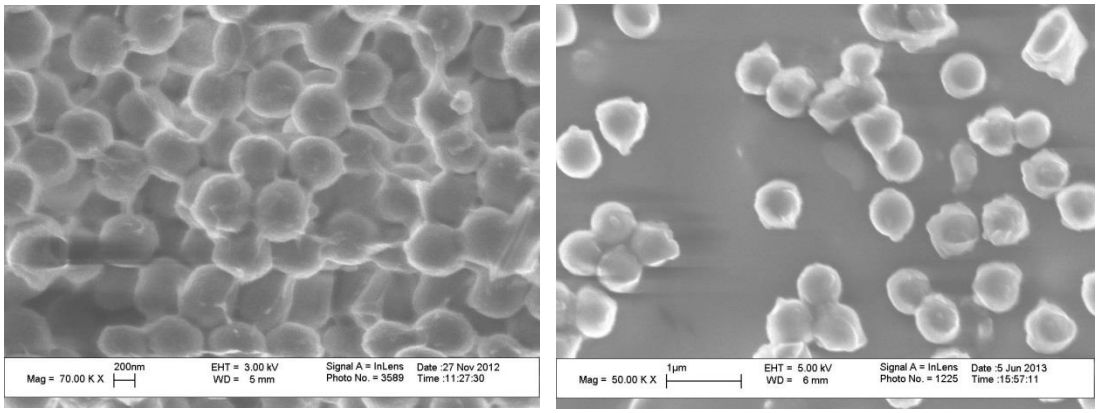

(a) (b)

Figure 2.12 SEM photographs of Eudragit RL 100 coated particles (a) without post treatment after filtration and (b) with post treatment after filtration.

Sonication was also used as a post-treatment after centrifugation. Similar to the results obtained by adding sonication after filtration, free flowing particles were also obtained by adding sonication as a post treatment after centrifugation.

2.3.7 Thermogravimetric Analysis of the Submicrometer Particles

Thermogravimetric analysis (TGA) allows measurement of the change in particle mass as a function of time by increasing the temperature of the sample continuously. Samples of dry, coated particles and dry, uncoated Cosmo 55 silica particles were analyzed by TGA. The temperature in the TGA was increased at a rate of 10 ^{o}C/min until it reached 550 ^{o}C. During this period, Eudragit RL 100 polymer coating decomposed as a result of heating while the mass of the uncoated silica remained almost unchanged as seen in Figure 2.13. The solid line shows that the weight % of the coated particles was reduced from 100% to 85%, which means that the 15% weight loss was due to decomposition of the polymer coated on the particles during heating.

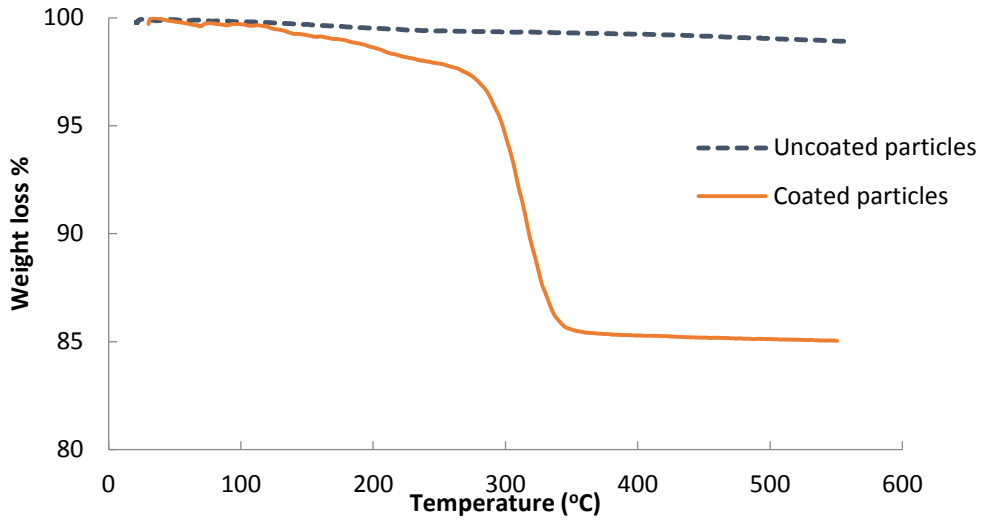

Figure 2.13 TGA micrographs of uncoated and Eudragit coated submicron silica particles subjected to post treatment methods after filtration.

To estimate the thickness of the coating, it is assumed here that the polymer is evenly coated on the spherical submicron particles of radius r and forms a uniform layer. The equation governing the relation between the mass of the polymer and the mass of the particles is

$$\frac{m_{Silica}}{m_{Polymer}} = \frac{\rho_{Silica}\frac{4}{3}\pi r^3}{\rho_{Polymer}\frac{4}{3}\pi\{(r+h)^3 - r^3\}} \tag{2.1}$$

The coating thickness h can be calculated as

$$h = r(1+\rho_{Silica}m_{Polymer} / \rho_{Polymer}m_{Silica})^{1/3} - r \tag{2.2}$$

where m_{Silica} and $m_{Polymer}$ are the mass of the particles and polymer, respectively. The densities of the host particles and polymer are ρ_{Sliica} (=2.65 g/ml) and $\rho_{Polymer}$ (=1.1 g/ml), respectively. Using the results from the TGA, the coating thickness for the submicron particles under optimized conditions was found to be about 33 nm.

2.3.8 Scale-up Using a Larger SHFCC Module

Scale-up can be achieved by simply using a larger module containing for example double the number of hollow fibers, 46 instead of 23 (see Table 2.1). The 25 mm diameter filter paper used with the smaller module was replaced by a 90 mm diameter filter paper so as to be able to handle a larger amount of product. Since the number of fibers inside the SHFCC module was doubled, the flow rate was also doubled without affecting the residence time, i.e., the velocity in each hollow fiber remains the same. Therefore the larger module should produce particles having a coating similar to that from the smaller module. Coated particles collected from both modules, large and small, (all other conditions are the same: 0.4 g silica, 16 inHg-based filtration speed) were characterized by TGA. The coating thickness of the particles calculated from TGA results was 33.1 nm for the large module and 33.3 nm for the small module. It should be noted that the coating thickness calculated from the TGA is an idealized value that assumes the coating on the particles to be perfectly uniform with no excess coating between the silica particles.

2.3.9 Laser Diffraction Spectroscopy

Sympatec Laser diffraction spectroscopy (LDS) coupled with RODOS dry dispersion and R1 lens (0.1- 35 μm) was used to identify the particle size distribution (PSD) of the products collected; most importantly, it can identify the amount of agglomeration present in the coated particles. A dry powder of particles coated in the small module was tested under different pressures (0.5 bar to 3 bar) to determine the average particle size. With an increase of the pressure, the powder exhibited a reduction in particle size until a plateau was observed. After the pressure reached 3 bar, the particle size did not decrease as the pressure was increased; this means that complete dispersal was achieved. Therefore, the

default primary pressure (PP) was set as 3 bar when measuring the PSD of the samples in Figure 2.14.

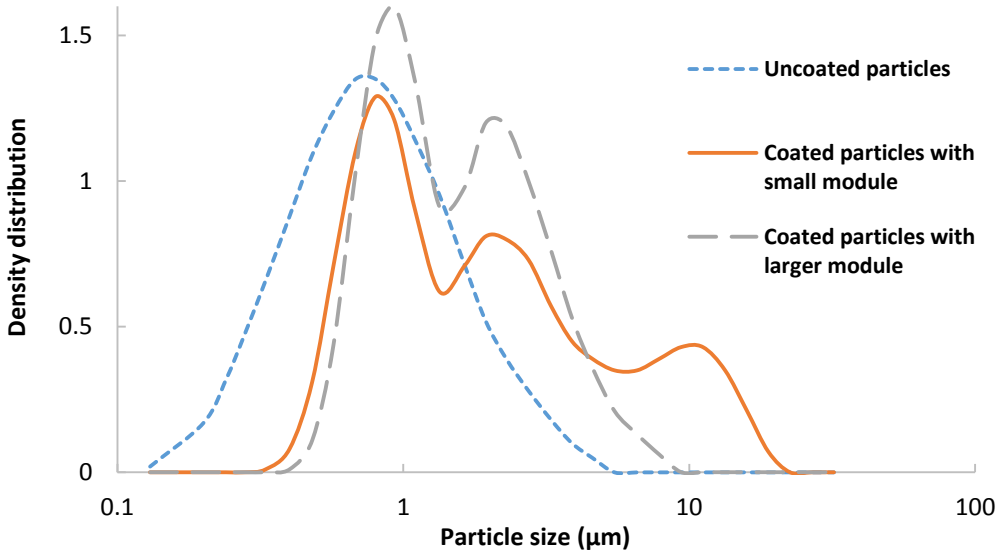

Figure 2.14 Particle size distribution for uncoated and Eudragit coated submicron particles from both the small and large modules.

The LDS analyzer was used to measure the PSD of uncoated Cosmo 55 silica, Eudragit coated Cosmo 55 silica particles from the small module, and Eudragit coated Cosmo 55 silica particles from the large module. Table 2.4 shows that the Sauter mean diameter (D_s) of the 3 samples are 640 nm, 1310 nm and 1250 nm, respectively. This indicates that the coated particles were somewhat agglomerated, forming mostly doublets and perhaps some triplets. After scale-up, the mean size of the coated particles from the large module is similar to that from the small module. However, there appears to be some difference in the extent of agglomeration of the coated particles obtained from the smaller module and the larger module (Figure 2.14). The coated particles go through a number of post-treatment steps after discharge from the SHFCC device. Any minor variation in these steps can contribute to the observed variation in the extent of agglomeration.

Table 2.4 Particle Size for Uncoated and Coated Submicron Particles

	Sauter mean diameter (μm)
Uncoated particles	0.64
Coated particles with small module	1.31
Coated particles with large module	1.25

2.3.10 Scanning Transmission Electron Microscopy (STEM)

The particle coating thickness and morphology can be much more precisely determined by TEM-STEM analysis which is used to check whether the coating thickness is in accord with the TGA results and also if it is uniform. Figure 2.15 (b) shows a photograph of a single coated particle under optimized conditions (0.4 g silica, 2.5 cc/min flow rate, surfactant concentration 0.0035 M, 4 ml water added to 20 ml of acetone, sonication post treatment after filtration at 16 inHg-based filtration rate, small module). The bright area is the silica particle and the transparent grey ring represents the polymer coating. From Figure 2.15, it is easy to see that a uniform, thin coating is covering the particle, while for uncoated silica particle shown in Figure 2.15 (a) no transparent ring is seen. Based on the scale bar, the thickness of the coating around the single submicron particle can be estimated to be about 25 nm.

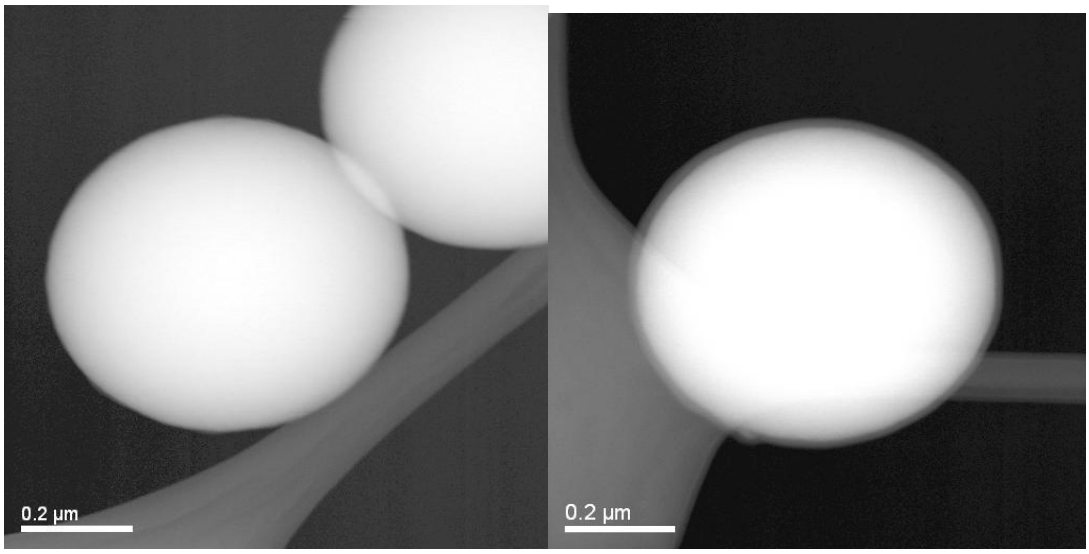

(a) (b)

Figure 2.15 STEM micrographs of (a) uncoated submicron particles and (b) coated particles under optimized condition.

Figure 2.16 shows the signal profile of various elements (carbon, silicon and oxygen) in the coated nanoparticle shown in Figure 2.15 (b). The probe detects various elements in the particle from the surface to the interior. The point at 0.022 µm in the x-axis is the surface point of the coating; the point at 0.05 µm is the coating end point and the beginning of the surface of the silica particle. The coating thickness can then be estimated as 0.028 µm or 28 nm.

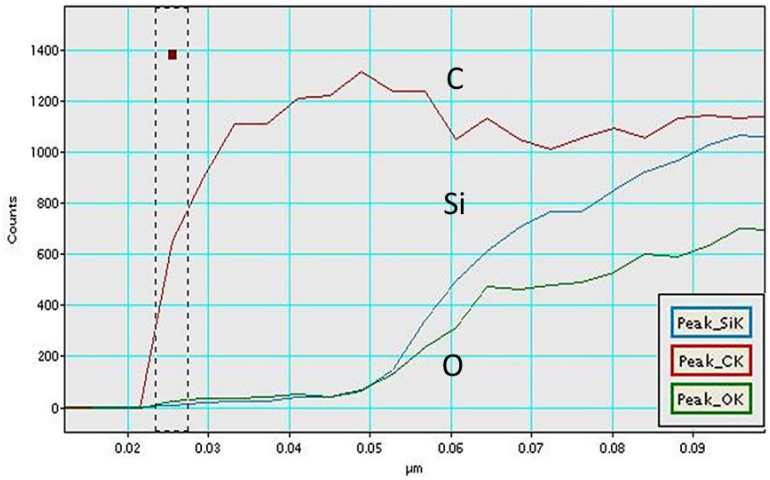

Figure 2.16 EDS results of single coated submicron particles under optimized conditions.

2.3.11 PLGA Coated Submicron Size Particles

Coating the silica particles with PLGA was also studied in the SHFCC device but not as extensively as with Eudragit. Therefore, only one figure is shown; it indicates that PLGA can also be coated onto the silica particles in the SHFCC device. Figure 2.17 (a) shows an SEM image of silica particles in a dioxane solution of PLGA before precipitation; Figure 2.17 (b), (c) and (d) show the SEM images of coated particles after the suspension was passed through the SHFCC and precipitation occurred.

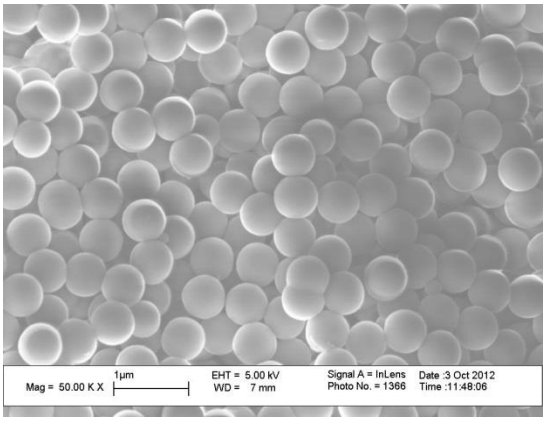

(a)

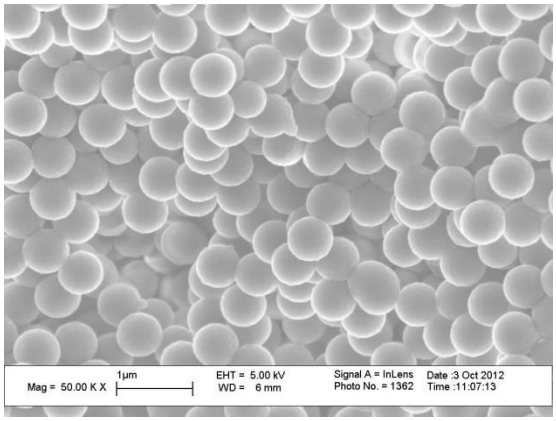

(b)

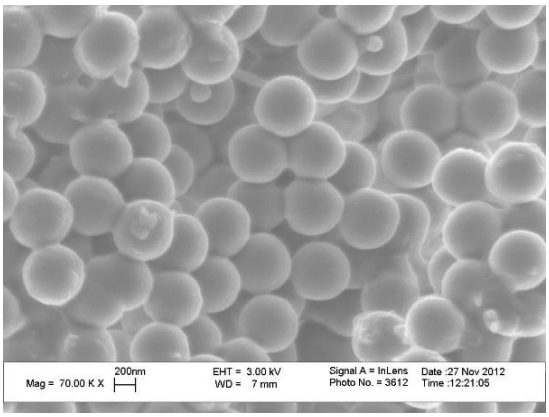

(c)

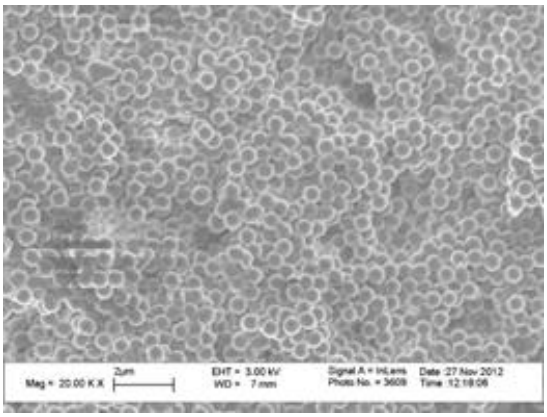

(d)

Figure 2.17 SEM photographs of solutions with PLGA and submicron particles (a) before passing through the SHFCC and (b),(c) and (d) after precipitation in the SHFCC under different magnifications.

Clearly, there is no coating in Figure 2.17(a); however Figure 2.17(b) shows a uniform polymer coating covering the particles. This result is in accord with the EDS result that shows a % carbon of 21.6 after post-treatment using fast filtration (16 in Hg), confirming that PLGA can also be used to coat the particles by the SHFCC method. It appears that the coating method developed is quite general and may be used with a variety of polymers; PLGA being biodegradable is an especially useful example since it is widely used in pharmaceutical industry.

2.3.12 Effect of Operating Parameters

It is useful to briefly summarize here the effects of various operating parameters in this technique one by one.

Residence time: The residence time in the hollow fiber device containing a certain number of hollow fibers having a certain I.D. and length is determined by the volumetric flow rate of the coating suspension; the higher the volumetric flow rate, the shorter is the residence time. From the TGA and EDS measurements it is clear that a longer residence time will lead to a higher amount of polymer precipitation as well as enhanced bridges between neighboring coated silica particles and agglomerates.

Lumen-side exit temperature: Other conditions remaining constant, the lumen-side exit temperature is controlled by the inlet temperature of the cooling liquid on the shell side. A lower temperature will lead to higher precipitation and thicker coating.

Polymer concentration: Higher polymer concentration will tend to enhance the coating thickness and the extent of bridging between neighboring particles and agglomerates. However, a higher concentration will also have other deleterious effects: there will be higher polymer loss in the exiting solution and increased solution viscosity

which will affect the processing capacity; the chances of clogging of the hollow fiber bore will increase.

Post-treatment time: Among the various post-treatment steps, the collection time, the filtration time and the centrifugation time are important in the sense that the coated submicron particles are in contact with a solution containing the polymer which is precipitating. Therefore, it is important to reduce the duration of various post-treatment steps especially when there is a volatile solvent namely, acetone, which will continue to evaporate and increase the polymer concentration in solution.

2.4 Results and Discussion for Coating of Silica Nanoparticles (SNPs)

After the cloud point measurements of the Eudragit/acetone/water solution were completed, attention was focused on coating of silica nanoparticles (SNPs) conducted in SHFCC modules of two sizes and characterizing the coatings so obtained. The characterization of the coatings was carried out after undertaking post-treatment steps mentioned earlier.

The amount of SNPs plays an important role in polymer coating using the SHFCC method since the precipitated polymer will coat every silica particle due to heterogeneous nucleation. It is expected that the higher the amount of silica addition, the higher is the amount of polymer that will be precipitated.

The coated SNP samples obtained after post-treatment steps of filtration, sonication, and vacuum drying were analyzed by TGA to determine the relationship between the average coating thickness on a SNP and the amount of silica added in the feed solution-suspension. It is useful to specify first the conditions used to obtain the coated SNPs which were subjected to TGA studies. Both the larger and the smaller SHFCC modules were

used to produce coated particles and the results compared vis-à-vis their effective coating thicknesses. For both modules, the operating conditions were kept the same: 0.1g SNPs, 20 ml acetone, 0.025g SDS, 2.4g Eudragit RL 100 and 4ml DI water. The only difference between the two modules was the number of hollow fibers. To maintain the same residence time for precipitation in both modules, a feed flow rate of 4 ml/min was maintained in the large module which was twice that in the small module (2 ml/min). Details of the results from TGA are provided below.

Figure 2.18 shows the observed weight loss results for uncoated and coated SNPs. The dotted line indicates that pure Aerosil 200 SNPs underwent hardly any weight loss during heating. However, both solid lines for the coated SNPs show considerable weight loss due to the decomposition of the polymer coating. The mass losses of coated particles from the large and smaller modules are estimated to be 60% and 55%, respectively; these values are quite close to each other. This result suggests that scale-up of the coating device and process may be easily implemented by maintaining the same residence time in SHFCC modules of different sizes having different numbers of hollow fibers.

If one assumes that the polymer coating was evenly spread over all SNPs and the particles are assumed spherical, the relation between the coating thickness h of the mass of the polymer and the silica nanoparticle of radius r can be deduced from equation (2.1) where m_{Silica} and $m_{Polymer}$ are the mass of the nanoparticle and the polymer coating. The coating thickness h can then be calculated from equation (2.2). The radius r of a silica nanoparticle is 6 nm. The densities of the host particles and the polymer are ρ_{Sliica} (=2.65 g/ml) and $\rho_{Polymer}$ (=1.1 g/ml), respectively.

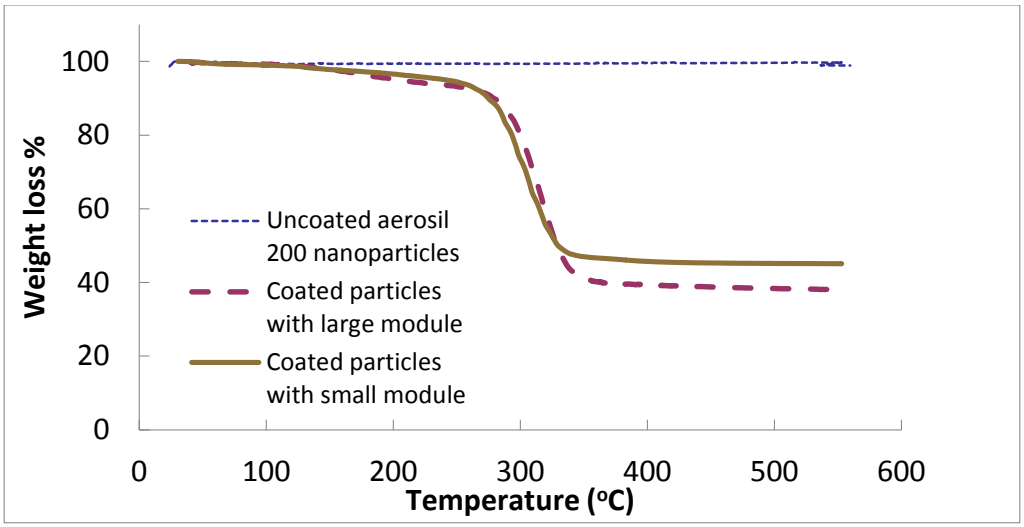

Figure 2.18 TGA micrographs for uncoated SNPs and Eudragit coated SNPs after post-treatments (filtration, sonication and drying).

Using the results of TGA experiments for different amount of SNPs added, one can estimate the average nanocoating thickness on the SNPs from equation (2.2). For example, 0.05 g of SNPs added to the original feed solution resulted in a thickness of 4.3 nm whereas 0.10 g of SNPs yielded a thickness of 3.9 nm. With a further increase in SNP addition to 0.15 g, the coating thickness decreased to 3.6 nm. The amount of SNPs plays an important role in polymer coating using the SHFCC method since the precipitated polymer will coat every SNP due to heterogeneous nucleation. The higher the amount of silica added, the lower the amount of polymer that will be precipitated on a given particle (resulting in a thinner coating) due to the much higher density of nucleation sites with increasing number of SNPs. All of these experiments were carried out in the larger SHFCC module.

The coating thickness can also be determined directly by measuring the coating thickness from the STEM micrographs of coated SNPs based on the scale bar at the bottom left side of the images (see Figure 2.21 provided later). Figure 2.19 shows that the measured coating thickness decreases as the amount of SNPs is increased. Figure 2.19 also shows the

coating thicknesses obtained from the TGA studies described above. The results from STEM measurements appear to be in reasonable accord with those from TGA measurements.

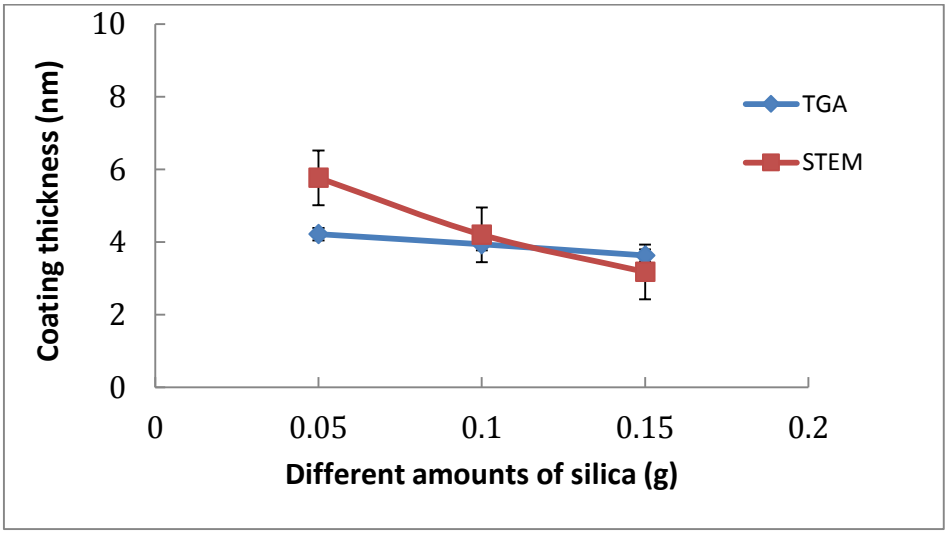

Figure 2.19 Results of coating thickness vs. silica addition (larger module) obtained by two methods: STEM and TGA.

STEM micrographs shown in Figure 2.20 are 2D mapping images obtained by EELS in which the green cover represents the polymer coating and silica nanoparticles appear as red and purple zones. This figure shows that all silica nanoparticles were uniformly coated by Eudragit RL 100 in both the small and the large module. One does not observe any significant difference in coating thickness between the two modules. Figures 2.20 (a) and 2.20 (b) show that the coating thickness in the small and large modules is 3.6 and 4.0 nm, respectively. The very limited difference in coating thickness from one module to another indicates that as long as the residence time is the same, scaling up by simply increasing the number of fibers is feasible.

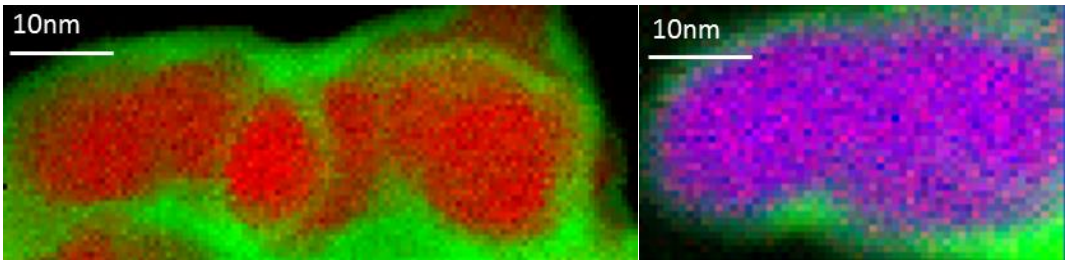

(a) (b)

Figure 2.20 EELS 2D elemental maps for coated SNPs, carbon K-edge in green, silicon $L_{3,2}$-edge in red or purple from (a) the small module and (b) the large module.

STEM analysis is a good way to characterize the film coating thickness, surface morphology, element distribution, particle size and degree of agglomeration. In the present case, a 1D line scan and 2D mapping provided by EELS add-on are used to analyze the samples. The blue straight line in Figure 2.21 (a) shows that the detector moves along the direction of arrow so that it first contacts the left side of the polymer coating boundary, passes through the interior of the SNP, and then across the right polymer coating boundary. Two peaks at the edge of the particle showing the carbon profile in Figure 2.21 (b) illustrate the polymer coating around the outer surface area of the nanoparticle. EELS spectrum (not shown here) confirmed that the nanoparticle is silica as it contains three elements, silicon, oxygen and carbon which comes from the coating. Figure 2.21 (c) is the silicon intensity profile across the particles following the same arrowed line in Figure 2.21 (a) which also shows that the material inside consists of only silica.

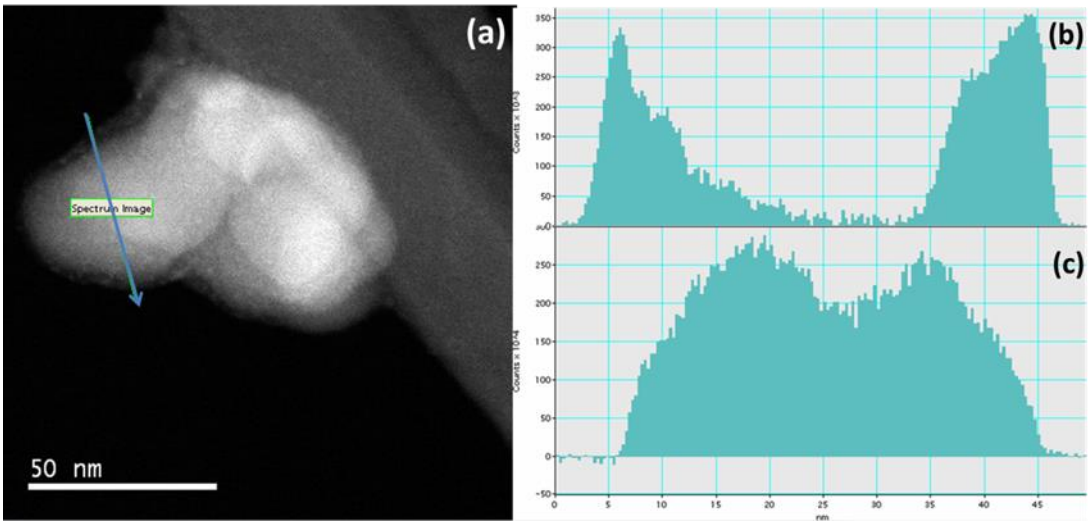

Figure 2.21 (a) STEM images of coated nanoparticles; (b) carbon intensity profile and (c) silicon intensity profile along the arrowed line in (a).

STEM 2D mapping (Figure 2.22) can directly visualize different element distributions to reveal the coating morphology. Figure 2.22 (b) shows that the polymer coating is evenly distributed over the entire SNP surface area and the thickness is quite uniform. The actual coating thickness can also be estimated by using the scale bar on the bottom left of Figure 2.22 (a). In this case the thickness is estimated to be 4 nm.

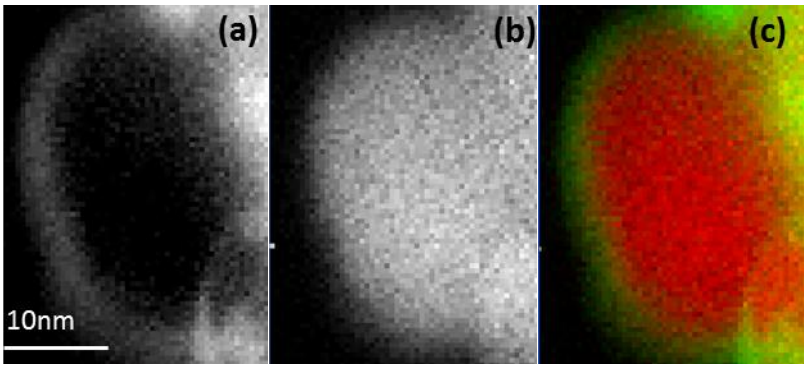

Figure 2.22 EELS 2D elemental map of (a) carbon K-edge, (b) silicon $L_{3,2}$–edge and (c) colorized map, carbon in green and silicon in red.

Whether the SHFCC technique can be employed to coat host nanoparticles having different surface properties such as hydrophilicity or hydrophobicity has also been investigated. For all of the results presented above, Aerosil 200 which is hydrophilic was used as the host particles. However, Aerosil R974, a hydrophobic silica particle having a primary particle size of 12 nm, was also successfully coated with Eudragit RL100 by applying the SHFCC technique (see Figure 2.23). The green area in this figure suggests that the polymer was evenly coated on the silica (red area) particle regardless of whether the particle surface is hydrophobic or hydrophilic. The thickness of the coating appears to be almost the same in both cases. This suggests that the SHFCC-based polymer coating technique can be broadly utilized to coat nanoparticles having different surface properties.

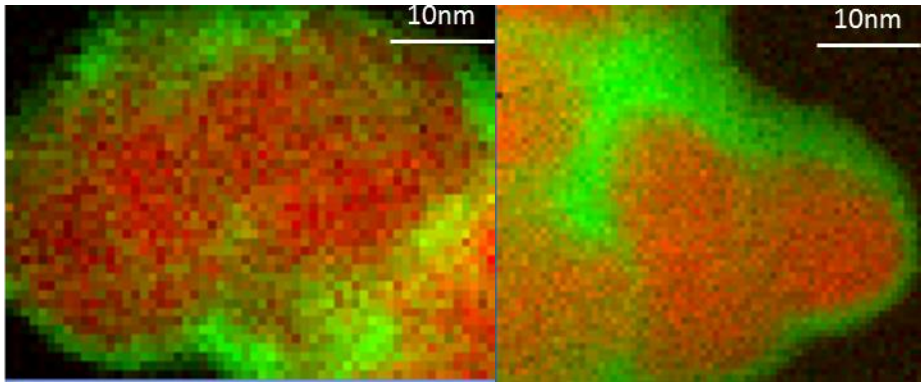

(a) (b)

Figure 2.23 EELS 2D elemental maps (carbon K-edge in green, silicon $L_{3,2}$–edge in red) of (a) Aerosil R974 and (b) Aerosil 200.

The images in Figure 2.23 also show that about 2 to 5 SNPs tend to stick to one another forming agglomerates due to the strong van der Waals forces between the nanoparticles. Another reason for agglomeration is that during polymer coating, precipitated polymer will not only cover the host particle, but also interconnect the coated particles via precipitated polymer bridges between the particles. To counteract the inherent

tendency for agglomeration by SNPs, an additional particle coating experiment was done by increasing the surfactant concentration and immediately applying sonication to break the soft bonding between the coated SNPs. In these experiments, the concentration of SDS was doubled from 0.0035M to 0.007M. After the coated products were collected on a filter paper, a certain amount of coated particles was immediately put in a small bottle containing water and sonicated for 1 minute. It was then dropped into the cuvette and analyzed in the Beckman Coulter N4 PLUS.

The mean particle size, the number of agglomerated SNPs and the PSD were determined for three samples: the uncoated SNPs; coated SNPs produced by the lower surfactant concentration (0.0035M); SNPs produced by higher surfactant concentration (0.007M) and the procedure just described above. Figure 2.24 illustrates the particle size distribution (PSD) of the three samples. It is clear that increasing the concentration of the surfactant and reducing any delay in further processing by undertaking sonication immediately reduces the extent of aggregation substantially. The inset on top of the figure identifies the mean size of the particles and the estimated aggregation or agglomeration of the nanoparticles based on the primary particle size of a single SNP (12 nm). Before coating it appears that on an average about four primary nanoparticles are sintered together and aggregated with an estimated size of 50 nm. After coating with Eudragit in the presence of a higher surfactant concentration based on the measured mean size (103 nm), about nine coated nanoparticles stick together to form agglomerates.

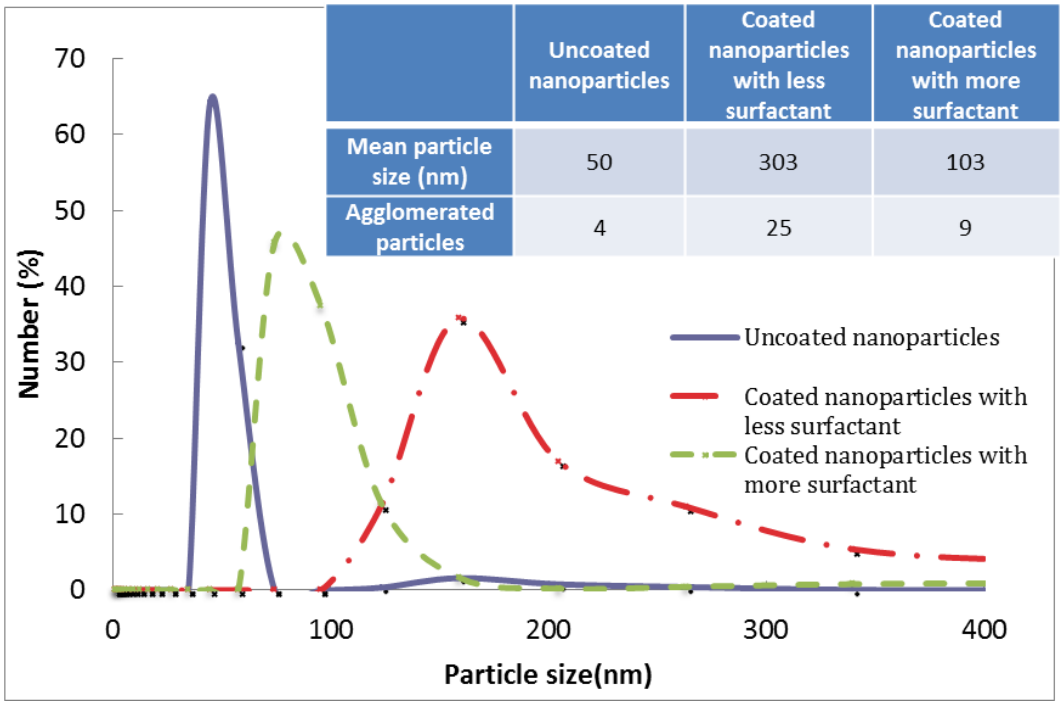

Figure 2.24 Particle size distribution by number for uncoated and coated SNPs by two methods; mean particle size and the extent of agglomeration of the particles are provided for the three cases in the inset at the top of the figure.

It is important to note that since the silica nanoparticles were produced in a high temperature furnace, sintering of the primary SNPs as well as attractive van der Waals force caused uncoated SNPs of 12 nm diameter (blue line) to show a certain level of aggregation. The PSD of the coated nanoparticles by the standard procedure using a lower level of surfactant is much wider than that of the uncoated particles due to the fact that polymer coating will also cause the particles to stick to one another and form solid bridges between particles upon drying even in the presence of a surfactant and sonication post treatment. This was also observed in the EELS images of Figure 2.23. However higher surfactant concentration and reducing post-treatment processing delays considerably reduced the level of observed agglomeration.

Nance et al. [8] have shown that, with the right coating, larger nanoparticles can

diffuse throughout the extracellular space in rat and human brains which is especially useful for diseases in the case of a compromised blood-brain barrier. However, recent literature evidence suggests that monodisperse NPs of size less than 50-60 nm exhibit superior drug delivery performance[39]. Surface functionalization of mesoporous SNPs with polyethylene glycol-polyethylenimine copolymers enhanced delivery of drugs loaded in 50 nm mesoporous SNPs[40]. Therefore it would be ideal to coat NPs which do not show any level of agglomeration or aggregation. In the present research, the Evonik fumed silica NP used is already aggregated to start with as a result of their manufacturing process. Use of host NPs and or drug nanoparticles which do not show any initial aggregation should lead to reduced agglomeration in coated NPs.

Coating of silica nanoparticles with a polymer by the solid hollow fiber cooling crystallization technique was investigated here. Both hydrophilic and hydrophobic SNPs having a primary size of 12 nm were successfully coated with Eudragit RL100 in two different SHFCC modules to demonstrate that scale-up can be relatively easy to achieve without affecting the quality/thickness of the coating. The only difference between the two modules is the number of hollow fibers. Different characterization techniques were employed to demonstrate that the polymer coating on the host SNPs was relatively uniform and the thickness of the coating can be tailored by varying the operating parameters. This technique was also successfully applied to coat submicron particles as shown in Section 2.3. Additional experiments focusing on polymer coating of drug particles will be illustrated in the following chapter.

CHAPTER 3

CONTINUOUS SYNTHESIS OF POLYMER COATED DRUG CRYSTALS BY SOLID HOLLOW FIBER MEMBRANE-BASED COOLING CRYSTALLIZATION

3.1 Introduction

To achieve the needed therapeutic effects in a host via controlled drug delivery, two methods are usually employed: dispersion of the drug in a polymer matrix which may degrade or swell with time or encapsulation of individual drug particles or crystals inside a polymeric coating. A polymeric coating of a drug particle or crystal is additionally useful when a fragile drug has to be protected from an adverse environment such as a highly acidic condition. This part of the thesis is focused on developing a polymeric coating on drug crystals by the novel SHFCC process which can be used for drug delivery systems and other potential applications [41][42].

Figure 3.1 (a) depicts a single polymeric solid hollow fiber. It can serve as a heat exchanger where the feed solution flowing in the tube side can be cooled down by the cold liquid circulating on the shell side. The hollow fiber was made of polypropylene (PP) which has a great deal of pH, chemical and solvent resistance. This nonporous fiber wall has a relatively smooth surface to minimize the possibility of clogging problem inside of the hollow fiber. Figure 3.2 (b) illustrates a solid hollow fiber cooling crystallizer (SHFCC) module that consists of a number of hollow fibers in the shell. The number of hollow fibers can be easily adjusted according to the needs of scale up.

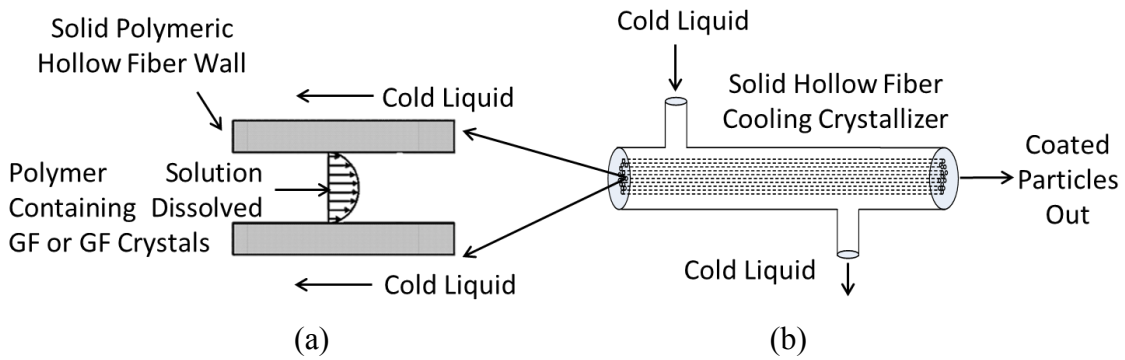

Figure 3.1 (a) Single solid hollow fiber heat exchanger; (b) Solid hollow fiber membrane based cooling crystallizer module.

3.2 Materials and Methods

3.2.1 Materials

Eudragit RL 100 (M_w, 150,000; a copolymer of methyl methacrylate, ethyl acrylate and methacrylic acid ester) was purchased from Evonik-Degussa (Parsippany, NJ). Drug particles Griseofulvin (GF) obtaining from Letco (Decatur, AL) was used as host materials (mean particle size < 10 μm, partially dissolved in acetone, practically insoluble in water) without further treatment. Sodium dodecyl sulfate (SDS) as a surfactant was also obtained from Sigma-Aldrich (St. Louis, MO).

3.2.2 Experimental Methods

Cloud point measurement was undertaken for the cooling experiments. Cloud point value of 15 ^oC was selected and the volume ratio of acetone/water used was 2.5/0.5. Detailed procedure was mentioned in Section 2.2.3.

A schematic diagram of the coating setup is the same as in Figure 2.1. An amount of 2.4 g of Eudragit RL100 granules was first placed into a flask containing 20 ml acetone solution and kept under stirring for about 30 min in order to fully dissolve the polymer. After the solution was clear, a given amount of drug particles was introduced in the solution.

Most of the drug particles were fully dissolved into the solution; there were some left-over drug crystals still suspended in the solution. Next 4 ml of DI water and 0.025 g of SDS as surfactant were added into the flask. After 30 min stirring, the flask containing the well-mixed solution was placed in a water bath at a constant temperature.

When the experiment was started, first an aqueous solution of 50 % by volume of ethylene glycol was circulated through the shell side; a chiller (Polystat CR250WS, Cole-Parmer, Vernon Hills, IL) cooled the glycol solution to -9 ^{o}C in the shell side. After about 2 min when the tube side wall was fully cooled down by the shell side cold liquid, the solution was fed into the lumen side of the SHFCC by a pump (Masterflex, model no.7523-20, Cole-Parmer, Vernon Hills, IL) at a rate of 3.5 ml/min. The temperature indicated by thermocouple T1 was 45 ^{o}C, the feed side polymer solution containing the drug was cooled down in the lumen side of the module from 45 ^{o}C to 5 ^{o}C (unless otherwise mentioned) by the cold liquid from the shell side. Polymer was crystallized from the solution and subsequently coated the drug particles due to the rapid temperature reduction. Coated drug crystals along with the excess polymer solution were swept out of the outlet of the SHFCC unit by the incoming feed solution since the SHFCC process is continuously operated. A vacuum microfiltration system (Omnipore Membrane, PTFE, 0.45 μm pore size, 90 mm filter diameter, Millipore, Billerica, MA) underneath the outlet was used to remove most of the solution at a pressure of 15 psig; the cake on the filter paper containing the coated particles was collected for post-treatment and characterization.

3.2.3 Characterization of Coated Griseofulvin Drug Crystals

The X-Ray Diffractometer by Empyrean (Philips, Westborough, MA) was used to measure the X-ray diffraction patterns of both coated and uncoated Griseofulvin drug samples at the

operating voltage and amperage of 45 kV and 40 mA, respectively. Sample powder was evenly dispersed on a sample holder and the surface was gently swept by a glass to maintain co-planarity in the area in order to get the accurate single source. The range of scanning was adjusted from 5 ^{o} to 45 ^{o} 2θ at a step size of 0.02 ^{o} 2θ and 15 ^{o} time per step under the scanning of 255 detecting channels.

Dissolution test was run to compare the difference between uncoated and coated GF drug particles via a Distek Dissolution tester (North Brunswick, NJ). 0.27 % of SDS solution in 900 mL volume was prepared as a buffer solution for the test according to the USP II paddle method. Medium temperature was maintained at 37 ^{o}C. An amount equivalent to a dose of 50 mg of Griseofulvin sample was dropped into a dissolution vessel containing buffer solution while a 50 rpm of the paddle stirring speed was maintained. After 1, 3, 5, 10, 20, 30, 40, 50 and 80 min, a syringe was used to extract the solution with a volume of 6 ml and immediately analyzed by UV spectroscopy (52100 UV+, Cole-Parmer, Vernon Hills, Illinois) at a wavelength of 296 nm. The transmissivity of 0.27 % SDS buffer solution was first analyzed as the benchmark before the test.

A differential scanning calorimetry (DSC 7, Perkin Elmer, Waltham, MA) was applied to determine if the melting peaks in the DSC thermogram are the same before and after the coating of drug particles. About 3 mg of the sample was heated over a temperature range of 30-250 ^{o}C at a rate of 10 ^{o}C/min, the melting point was detected by Pyris software.

A Raman Microscope (DXR, Thermo scientific, Waltham, MA) was used for identifying the molecular structures for uncoated/coated drug crystals. Laser wavelength was set at 780 nm while the Laser power was 10 mw for the run.

A laser diffraction particle size analyzer (LS230, Beckman Coulter, Brea, CA) was

applied to measure the particle size distribution. An aqueous sample containing the suspension of uncoated/coated drug particles was first under sonication for 30s before the testing in order to break the soft bonding among coated particles.

SEM, TGA instruments were already mentioned in Section 2.2.4

3.3 Results and Discussion

3.3.1 Crystallization of Griseofulvin Drug Particles in SHFCC Unit

A small amount of dry GF powders as received was put on a stub pin mount and characterized by SEM without any treatment. Figure 3.2 illustrates micrographs of pure GF particles under different magnifications. It illustrates the drug particles as received have very rough surfaces and irregular shapes with a diameter around 10 micrometer.

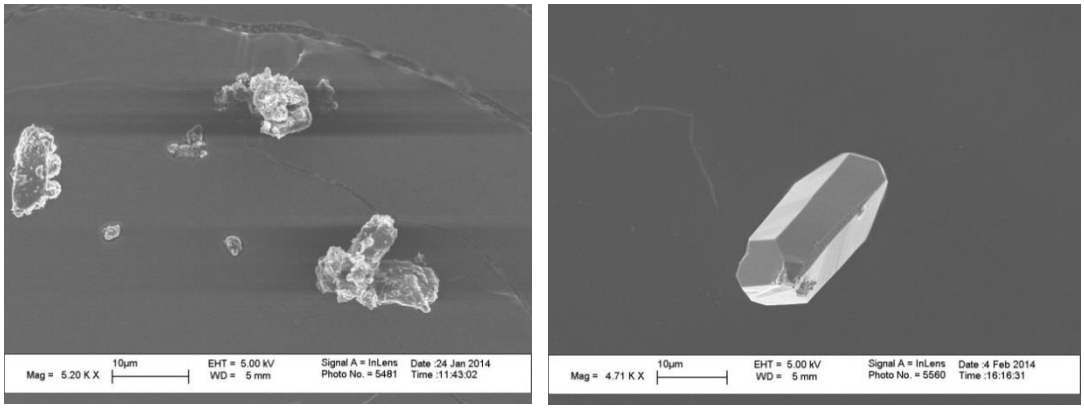

(a) (b)

Figure 3.2 SEM micrograph of (a) pure drug powders as-received and (b) drug powders after precipitation in a SHFCC unit without any polymer.

In order to identify whether SHFCC process will affect the characteristic of drug particles, the as-received GF particles were analyzed by SEM after the SHFCC process without the presence of any polymer. GF particles were first fully dissolved into solution in acetone in a flask which was then submerged in a water bath at 45 ^{o}C under stirring;

after about 30 min mixing when there were no drug particles suspended in the solution, the solution was passed through the tube side of the SHFCC device while the cold liquid was circulating in the shell side; drug particles were collected at the outlet in the other end by a filter paper and subjected to characterization.

Figure 3.2 (b) is the micrograph of pure GF particles after pumping through SHFCC device without the addition of Eudragit RL 100. Compared to Figure 3.2 (a) in which the drug shows no crystalline shape, drug particles in Figure 3.3 (b) have grown up to be well-defined crystals after SHFCC process. The surface is relatively smooth with only some tiny crystals attached to it. That is because the drug was first fully dissolved in the acetone solution (0.55 g GF in 20 mL acetone) in the flask; after passing through the SHFCC heat exchanger, GF particles precipitated out from the solution due to rapid temperature reduction in the SHFCC module.

3.3.2 Coating of Griseofulvin Drug Particles with Eudragit Polymer in SHFCC unit

First, the polymer has to be dissolved in the acetone solution prior to the drug particles in order to provide the coating material for Griseofulvin. The fully dissolved polymer solution in acetone with small amounts of drug particles suspended (most of the drug particles were fully dissolved in the solution) was pumped through SHFCC cooling crystallizer, the drug will crystallize first, polymer will precipitate later and cover the drug particles. In Figure 3.3, a thin polymer coating can be seen on each drug crystal. Compared to Figure 3.2 (b) in which the drug particles were crystallized without the presence of any polymer, the surface morphology around the drug crystals also appears to be different which implied the polymer successfully encapsulated the GF particles after the SHFCC process.

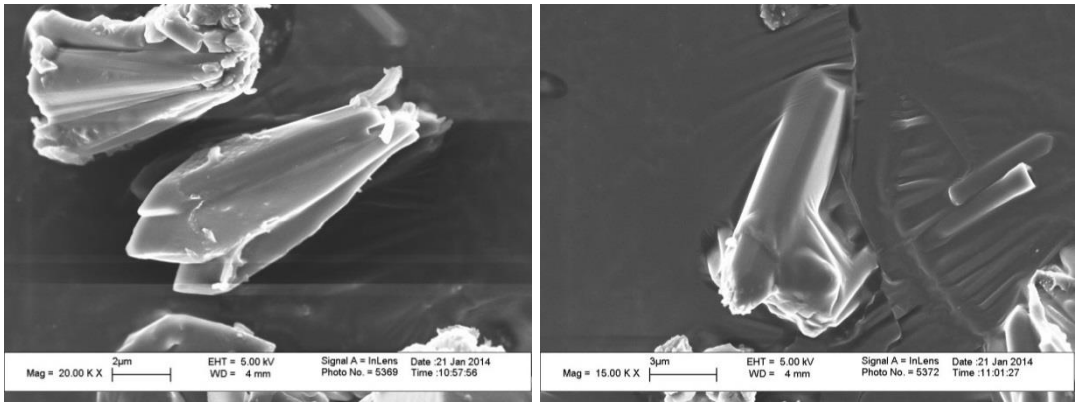

Figure 3.3 SEM micrographs of polymer coated drug particles after precipitation.

3.3.3 TGA Characterization of Polymer Coated Drug Particles

TGA is a precise thermal analysis method to identify percent weight loss of sample as a function of increasing temperature. It can be used in the case of polymer coated drug particles to measure the weight of polymer coating if one can identify the temperature range of weight loss caused by drug decomposition and polymer decomposition since drug particles and polymer will both decompose to cause weight reduction of the TGA thermograms when heating up.

The polymer decomposition range can be identified by the TGA graph of previous experimental results of coating silica particles by polymer. In the case of silica particles coated by the polymer Eudragit RL 100, since the silica (host particles) will not decompose during the heating up process, weight loss is almost completely contributed by polymer decomposition. Figure 3.4 (a) shows that the primary range of polymer decomposition is from 270 to 400 ^{o}C. Figure 3.4 (b) shows the TGA results for the uncoated/coated drug particles by SHFCC method in which the blue curve illustrates the results for the uncoated GF while the red dash curve shows the TGA results for polymer coated GF particles. The decomposition range for the as-received GF is easily determined to be 150 to 270 ^{o}C. Base

on this information, the actual polymer weight loss ($m_{polymer}$) can be estimated to be 13 % (The Y-axis value difference from the range of 270 to 400 ^{o}C) from the dashed curve in Figure 3.4 (b) so that the weight loss of GF particles (m_{drug}) is thus to be 87 %.

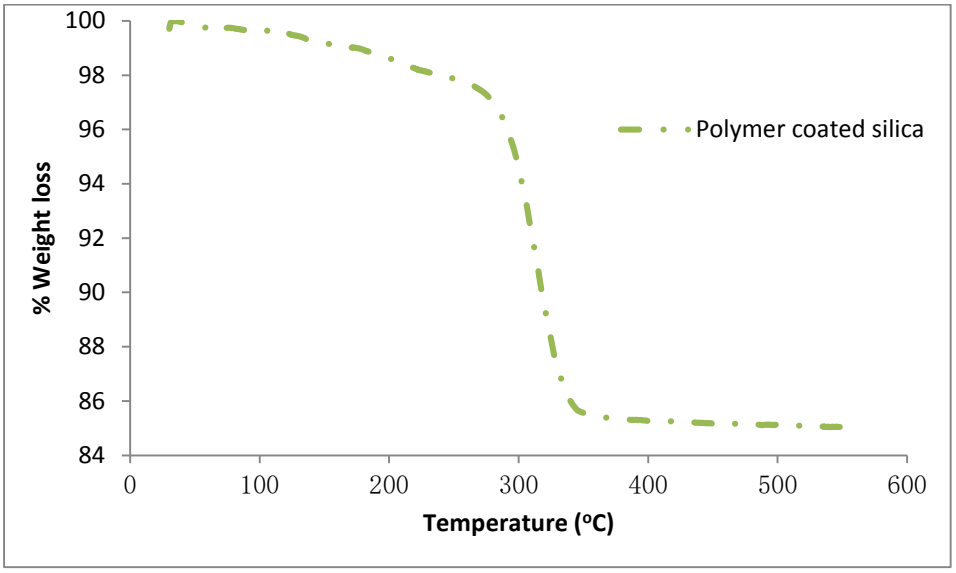

(a)

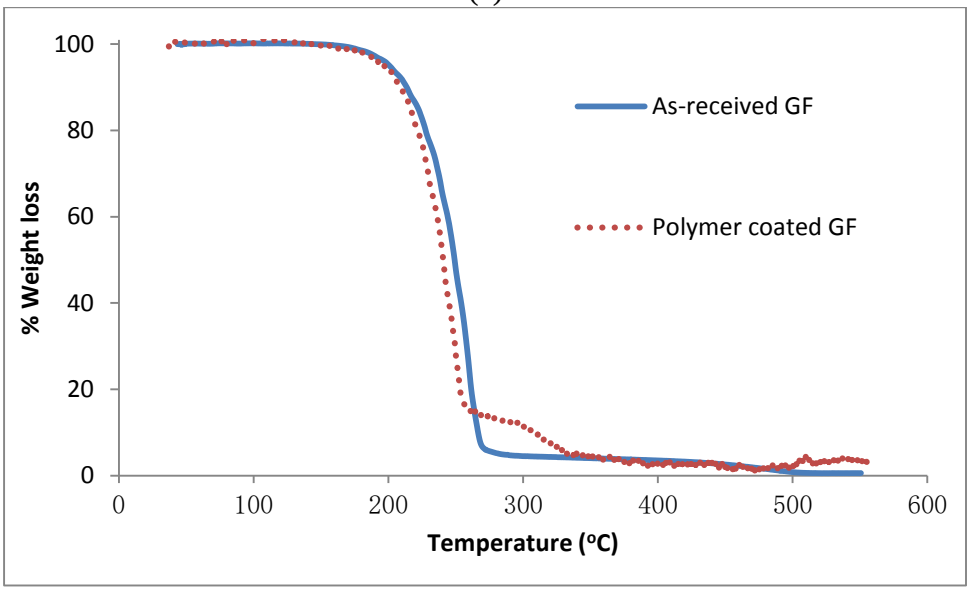

(b)

Figure 3.4 TGA results of (a) polymer coated silica particles; (b) as-received GF and coated GF particles by SHFCC device.

Every drug particle is assumed before coating to be a perfect rectangular parallelepiped with three dimensions of H_{drug}, W_{drug} and L_{drug}; the polymer coating thickness h is covering the entire drug particle. The thickness of the polymer coating on GF particles can be estimated by equation (3.1)

$$\frac{m_{drug}}{m_{polymer}} = \frac{\rho_{drug} H_{drug} \times W_{drug} \times L_{drug}}{\rho_{polymer}[(H_{drug} + 2h) \times (W_{drug} + 2h) \times (L_{drug} + 2h) - H_{drug} \times W_{drug} \times L_{drug}]} \quad (3.1)$$

Here the ratio $m_{drug}/m_{polymer}$ = 87 %/13 %= 6.7 was determined by the weight loss of drug and polymer from Figure 3.4 (b). The densities of the drug particles and polymer are ρ_{drug} (=1.4 g/ml) and $\rho_{polymer}$ (=1.1 g/ml), respectively. The height, width and length can be estimated from Figure 3.2 (b) to be 17 μm, 6 μm and 8 μm, respectively. The polymer coating thickness was estimated to be 0.26 μm by using equation (3.1).

3.3.4 XRD and Raman Spectroscopy

XRD analysis was first performed to identify the crystal structure of the sample. Figure 3.5 (a) shows the XRD results for uncoated and coated GF particles. As can be seen from the graph, there was no alteration in every peak position which implied that the polymer coating of drug particles did not damage the crystal structure of Griseofulvin since the characteristic peaks of the two samples are identical. Figure 3.5 (b) describes the Raman spectra for the uncoated/coated drug crystals at the shift range from 0 to 3500 cm^{-1}.In accordance with the XRD results, the characteristic peaks for both uncoated GF and coated GF particles are all the same. This suggests that coating of the drug particles by the precipitation of the polymer from the solution by SHFCC process did not alter the drug molecular structure; therefore the drug can retain its pharmaceutical effect even after the coating with polymer.

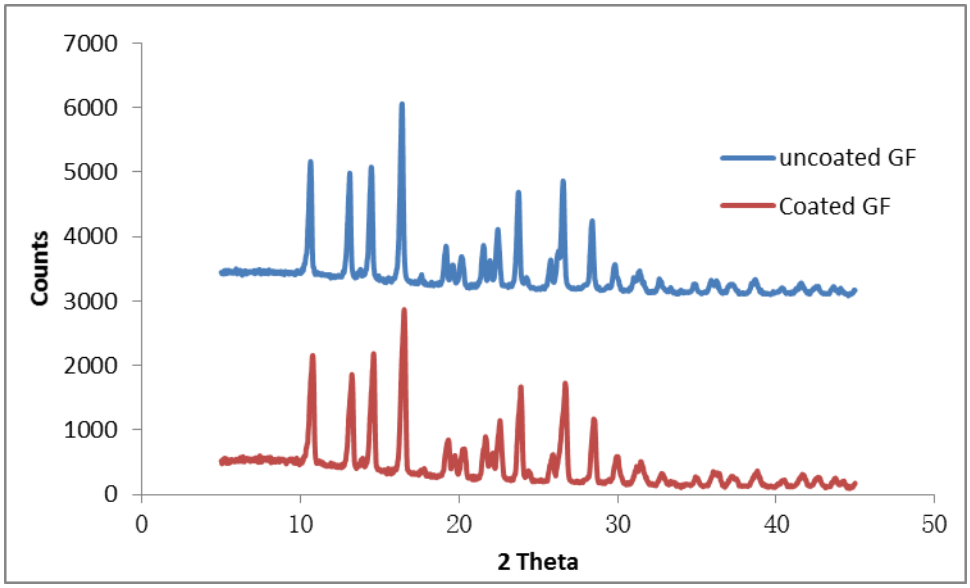

(a)

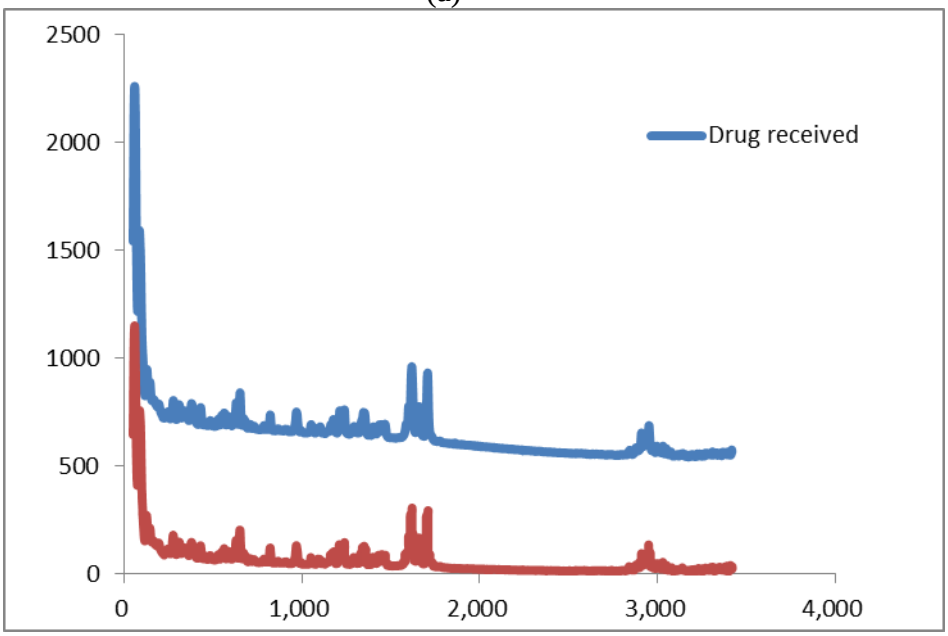

(b)

Figure 3.5 (a) X-ray diffractograms of uncoated GF and coated GF samples; (b). Raman spectra for uncoated GF and coated GF samples.

3.3.5 Differential Scanning Calorimetry (DSC)

Differential scanning calorimetry analysis was performed for the as-received GF and the Eudragit coated GF particles as shown in Figure 3.6. The peak position determined by the Pyris software is 220.20 ^{o}C for the as-received Griseofulvin particles, which is almost

identical to the peak value of 221.37 ºC for the polymer coated GF. The slight intensity difference may be due to the polymer coating covering the entire drug particles that prevent the signal from penetration.

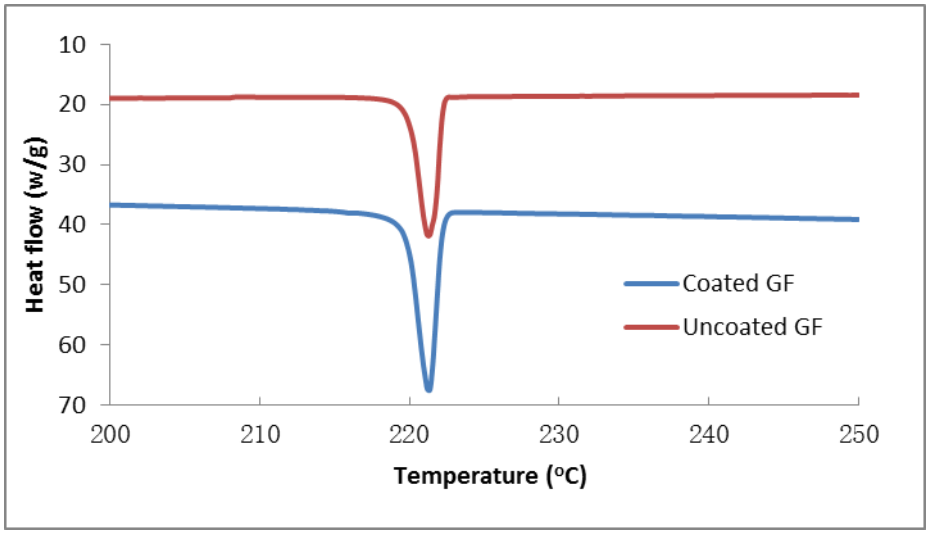

Figure 3.6 Differential scanning calorimetry patterns for uncoated GF and coated GF.

3.3.6 Dissolution Testing Study

To identify the effect of controlled release of drug when GF was coated by the polymer using solid hollow fiber membrane-based cooling crystallization method, the dissolution study of the as-received drug, uncoated drug and the polymer coated drug were carried out. The dissolution test results are shown in Figure 3.7. The dissolution profiles for as-received GF and uncoated GF are very similar which indicated that even when the GF particles was re-precipitated from the solution by SHFCC device with different crystal shapes, it did not prevent or change the estimate of the time for the drug to be 100 % dissolved in the buffer solution. The dissolution profile of the coated GF particles (green curve) is completely different from the others; the coated GF crystals only dissolved about 18% even after 80

min which implied that the polymer coating was acting as a barrier to prevent the drug component from dissolving in the solution.

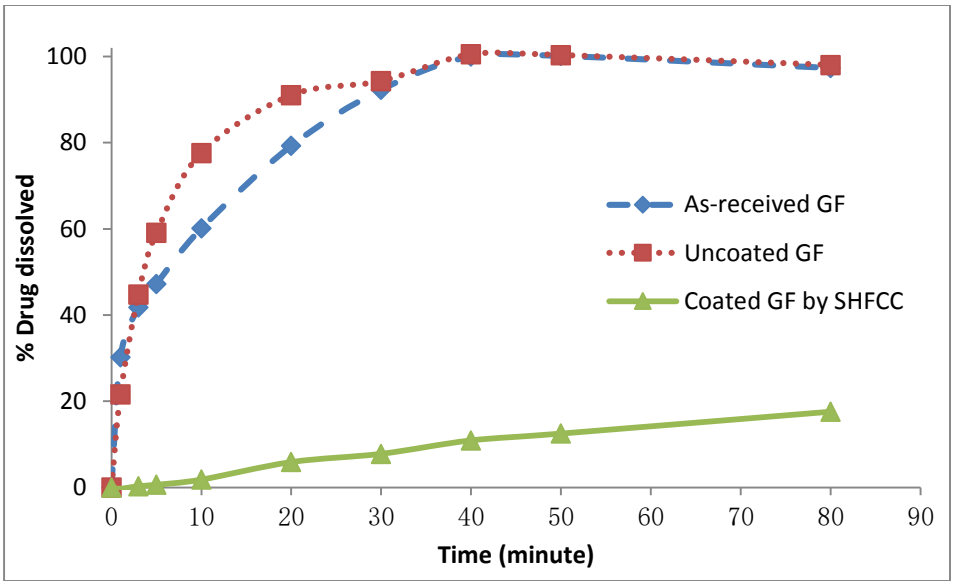

Figure 3.7 Dissolution profiles for crystals of as-received GF, uncoated GF, and polymer coated GF, the latter two obtained by the SHFCC technique.

3.3.7 Crystal Size Distribution Measurement

The crystal size distributions (CSD) of the as-received uncoated drug particles as well as Eudragit RL 100 coated Griseofulvin drug particles collected from the SHFCC process were measured by LS 230 laser diffraction analyzer to compare of the level of agglomeration before and after coating. Figure 3.8 illustrates the CSD profiles of the uncoated and coated drug crystals in which the median size of the as-received GF (11.6 μm) was about 3 times smaller than that of the polymer encapsulated GF (31.19 μm). One possible reason is due to the high level of polymer connectivity over the coated GF crystals that led to a certain amount of agglomeration since the precipitated polymer will form bridges attaching the neighboring drug particles.

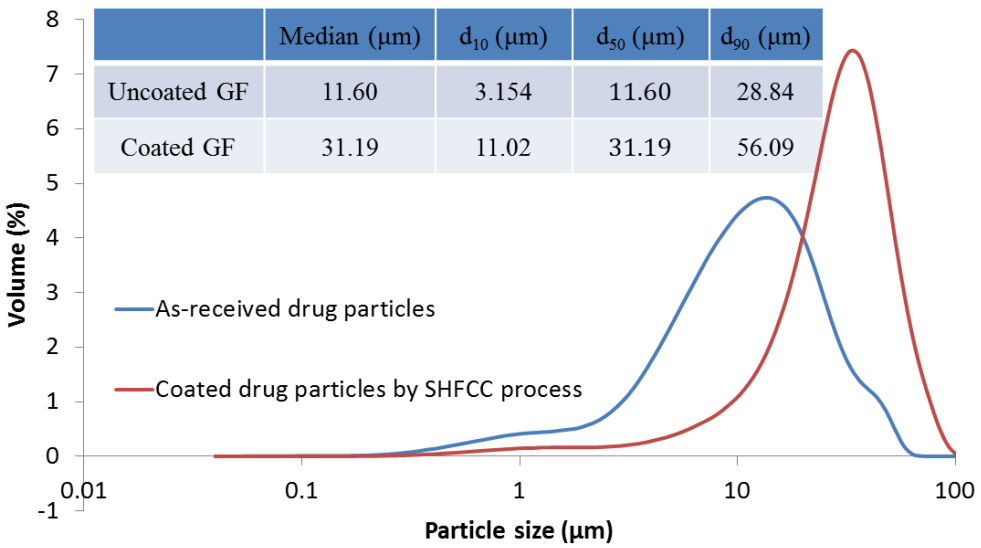

Figure 3.8 Crystal size distribution of as-received and coated Griseofulvin drug particles.

A novel approach for continuous synthesis of polymer coated of Griseofulvin drug particles has been developed by using the solid hollow fiber cooling crystallizer. Following the previous determination of the cloud point for Eudragit RL 100/acetone/water solution by an UV spectrophotometer, the cloud point temperature of the ternary system was set to be 15 ^{o}C. Drug particles were evenly coated by the polymer precipitated from the acetone solution inside of the SHFCC module. Further tests using XRD, Raman and DSC indicated that the polymer coating covering the drug particles will not influence the pharmaceutical effects of the drug. The dissolution test results suggest that the coated drug demonstrated a controlled release potential for drug delivery system since the coated drug has a much slower dissolution rate with time compared to the uncoated drug.

This novel method for coating of drug particles should be attractive for the pharmaceutical industry especially in the area of drug delivery. The relatively simple set up and the modest requirements for experimental conditions provide an economic advantage compared to other coating techniques. The continuous process of coating should

be contrasted with most of coating techniques also suggests a possibility of mass production. Next chapter will introduce another novel coating technique – PHFAC, to coat the host particles such as silica and drug particles by polymer.

CHAPTER 4

CONTINUOUS POLYMER COATING/ ENCAPSULATION OF SUBMICRON AND NANOPARTICLES USING A POROUS HOLLOW FIBER ANTI-SOLVENT CRYSTALLIZATION METHOD

4.1. Introduction

Conventional crystallization/precipitation processes for coating particles with a polymer from its solutions rely on either cooling or solvent evaporation or anti-solvent methods or chemical reactions. Of these methods, anti-solvent techniques continue to be of considerable interest. Even though impinging-jet mixers are being utilized to this end in preference to standard crystallization devices, they are plagued by many shortcomings. Another novel technique is proposed here for continuous polymer coating of crystals/particles by adapting the porous hollow fiber anti-solvent crystallization (PHFAC) technique besides the SHFCC process which was already introduced in Chapter 2. This technique is facile and easily scalable and can be used for a variety of polymers and solvents. How submicron (550 nm) and nanoparticles (12 nm) of silica can be coated continuously with thin layers of the polymers Eudragit RL 100 and PLGA is illustrated here.

4.1.1 Porous Hollow Fiber Anti-solvent Crystallizer/Precipitator

Two potential configurations of a single porous hollow fiber anti-solvent crystallizer (PHFAC) are shown in Figure 4.1. The porous hydrophilic hollow fiber was made of the polymer Nylon 6; it has an excellent resistance to pH and a variety of organic solvents. This fiber has an inner diameter (ID) of 600 μm and an outer diameter (OD) of 1000 μm. The hollow fiber wall porosity is 0.75; the pore size ranges from 0.2 to 1.5 μm with only a

few pores having the largest size. Anti-solvent crystallization using the hollow fiber-base membrane may be carried out in two ways shown in Figures 4.1 (a) and 4.1 (b). In both of these configurations, the anti-solvent is made to permeate through the pores. Alternate configurations wherein the feed suspension is made to permeate through the pores are not possible for the particular hollow fiber selected since in the case of submicron particles the diameter of the host silica particles used (0.55 μm) is larger than most of the pores. Some agglomeration of the silica particles can occur in the feed suspension leading to clogging of the pore mouths.

Figure 4.1 (a) illustrates the scheme wherein polymer crystallization/precipitation takes place in the tube side. The anti-solvent permeates through the pores from the shell side into the tube side while the feed polymer solution-suspension of silica particles flows in the tube side. Injection of the anti-solvent through numerous pores generates intense mixing between the two liquids leading to precipitation of the polymer and covering of the host silica particles present in the feed solution-suspension in the tube side.

Figure 4.1 (b) illustrates a reversed configuration. The feed solution-suspension was pumped through the shell side; the anti-solvent was pumped through the tube side such that it permeated into the shell side as numerous jets streaming into the polymer solution-suspension. This led to rapid precipitation/crystallization of the polymer in the shell side and coating of the silica particles in the suspension. This particular configuration is preferred over that shown in Figure 4.1 (a). Due to the larger cross-sectional area in the shell side, silica particles are more easily swept away compared to that in the tube side crystallization/precipitation since the internal diameter of a single hollow fiber is less than

the average inter-fiber spacing on the shell side. All experiments were done using the configuration shown in Figure 4.1 (b).

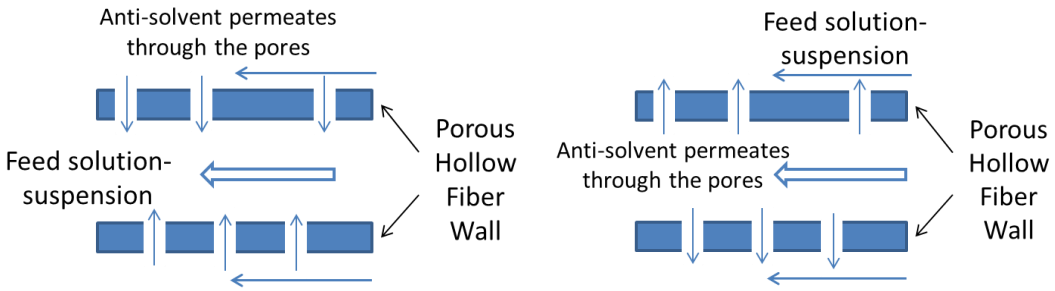

Figure 4.1 Porous hollow fiber anti-solvent crystallization (PHFAC) -- operating approach for the permeation of anti-solvent through the pores: (a) crystallization in the tube side; (b) crystallization in the shell side.

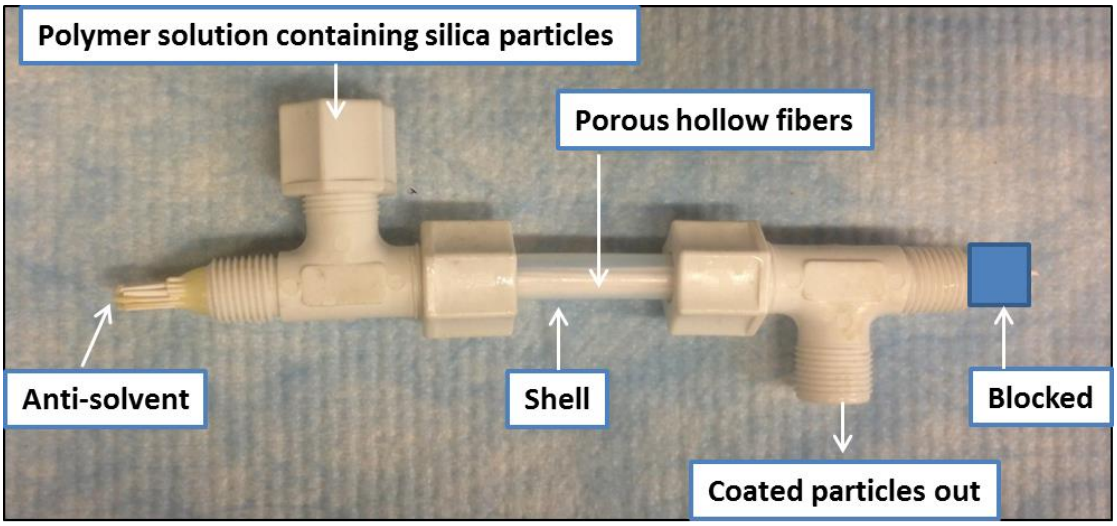

Figure 4.2 Schematic of porous hollow fiber anti-solvent crystallizer (PHFAC).

Figure 4.2 is the photo of a typical porous hollow fiber-based anti-solvent crystallizer (PHFAC). It contains 23 porous nylon hollow fibers inside the shell made of fluorinated ethylene propylene (FEP). The shell internal diameter is 8 mm and the effective length is 8 cm. The two ends of the hollow fibers at the end of the shell side tube were potted within polypropylene male run tees (Cole-Parmer, Vernon Hills, IL) using an epoxy

resin (C4 and D, Armstrong, Easton, MA). As shown in Figure 4.2, water, the anti-solvent, was passed through the lumen of the hollow fibers in the tube side while the polymer solution containing a suspension of silica particles was pumped in the shell side of the module co-currently.

4.2. Materials and Methods

4.2.1 Materials

The host submicron silica particles, Cosmo 55 (550 nm nonporous hydrophilic spherical particles), were obtained from Presperse (Somerset, NJ). Silica nanoparticles used were Aerosil 200 (non-porous hydrophilic fumed silica with a diameter of 12 nm) (Evonik-Degussa, Parsippany. NJ). Coating polymers were: Eudragit RL 100 (M_w, 150,000; a copolymer of methyl methacrylate, ethyl acrylate and methacrylic acid ester) from Evonik-Degussa (Parsippany, NJ); PLGA (Poly (D, L-lactide-co-glycolide), M_w, 7,000-17,000) from Sigma-Aldrich (St. Louis, MO). Acetone, a good solvent for Eudragit RL 100, dioxane, a good solvent for PLGA, and the surfactant sodium dodecyl sulfate (SDS) were obtained also from Sigma-Aldrich. Deionized water was used as the anti-solvent.

4.2.2 Experimental Methods

Feed solution-suspension was prepared in a flask by first introducing 2.4 g of Eudragit RL 100 (or PLGA) in 20 ml acetone (or dioxane) solution. After about 30 min when the polymer was fully dissolved, 4 ml of water was added in the solution to slightly decrease the solubility of the polymer. This was done to make the polymer solution more sensitive to the anti-solvent as will be seen later. Next 0.4 g of Cosmo 55 silica particles was added along with 0.025 g of SDS. The flask was placed under a magnetic stirrer and kept stirred

during the experiment.

Figure 4.3 illustrates the process schematic used for the PHFAC-based coating of the silica particles. A peristaltic pump (Masterflex L/S model 7518-60, Cole-Parmer, Vernon Hills, IL) was used first to pass DI water to the tube side of the module. Since the other end of the module tube-side was blocked by a valve, tube side pressure increased from 0 to 15 psig so that the water permeated through the pores in the hollow fiber wall to the shell side. The feed solution-suspension was introduced into the shell side of the PHFAC unit by another identical pump after 2 min.

The order of pumping the liquids should not be reversed. If the feed solution is first passed to the shell side, then part of this solution would have permeated to the lumen side; that would have led to subsequent mixing of the anti-solvent with the polymer solution and the precipitated polymer would have stayed in the tube and eventually would have led to clogging of the tube side. The reading on the pressure gauge 2 (Figure 4.3) was close to zero psig since the volume of the shell side is relatively large offering the solution almost no resistance to pass through. Innumerable water streams from the pores were injected into the feed polymer solution-suspension in the shell side generating strong mixing of the solutions. The solubility of the polymer drastically deceased because of the introduction of the anti-solvent so that polymer precipitated and covered the silica host particles. The coated product along with the excess polymer solution and water were continuously pumped out through the shell side outlet. A microfiltration device was placed under the outlet to collect the particles on a filter paper (Omnipore Membrane JHWP09025, PTFE, hydrophilic, 0.45 μm, 90 mm; Millipore, Billerica, MA). The coated silica particles were recovered from the filter paper and vacuum dried to make them ready for characterization.

The flow rate on the hollow fiber lumen side was kept at 11 ml/min and the shell side flow rate was maintained at 6 ml/min. It is important to maintain a reasonable flow rate in the shell side. First, a polymer such as PLGA is highly sensitive to the anti-solvent; the presence of just a little anti-solvent in the shell side will lead to extensive precipitation of the PLGA. Unless the shell-side flow rate is high enough to flush out the precipitates once they are formed, the precipitates can block the shell side. Secondly, the shell side flow rate is related to the pressure in the tube side. The shell side flow rate has to be held at a certain level to increase the pressure difference between the tube side and the shell side so that the anti-solvent water can successfully permeate from the tube side to the shell side and achieve intense mixing with the feed solution-suspension. One can generate a high super-saturation level if a high water flow rate is created so that a maximum amount of the polymer can be crystallized out without any waste.

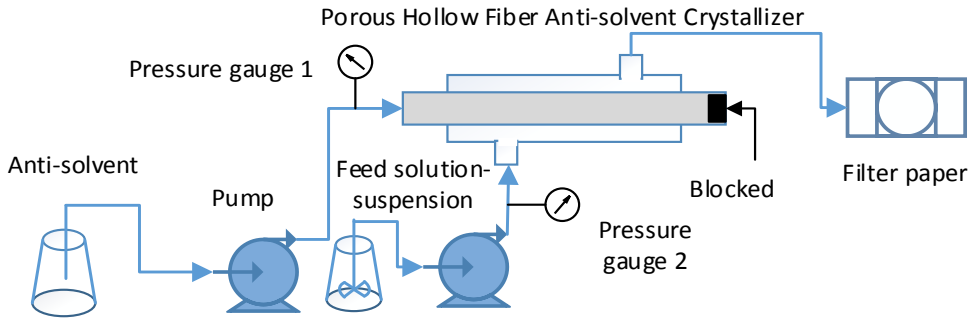

Figure 4.3 Experimental setup for continuous polymer coating of silica particles in a porous hollow fiber anti-solvent crystallization (PHFAC) device.

4.3. Results and Discussion

4.3.1 Coating of Submicron Silica Particles with Eudragit RL 100

Submicron silica particles (Cosmo 55, 550 μm) were first coated with the polymer Eudragit RL 100. The polymer was precipitated in the PHFAC module due to the rapid solubility reduction when DI water was introduced from the tube side thus coating the silica host particles. Eudragit RL 100 is not as sensitive to the anti-solvent water compared to PLGA. Even when a considerable amount of water was quickly introduced into a solution of Eudragit, limited precipitation happened; the color of the solution changed from clear to slightly cloudy per visual inspection. Therefore, a high concentration of polymer (10 wt%) as well as a high water permeation rate from the tube side has to be maintained to ensure sufficient polymer precipitation on the silica particles.

It appears that the quantity of the host silica particles plays an important role in determining the coating thickness since the polymer concentration of the solution was fixed. Other conditions remaining fixed, the magnitude of the residence time of the feed solution-suspension in the shell side essentially determines the amount of the polymer that will precipitate. Therefore, the higher the number of host particles present in the solution, the lower will be the amount of polymer that will precipitate on each silica particle and coat it. To that end, three identical Eudragit solutions were prepared containing exactly the same amount of water, acetone, polymer and SDS; the only difference between these solution-suspensions was the amount of silica added (0.2 g, 0.4 g and 0.8 g).

Thermogravimetric analysis (TGA) was used to analyze the weight loss of the polymer coated silica particles. The polymer coating that covered the silica particles started decomposing gradually during heating resulting in a weight loss of the sample. Figure 4.4

illustrates the TGA results for coated Cosmo 55 particles for three different amounts of silica in the feed solution-suspension and the uncoated Cosmo 55 particles as received. The as received silica sample lost less than 1% of its weight after heating (the solid line in Figure 4.4). This suggests that the weight loss of the coated silica samples was essentially due to polymer loss. According to the TGA results, the % weight loss decreased when more silica was added to the solution implying a thinner coating on the silica particles. The % weight losses for the cases of 0.4 g silica and 0.2 g silica addition are relatively close implying that the amount of polymer that can be deposited on the silica particles has an upper limit. Most of the experiments were therefore run with 0.4 g as the mass of silica. A lesser amount of silica addition will lead to a somewhat thicker coating and potentially increase the agglomeration of the polymer coated particles. Too many silica particles may lead to a thinner and defective coating.

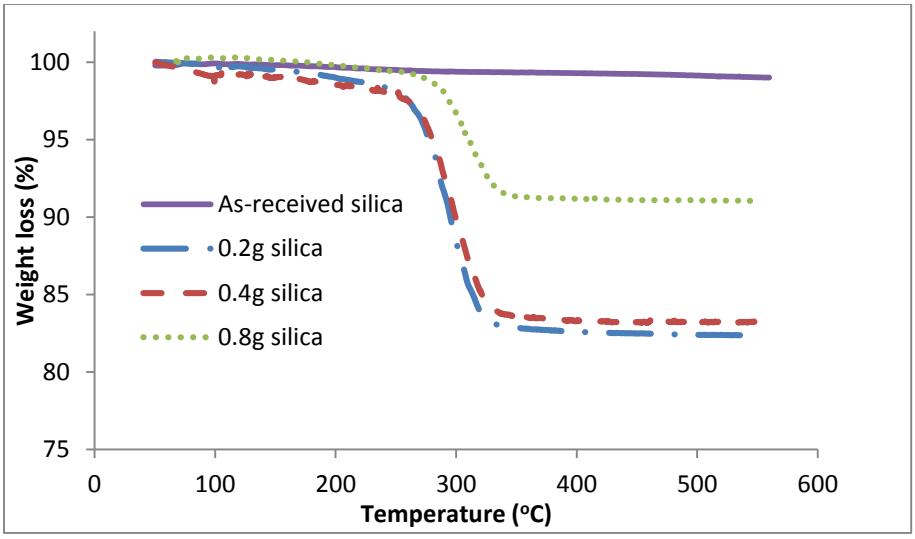

Figure 4.4 TGA micrographs of the as-received silica (Cosmo 55) as well as Eudragit RL 100 coated silica particles under different feed conditions.

Since the as-received Cosmo 55 particles are almost perfectly spherical with a very narrow particle size distribution, one can assume that these silica particles are spheres of diameter 2r. The relationship between the mass of silica and the polymer mass has been expressed in Equation (2.1). The polymer coating thickness h can then be calculated from this equation to be 36.9 nm.

4.3.2 Characterization by Scanning Electron Microscopy

After about 20 min of operation, a sample was obtained on the filter paper for characterization. SEM was used to detect the actual surface coating topography and composition of the polymer coated Cosmo 55 particles. Figure 4.5 shows the SEM micrographs of coated and uncoated dry silica particles. Compared to Figure 4.5 (a), Figure 4.5 (b) clearly shows that the polymer was coated on every silica sphere due to heterogeneous nucleation. Limited amounts of polymer bridges between neighboring silica particles suggest soft bonding or agglomeration between particles, which can be separated by the external forces experienced in an ultrasonicator to obtain free-flowing coated particles.

Surface elemental analysis by EDS can provide additional information of the composition of the coating on the silica particles. The EDS results of the uncoated and the coated Cosmo 55 samples are shown in Figures 4.6 (a) and 4.6 (b), respectively. No carbon peak appears in Figure 4.6 (a) suggesting that there was no carbon element on the as-received silica particles. On the contrary, a clear carbon peak shown in Figure 4.6 (b) indicates that Eudragit RL100 polymer successfully coated the Cosmo 55 silica particles since only the polymer contains the element carbon. The EDS results are in accordance with the SEM results.

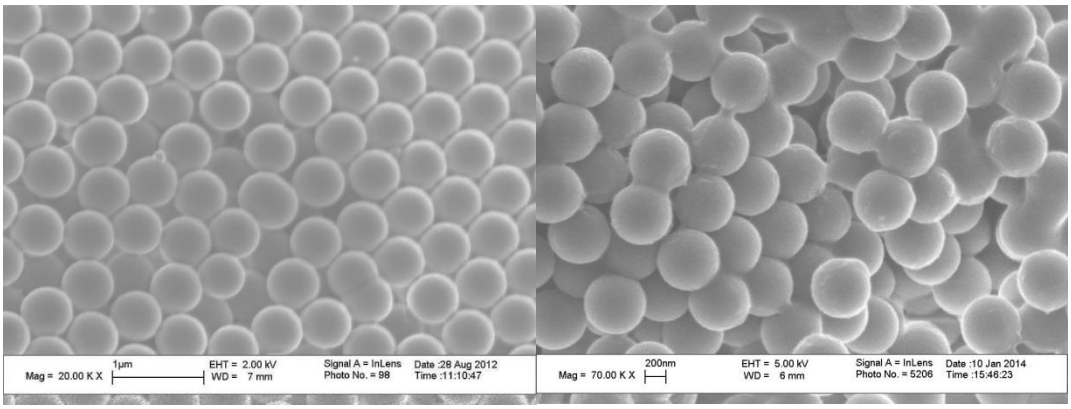

(a) (b)

Figure 4.5 SEM micrographs of (a) uncoated and (b) Eudragit coated silica (Cosmo 55) under different magnifications.

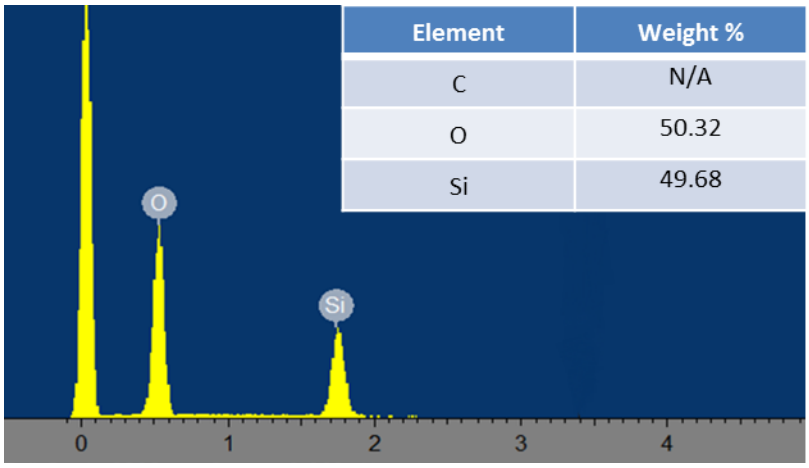

Element	Weight %
C	N/A
O	50.32
Si	49.68

(a)

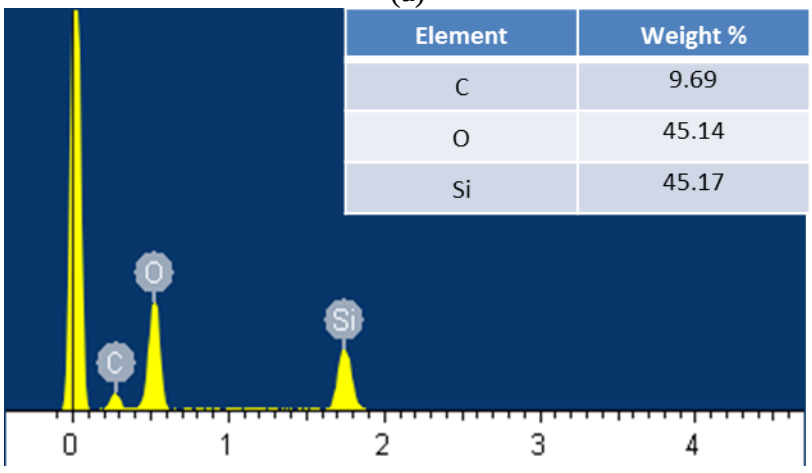

Element	Weight %
C	9.69
O	45.14
Si	45.17

(b)

Figure 4.6 EDS results of (a) uncoated and (b) Eudragit RL 100 coated submicron silica particles (Cosmo 55).

4.3.3 Characterization by Scanning Transmission Electron Microscopy

Scanning transmission electron microscopy is another tool that can be used to determine the coating thickness of the polymer around the silica particles. Compared to SEM, it can display the coating morphology more precisely. The micrograph in Figure 4.7 (a) shows parts of two uncoated silica particles while that in Figure 4.7 (b) shows sections of two Eudragit coated silica particles. The two dark partial spheres in Figure 4.7 (b) represent two silica particles: the polymer coating covering the particles is shown in grey. The two silica particles in Figure 4.7 (b) are seen to be interconnected by a polymer bridge; a thin polymer coating is seen around the periphery of the particles. Based on the scale bar in the micrograph, the thickness of the coating on a single submicron silica particle is estimated to be between 10 nm and 20 nm.

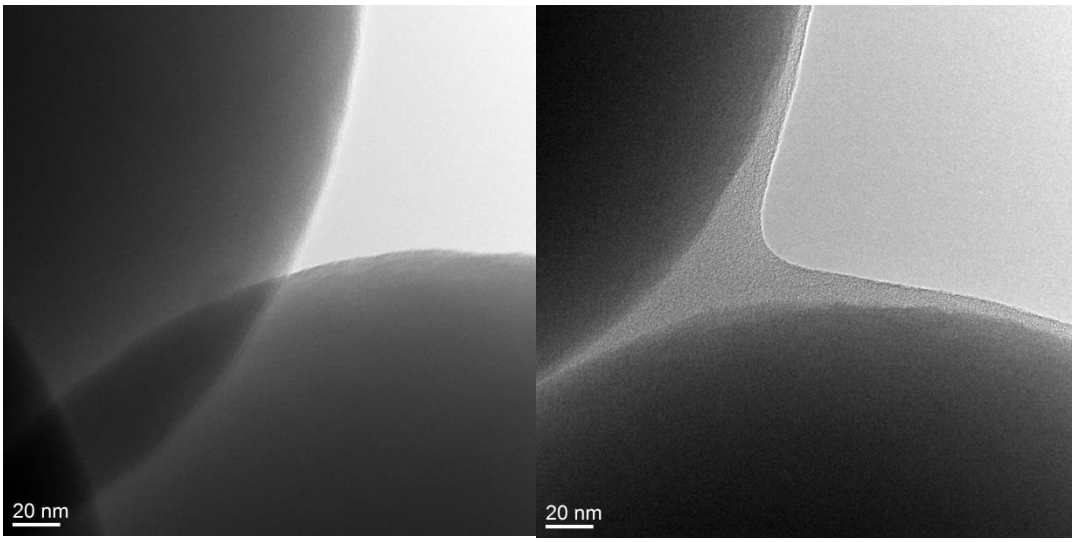

(a) (b)

Figure 4.7 STEM micrographs of (a) uncoated silica particles and (b) polymer coated silica particles after PHFAC process (0.4 g silica, 2.4 g Eudragit RL, 20 ml acetone and 4 ml water).

4.3.4 Coating of Cosmo 55 Silica Particles with PLGA

PLGA is frequently used as a coating material in the pharmaceutical industry since it is a biodegradable and biocompatible copolymer approved by FDA. Compared to a solution of Eudragit RL 100 in acetone, a solution of PLGA in dioxane is much more sensitive to the addition of an anti-solvent such as water into the polymer solution than a solution of Eudragit RL 100 in acetone. High levels of precipitation will take place in the shell side if 10 wt% PLGA was added into solution. The PLGA concentration level can be a determining factor in the coating of submicron particles. Solutions having different concentrations of PLGA were therefore prepared to explore how the amount of PLGA will affect the coating since PLGA is much more sensitive to the anti-solvent compared with Eudragit RL 100.

Figure 4.8 illustrates the results from TGA of the as received (uncoated) silica particles and PLGA-coated silica particles. As the solution PLGA concentration was increased, the amount of the precipitated polymer increased drastically, indicating that the extent of supersaturation of PLGA increased with the anti-solvent addition very rapidly and the precipitation kinetics was very fast. From the results of TGA, the percentage weight loss of the polymer were estimated to be 90%, 60% and 37% corresponding to PLGA concentrations in the solutions of 10%, 7.5% and 2.5% respectively. These extraordinarily high amounts of precipitation demonstrate the sensitivity of the dioxane solutions of PLGA used in this study to the addition of the anti-solvent water. Unlike coating with Eudragit RL 100, when the PLGA solution was mixed with the anti-solvent jet streams in the PHFAC module, PLGA was fully precipitated out from the solution.

Figures 4.9 (a) and 4.9 (b) show the SEM micrographs for polymer-coated silica particles from 10% and 2.5% PLGA solutions respectively. In Figure 4.9 (a), silica particles appear to be immersed in a huge amount of PLGA precipitate. However, for 2.5% PLGA solution, Figure 4.9 (b) shows that the silica particles had a thick coating and were somewhat inter-connected but not embedded in the polymer matrix. This suggests that reduction of the solution concentration of PLGA can effectively decrease the coating thickness as well as the extent of agglomeration. Calculations using equation (2.1) suggest the thickness of the coating for 2.5 wt% PLGA solution to be 94 nm. Since there were some polymer bridges between the particles, the real coating thickness along the particle periphery should be less than 94 nm.

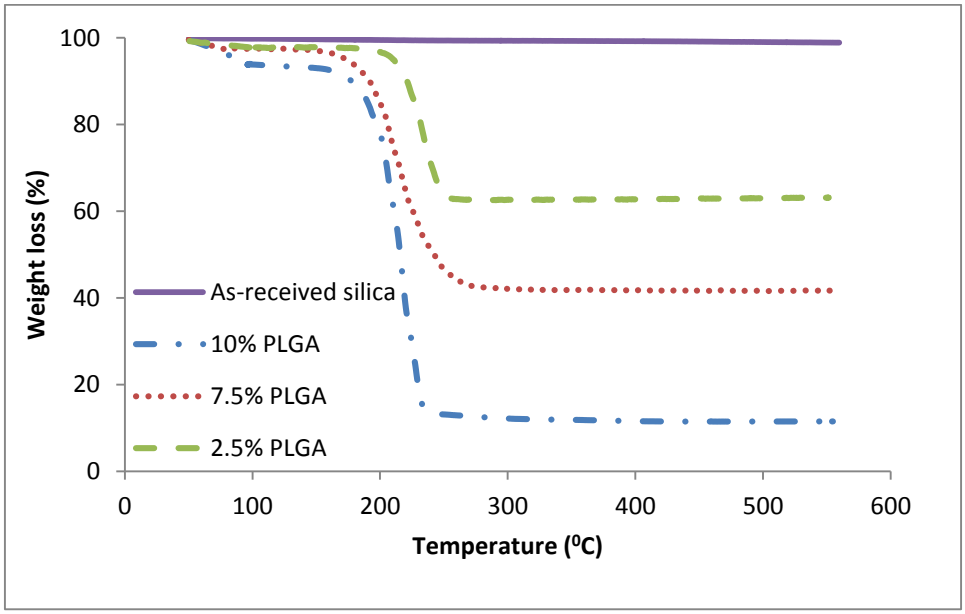

Figure 4.8 TGA micrographs of the as-received silica (Cosmo 55) as well as PLGA coated silica particles (0.4 g silica, 20 ml dioxane and 4 ml water) for different feed solution concentrations of PLGA.

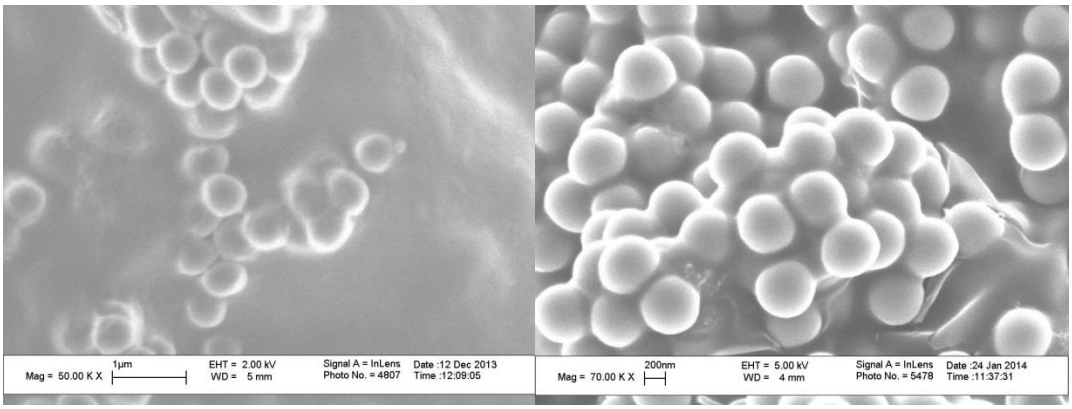

(a) (b)

Figure 4.9 SEM micrographs of PLGA coated particles from solutions containing two different levels of PLGA: (a) 10 wt% (b) 2.5 wt%.

Could one reduce the solution concentration of PLGA further to reduce the amount of bridging and the coating thickness? Figure 4.10 illustrates SEM micrographs of uncoated silica and PLGA-coated silica for the case of a 1% PLGA solution. There is very little difference between the two micrographs at the level of magnification used. Compared with the as-received Cosmo 55, the coating in Figure 4.10(b) appears to be quite limited. The small amount of precipitation of PLGA was not enough to cover the particles; instead small amounts of polymer appear to be attached to the surface of some of the silica particles or lie in between particles. It appears that PLGA concentration cannot be reduced too much since it may result in an imperfect coating.

Therefore, the 2.5 wt% solution of PLGA was selected for further anti-solvent crystallization/precipitation experiments and characterization. The EDS results of uncoated silica as well as 2.5 wt% PLGA solution-based coated silica particles are shown in Figure 4.11. Compared to Figure 4.11 (a), the carbon peak in Figure 4.11(b) demonstrates the existence of PLGA coating on the silica particles.

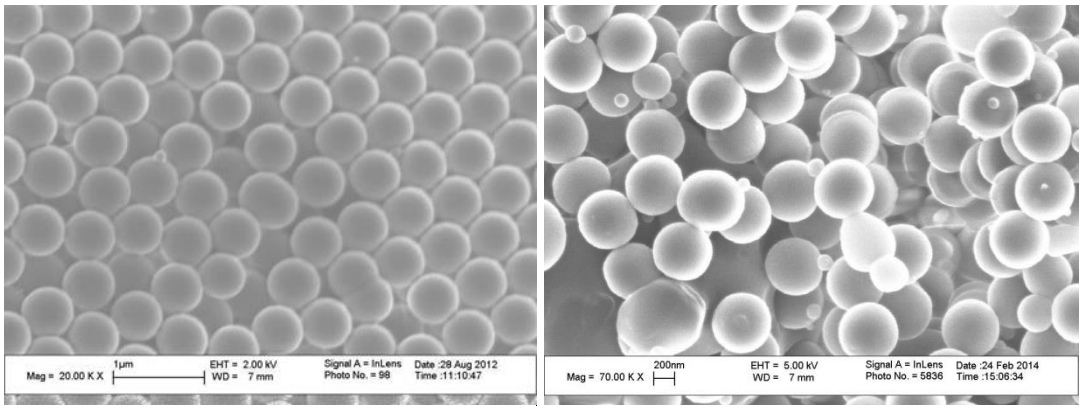

(a) (b)

Figure 4.10 SEM micrographs of uncoated and PLGA coated particles: (a) uncoated (b) 1 wt% PLGA coated.

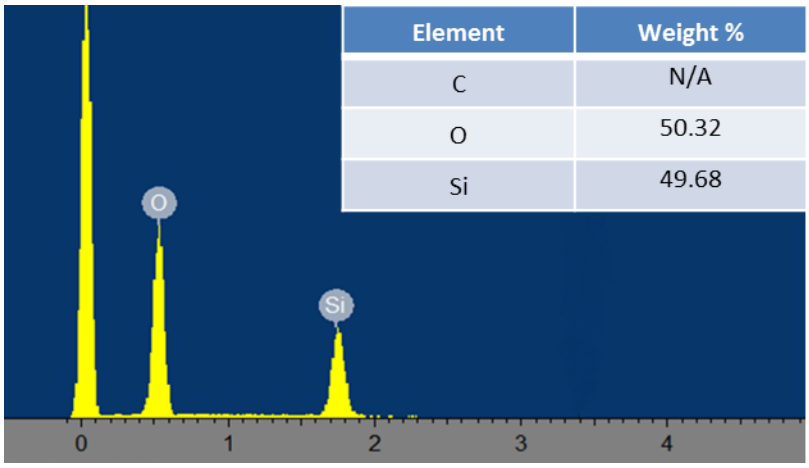

Element	Weight %
C	N/A
O	50.32
Si	49.68

(a)

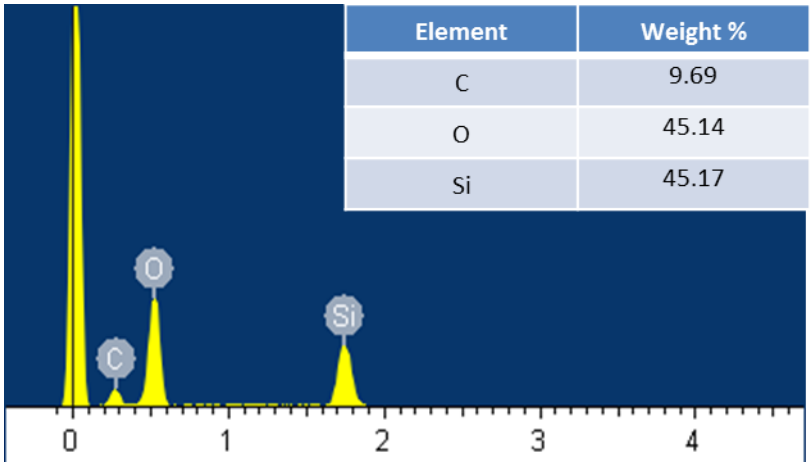

Element	Weight %
C	9.69
O	45.14
Si	45.17

(b)

Figure 4.11 EDS results of (a) uncoated and (b) PLGA coated Cosmo 55 submicron particles.

4.3.5 Particle Size Distribution

The particle size distributions of the Cosmo 55 silica particles coated by Eudragit RL 100 or PLGA as well as the as-received silica particles were analyzed by laser diffraction to quantify the level of agglomeration of the particles after coating. Figure 4.12 shows the results for the particle size distributions of the as-received silica, Eudragit-coated silica and PLGA-coated silica. As expected, the mean size of Eudragit-coated silica was smaller than that of the PLGA coated silica as shown in Table 4.1 and Figure 4.12. It is clear that the high level of particle connectivity witnessed in PLGA precipitation led to a greater agglomeration of the coated particles.

Table 4.1 Specifications of PSD Results for the As-received Silica, Eudragit Coated Silica and PLGA Coated Silica Particles for Cosmo 55

	Mean size (μm)	d_{10} (μm)	d_{90} (μm)
As received silica	0.595	0.266	0.969
Eudragit coated silica	1.398	0.704	2.324
PLGA coated silica	1.810	1.451	2.215

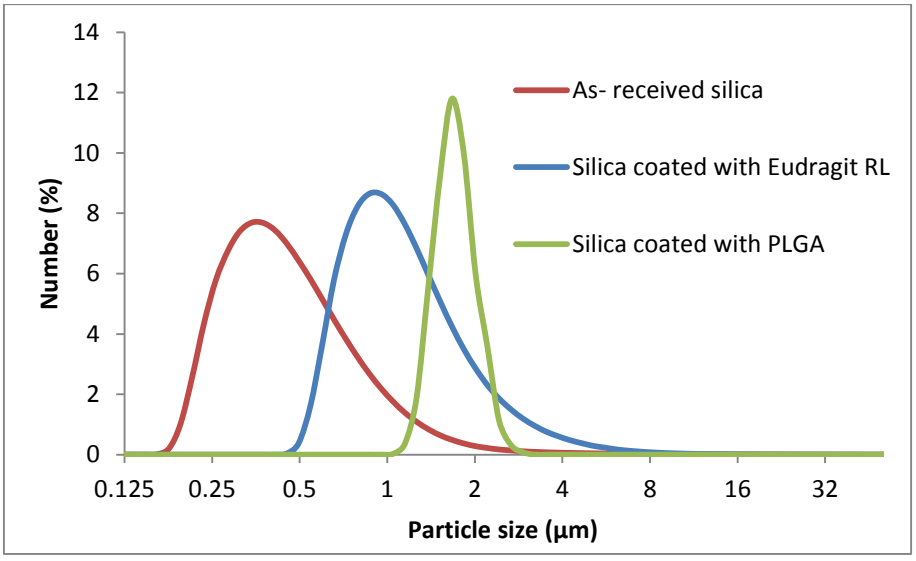

Figure 4.12 Particle size distributions of as-received silica, Eudragit and PLGA coated silica particles (Cosmo 55).

4.3.6 Comparisons of Two Different Polymer Coatings on Submicron-size Silica Particles

Both the polymers, Eudragit RL 100 and PLGA, were used to successfully coat the host silica particles. Each polymer has its own advantages as a coating material for the PHFAC process. Eudragit RL 100 produces somewhat more uniform coating and lesser amount of polymer bridging between neighboring silica particles; the coating thickness can be adjusted by controlling the amount of added silica in suspension for a given residence time. The coating formed by Eudragit is also thinner than that of PLGA. Agglomeration was also reduced considerably because of the smaller amount of polymer precipitation. On the other hand, PLGA is a widely used coating material especially in the field of drug delivery for controlled release. Due to the high sensitivity of the dioxane solutions of PLGA to the anti-solvent used, the coating thickness can also be adjusted simply by changing the concentration of PLGA in solution. From the results of Figure 4.4 with Eudragit, one may expect that the amount of silica particles added to a solution can also influence the coating thickness.

4.3.7 Continuous Polymer Coating of Nanoparticles by PHFAC

Coating of silica nanoparticles (Aerosil 200) by Eudragit RL 100 has also been studied using the novel PHFAC method but not as extensively as the coating of the submicron silica particles. The preliminary results are illustrated here to demonstrate that silica nanoparticles can be coated with the Eudragit RL 100 polymer as well. Figure 4.13 (a) shows a SEM micrograph of the coated silica nanoparticles. The micrograph shows that the silica particles were covered by the precipitated polymer although there was a significant level of agglomeration among the coated particles. One reason for the agglomeration is that the silica particle size is so small (12 nm) that they have a strong

tendency to stick to each other due to the strong van der Waals forces between the nanoparticles. Another reason is that the precipitated sticky polymer not only covers the particles but also connects the particles by forming polymer bridges between the particles. This type of agglomeration may be minimized by adding increased amounts of surfactants and applying sonication to break the soft bonding of the coated nanoparticles. Figure 4.13 (b) shows EDS results for the coated nanoparticles in which the carbon profile demonstrates that the nanoparticle was coated by the polymer since silica particles contains no carbon.

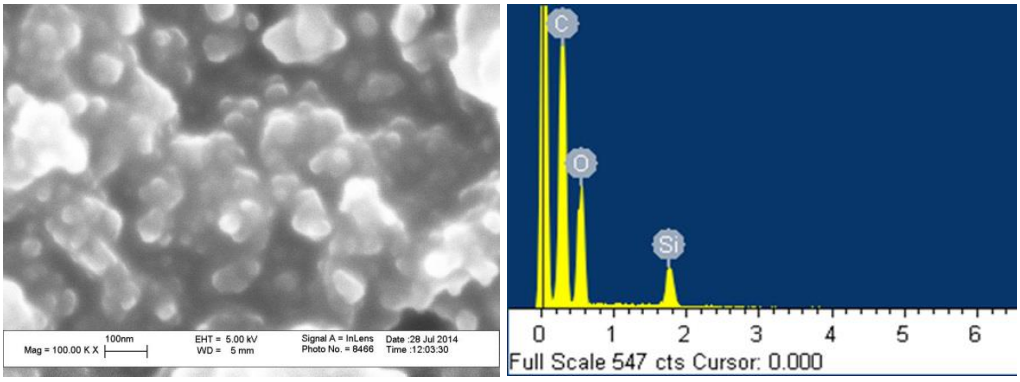

(a) (b)

Figure 4.13 (a) SEM micrograph and (b) EDS results of polymer coated silica nanoparticles using the PHFAC process.

For the silica nanoparticles, TGA results are shown in Figure 4.14. The dashed blue line represents the weight loss profile of the as-received silica nanoparticles as the temperature was increased to 550 ^{o}C. As expected, there was negligible weight loss since silica nanoparticles do not decompose during the heating. However, the polymer-coated silica nanoparticles shown by the red curve lost about 70% of the weight since the polymer decomposed during the heating. The coating thickness on the nanoparticles can be estimated using equation (2.1) to be around 5 nm.

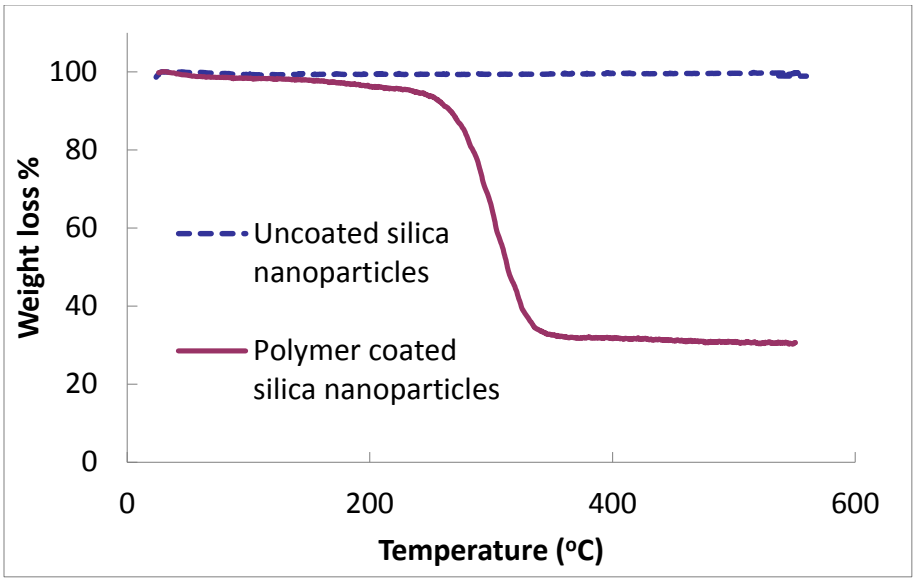

Figure 4.14 TGA micrographs of as-received silica as well as Eudragit RL coated silica nanoparticles (Aerosil 200).

The technique of porous hollow fiber anti-solvent crystallization (PHFAC) was successfully adapted to continuously coat submicron (550 nm) and nanoparticles (12 nm) of silica with a polymer. After vacuum drying and sonication, free-flowing polymer-coated silica particles were obtained by this continuous process. By varying a number of conditions such as the silica loading in the solution-suspension and the solution concentration of the polymer, one can adjust the polymer coating thickness over certain ranges. Both the polymers, Eudragit RL 100 and PLGA, were successfully used to coat the silica particles using this novel method. Chapter 5 will focus on the continuous synthesis of polymer coated drug crystals by the PHFAC method.

CHAPTER 5

CONTINUOUS SYNTHESIS OF COATED DRUG CRYSTALS BY A POROUS HOLLOW FIBER ANTI-SOLVENT CRYSTALLIZATION METHOD

5.1 Introduction

In controlled drug delivery systems, well-characterized and reproducible dosage forms are utilized to ensure that the rate and duration of drug delivery achieves the required concentration at the target site to provide optimum therapeutic effects. The subject of the controlled drug delivery by encapsulating individual drug particle in a polymeric coating is of interest here.

The size range of drug particles can vary between micron-sized, sub-micron (100-1000 nm) and nanoparticles (10-100 nm). Due to their greater solubility, high stability, high carrier capacity, incorporation of biodegradable and hydrophobic/hydrophilic substances and administration by a variety of delivery vehicles, nanoparticle-based systems have attracted considerable attention in the application of drug delivery [43-48]. However, the focus of this chapter will be micron-sized drug crystals.

A porous hollow fiber membrane-based anti-solvent crystallization (PHFAC) technique was used to develop a continuous technique whereby micron-size drug particles having a thin polymeric coating are produced continuously from an acetone solution of the drug as well as the polymer used to coat it. This chapter describes the results of a facile and continuous method of synthesizing micron-size GF drug particles having a thin polymer coating based on the PHFAC technique. The polymer used to coat the crystallized drug particles is Eudragit RL 100. The reasons for selecting this polymer are as follows.

The Eudragit family of polymers has very useful characteristics under physiological conditions. They are not degraded by enzymatic attack; they do not undergo absorption in the digestive tract and are physiologically inert. As enteric coating agents they find wide use and can control the dissolution rate of drugs in the stomach and intestine, and they are frequently employed in the formulation of controlled release drugs. That Eudragit RL100 can be used to successfully coat submicron particles as well as nanoparticles using the technique of cooling crystallization has been shown already in Chapter 2. Further, Eudragit has limited sensitivity to anti-solvent addition as was observed in these earlier studies.

The nature of the porous hollow fiber will be preferentially dictated by the anti-solvent being pushed through and the dimensions of the submicron and nanoparticles under consideration. The material of the hollow fiber should not swell in the solvent environment. Further the pore size should be lower than the smallest particles being formed to prevent accidental pore clogging. With water as the anti-solvent, a hydrophilic hollow fiber, e.g., the nylon hollow fiber used here is needed. One can also use hollow fibers of for example, regenerated cellulose, hydrophilized polyvinylidene fluoride, and polyethersulfone as long as there is sufficient solvent resistance. If porous hydrophobic hollow fibers, e.g., Celgard polypropylene hollow fibers, are used, prior wetting of the pores is necessary if an aqueous non-wetting solution is the anti-solvent. However, a hydrophobic hollow fiber will remain susceptible to spontaneous wetting by the organic solvent on the shell side unless appropriate care is taken.

Figure 1.12 in Chapter 1 depicted a PHFAC module containing a number of porous hollow fibers for continuous synthesis of polymer-coated drug crystals. As shown, each hollow fiber serves as a separate anti-solvent crystallizer. The anti-solvent flowing through

the hollow fiber tube side at a higher pressure permeates to the shell side where the polymer solution containing the dissolved drug molecules is flowing. Zarkadas and Sirkar (2006) [24] have demonstrated that the mixing efficiency of this process for the two liquids, the shell-side flowing liquid and the liquid injected from the tube side through the pores is extraordinary. Here in the studies using anti-solvent crystallization, the rapid local addition of the anti-solvent through every pore mouth in the porous hollow fibers drastically decreases the solubility of the drug as well as the polymer in the shell-side feed solution. A very high level of supersaturation is created throughout the shell-side cross section at every axial location in the module causing precipitation of the drug and the polymer resulting in the production of polymer coated drug particles. The suspension of the coated particles along with the excess solution and the anti-solvent are pumped out continuously from an outlet of the shell.

This novel PHFAC device and the process of synthesizing polymer coated drug crystals has certain advantages compared to other anti-solvent crystallizers. There is an extraordinarily intense contacting of the anti-solvent and the feed solution everywhere in the shell side of the PHFAC module. Since the fractional porosity of the hollow fiber wall is around 0.75, a large number of hollow fibers will result in anti-solvent jets emanating from all of the pores in the membrane module. Therefore, almost the entire shell side will be subjected to an intense contacting due to the very large interfacial area created between the two miscible liquid streams. A very high level of supersaturation is created throughout the shell side resulting in very rapid crystallization of the drug molecules. The rate of crystallization of the drug is very rapid; however, that for the polymer is not as rapid as will be shown below. The growth of the crystals and the coating thickness will depend on

a balance between the rate at which the supersaturation is created locally, the level of supersaturation created, and the time allowed for the growth process to occur which is largely determined by the residence time of the shell-side liquid stream.

Another advantage of the PHFAC device is the high surface area/volume ratio that can be achieved if there is a reasonably high packing density of the hollow fiber membranes. That will lead to maximization of the rate of production of the coated drug particles and achievement of a high product recovery rate. Furthermore, scale-up is relatively straightforward since the number of hollow fibers in a module can be increased or decreased according to the needs of production; correspondingly, the module shell diameter can be increased or decreased. Theoretically, the larger the number of hollow fibers in the tube side of the PHFAC module, the higher the rate of production. The morphology and dimensions of the coated drug particles are likely to remain the same if the flow rates can be increased in proportion to the increase in the number of hollow fibers.

5.2. Materials and Methods

5.2.1 Materials and Preparation of The Feed Solution

Eudragit RL 100 (M_w, 150,000; a copolymer of methyl methacrylate, ethyl acrylate and methacrylic acid ester) was purchased from Evonik-Degussa (Parsippany, NJ). Drug particles of Griseofulvin (GF) were purchased from Letco (Decatur, AL) and used without further treatment. This drug has a solubility of 0.116 M in acetone. It is practically insoluble in water; at 25°C the aqueous solubility is 8.64 mg/L. Sodium dodecyl sulfate (SDS) used as a surfactant was obtained from Aldrich. Deionized water was used as the tube side anti-solvent liquid. The Nylon 6 hollow fibers were obtained from ENKA America Inc.,

Asheville, NC. Theses fibers are hydrophilic, allowing easy permeation of the anti-solvent water through the pores.

Eudragit RL 100 polymer was selected as the coating polymer for GF. An amount of 2.4 g of polymer granules was first put in a glass flask containing 20 mL acetone. After about 1 hr when the polymer was fully dissolved, a small amount (4 mL) of the anti-solvent, water was added to keep the polymer solution highly sensitive to further anti-solvent addition. Then 0.025 g of SDS was added before the addition of GF to keep the polymer-coated particles to be produced well dispersed. Finally, 0.55 g GF powder was added to the acetone solution, and after about 30 min, the solution turned from cloudy to clear indicating that the GF powder was fully dissolved in the solution.

5.2.2 Experimental Methods

A schematic diagram of the porous hollow fiber anti-solvent crystallization/coating setup for developing polymer coated GF drug particles was shown in Figure 4.3 (Chapter 4). A flask containing the solution of dissolved GF and polymer was placed over a magnetic stirrer. A peristaltic pump (Masterflex L/S model 7518-60, Cole-Parmer, Vernon Hills, IL) was used to first pump DI water to the tube side. Subsequently, the polymer-drug solution was passed into the shell side of the PHFAC module by another peristaltic pump after 2 min. Since the other end of the tube side was blocked, water was forced to go through the pores in the hollow fiber membrane into the shell side. Tiny water jets from the pores of the hollow fibers were injected into the acetone solution of the drug and the polymer on the shell side generating intense mixing of the feed solution with water.

For submicron-sized pores and nanopores, normally porous membrane-based emulsifications in immiscible systems, i.e., liquid forced through the pores into an

immiscible liquid, indicate creation of liquid droplets of size 1-3 times the membrane pore size of the liquid being forced through the pores into an immiscible liquid [49]. Due to the miscible nature of the organic–aqueous liquid system employed here, there will be a water jet emanating from each pore; however, the jet will disappear quickly via dissolution. Here the membrane pore size range is 0.2-1.5 μm.

The anti-solvent water can dramatically increase the supersaturation by decreasing the solubility of the drug as well as the polymer in the resulting solution. The tube side water flow rate was kept at 11 mL/min while the shell side flow rate for the drug-polymer solution was maintained at 6 mL/min (unless otherwise noted). This flow rate combination is identified as X3; other combinations used will be identified below. The pressure difference maintained between the shell side and tube side was 15 psi.

Crystals of GF appeared as expected. The polymer also precipitated from the solution and rapidly coated the GF drug crystals. In fact, heterogeneous nucleation of the polymer occurred around the growing drug crystals. The suspension of coated drug particles was continuously flushed out through the shell-side outlet of the PHFAC module into a microfiltration device (Omnipore Membrane JHWP09025, PTFE, hydrophilic, 0.45 μm, 90 mm; Millipore, Billerica, MA) to collect the coated drug particles from the slurry. Products were vacuum dried and subjected to various characterization steps.

The sequence of pumping is important, since the anti-solvent water has to permeate through the pore first; otherwise the viscous polymer solution can permeate to the tube side due to a pressure difference. There are four reasons for selecting the relatively high levels of the flow rate levels used in most of the experiments. i.e., 11 mL/min for the tube side water flow rate and 6 mL/min for the shell side flow rate of the drug-polymer solution.

First, it is necessary to generate sufficient pressure in the tube side for DI water to permeate through the pores in the wall of the hollow fibers. Secondly, the velocity of the water streams emanating from the pores should be high enough to facilitate intensive mixing of the drug-polymer solution and the anti-solvent. Thirdly, after precipitation of both the drug particles and the polymer from the solution in the shell side, high levels of precipitation can create blockages in the shell side even with a relatively smooth FEP shell surface. The high flow rates of the incoming water streams and the acetone-based feed solution will flush out the coated drug particles formed, as well as any excess polymer precipitation, so that the module can be run continuously to maximize productivity. Lastly, the addition of a large excess of the anti-solvent water generated a very high level of supersaturation to precipitate the maximum amount of the drug and polymer.

5.3 Results and Discussion

5.3.1 Crystallization of GF Drug Particles in a PHFAC Unit w/wo Polymer

Dry GF powder as received was first analyzed by SEM without any treatment. Figure 5.1 (a) shows the micrograph of pure GF particles as received at a given magnification. The surface of these drug particles as received appears to be very rough with a non-fractal structure; the particle size of GF is close to 10 μm. To find out whether the PHFAC process affects the characteristics of the drug particles compared to the drug particles as received, pure GF crystals were formed using the PHFAC process without the presence of any polymer. Drug particles were first fully dissolved in an acetone solution in a flask under stirring. The solution was directly passed through the shell side of the PHFAC device without any addition of Eudragit RL 100 while water was introduced from the tube side as

the anti-solvent. The product was collected at the outlet in the other end on a filter paper and subjected to SEM characterization.

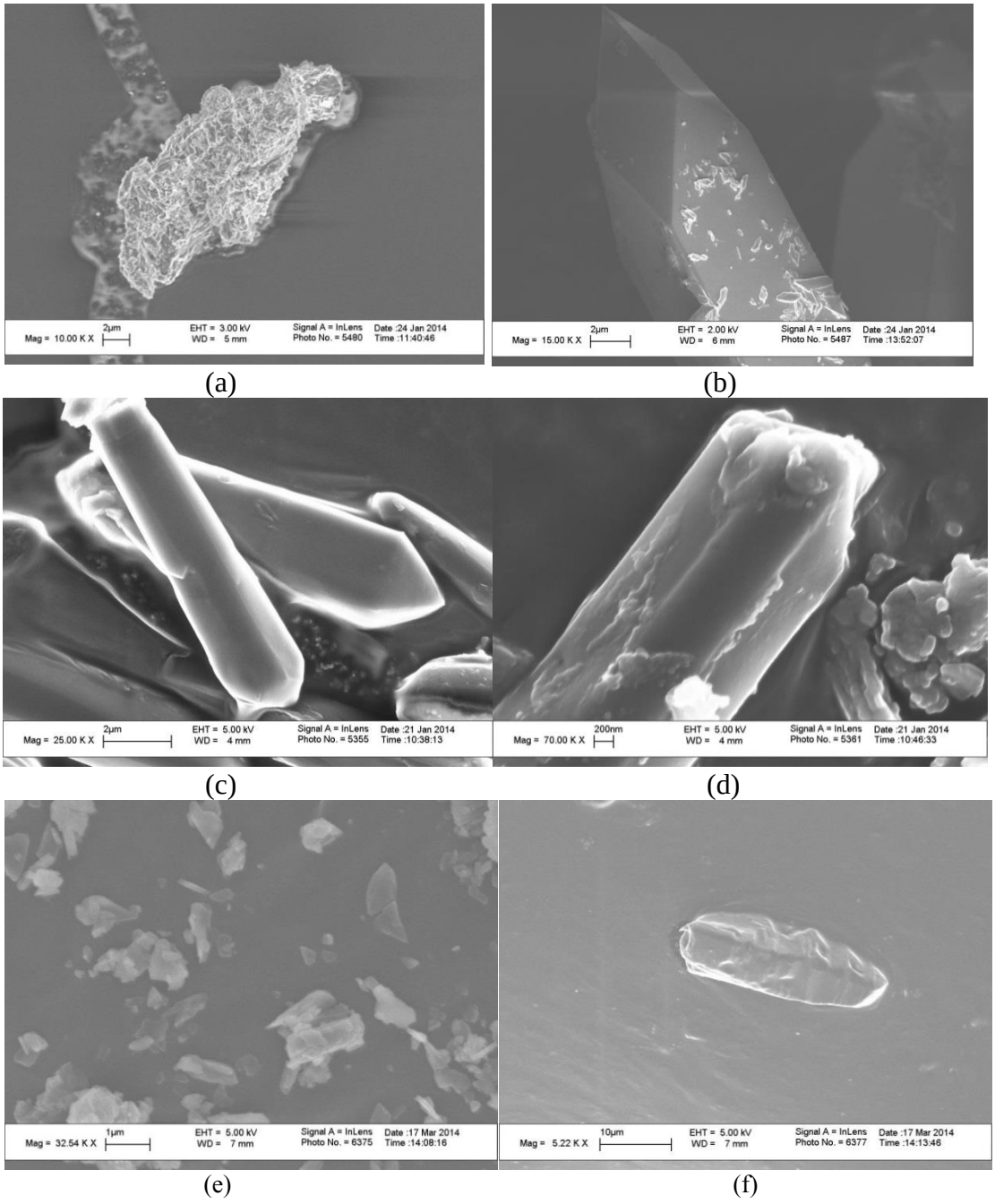

Figure 5.1 SEM micrographs: (a) Pure GF drug powder as received; (b) pure GF drug crystals after precipitation in a PHFAC device without any polymer; (c) and (d) polymer coated GF drug crystals after precipitation (X3) under different magnifications; (e) uncoated GF sample prepared under flow-rate combination X0 (see Table 1); (f) polymer-coated GF crystals prepared using flow-rate combination X2 (Table 1);

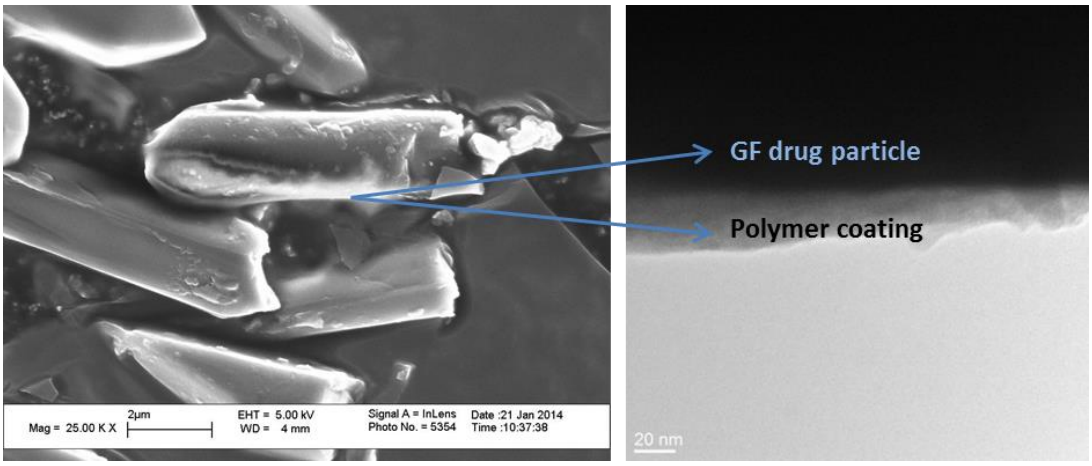

(g) (h)

Figure 5.1 SEM micrographs: (g) and (h): SEM and STEM micrographs respectively of polymer-coated GF crystals after precipitation under different magnifications (X3). (Continued)

Figure 5.1 (b) shows the SEM micrographs of pure drug particles crystallized after pumping through the PHFAC device without any polymer. Compared to Figure 5.1 (a) where the GF particle hardly shows any crystalline shape, drug particles in Figure 5.1 (b) have a well-defined crystal structure. The surface is a lot smoother with only some tiny crystals attached to it. This is because the drug was first fully dissolved in acetone (0.55 g GF in 20 mL acetone) and the GF particles precipitated out from the solution as a result of rapid solubility reduction in the PHFAC device.

5.3.2 Synthesis of Eudragit-coated GF Drug Crystals in a PHFAC Module

When the acetone solution containing both dissolved drug molecules and polymer was pumped through the PHFAC crystallizer with the anti-solvent water coming in from the tube side, it appears that the drug molecules crystallize rapidly from the solution first, and then the polymer precipitates and coats the drug crystals. In Figures 5.1 (c) and 5.1 (d), a polymer coating can be seen on each drug crystal. Compared to Figure 5.1 (b) in which the

drug particles were crystallized without the presence of any polymer, the surface morphology around the drug crystals also appears to be different.

5.3.3 Residence Time Variation

Residence time plays an important role in the PHFAC process since precipitation of both the polymer and the drug can be affected by the variation of residence time in the shell side of the module. Residence time can be simply altered by changing the shell-side feed solution flow rate. To identify the influence of the feed solution flow rate on the particle size distribution (PSD) of GF crystals, the solution containing the dissolved drug without any polymer was passed through the PHFAC module at different rates. The particle size distribution will also be affected by the extent of supersaturation, and the rate at which the anti-solvent is introduced from the tube side to the shell side for a given feed solution flow rate.

Results of the PSD of the drug crystals under different combinations of flow rates of the two streams (X0, X1, X2, X3 and X4) are listed in Table 5.1. The combination X0 has the lowest tube side anti-solvent flow rate and the highest shell-side feed flow rate, which reduces the level of interaction between the feed and the anti-solvent to the lowest level. As a result, it has the lowest extent of supersaturation and rate of supersaturation development and the median particle size of drug crystals is only 1.61 μm (Figure 5.1 (e)). Also, the recovery rate of the drug crystals is the lowest among all five conditions since most of the drug was still dissolved in the solution without precipitation. If we keep the tube side anti-solvent flow rate at the same level but decrease the shell-side feed solution flow rate to 6 mL/min (combination X2), the median particle size increased to 7.33 μm. This is due to an increase in the feed solution residence time which allows for more GF

crystal growth time and consumption of the supersaturation created. Combination X1 has a larger residence time than that in X0 but smaller than that in X2. As a result the average particle size is intermediate between those from combinations X0 and X2.

Table 5.1 The PSDs of Drug Crystals from PHFAC Module Without Any Polymer in the Feed Solution for Various Flow Rates of the Feed Solution and the Anti-solvent Stream

Experimental run	Shell side flow rate (mL/min)	Tube side flow rate (mL/min)	Median size (μm)	d_{10} (μm)	d_{90} (μm)
X0	11	6	1.61	1.00	2.21
X1	8.5	6	3.95	1.70	16.16
X2	6	6	7.33	1.87	15.29
X3	6	11	11.83	2.11	30.30
X4	12	11	11.76	2.94	26.62

For flow combinations of X3 and X4, the tube side anti-solvent flow rate was increased from 6 to 11 mL/min giving rise to intensive mixing of the feed solution with the anti-solvent resulting in rapid development of very high levels of supersaturation. When comparing the combination X4 with the combination X3, it appears that in spite of doubling the shell side feed flow rate, the median size of particles still remained essentially the same. It is possible that with such a high tube side flow rate, the rate of supersaturation development and the growth rates are high enough to allow for ample growth of the drug particles. Further, the shell–side residence time variation employed was not high enough to affect the final PSD of the drug particles. In addition, it appears that the drug was fully precipitated from the solution and grew to its maximum size.

It is clear that the drug crystal size can be altered by variation of both the feed solution flow rate and the tube-side anti-solvent flow rate. Polymer coating experiments were also performed under these conditions to show that after the drug crystal size was

controlled by varying the residence time, the drug crystals can still be coated with polymer that precipitated in the PHFAC module. Figure 5.1 (e) shows an SEM micrograph of uncoated crystals prepared under the flow-rate combination X0 involving the smallest residence time and the lowest extent of supersaturation (Table 5.1), while Figure 5.1 (f) shows the SEM micrograph of a coated GF crystal obtained under the combination X2 (Table 5.1). Figures 5.1 (g) and 5.1 (h) illustrate the thickness of the polymer coating on the crystals at two levels of magnification. The flow combination of X3 was employed for these samples. Figure 5.1 (h) based on a higher magnification has a scale length of 20 nm; one can clearly observe a coating of around 20 nm thickness around the crystal. Figure 5.1 (g) shows the scale bar length is 2 μm. But one can still see a thin coating, about 20 nm, around the crystal.

It is important to know the sequence of precipitation and extent of co-precipitation if any of the drug and the polymer when introducing the anti-solvent from the tube side of the PHFAC module. If the drug particles precipitate/crystallize first, then the final product is most likely to be polymer-coated drug particles. However if both the drug and the polymer crystallize or precipitate at the same time, the product will be either the drug dispersed in a polymeric matrix or vice versa. To explore these concepts, an experiment was run under the flow-rate combination of X2 (Table 5.1) with the acetone solution on the shell side containing only Eudragit RL 100 polymer; the drug GF was not present in the feed solution.

After the PHFAC process was completed, no polymer precipitate was collected on the filter paper from the module outlet. This suggested that the rate of polymer precipitation in the absence of the drug crystals was zero for the low residence time used and the extent

of anti-solvent induced supersaturation created in this experiment. Thus the polymer appears to precipitate rapidly only in the presence of crystals of drug particles which serve as nuclei for polymer crystallization. As a result, when the polymer solution containing dissolved drug molecules is pumped into the PHFAC unit, the drug crystals precipitate out of the solution first and then the polymer precipitates and coats the GF particles as described above

5.3.4 Particle Size Distribution

Since one of the objectives of the study is to understand the impact of this novel PHFAC coating technique on the synthesized drug particles, both the as-received uncoated GF particles and the Eudragit-coated GF particles obtained from the PHFAC were selected for particle size distribution analysis. A suspension of the samples in water was carefully dropped into the inlet of the laser diffraction particle size analyzer. Results of the two samples are shown in Figure 5.2. The median size of the uncoated GF sample (11.6 μm) was close to the manufacturer's specification (10 μm). After polymer coating, the median size of the coated drug particles increased to 19.2 μm. One reason for the median size increase is obviously due to the coating which increases the particle size. A more relevant reason is that the coating of GF by the polymer results in a certain amount of agglomeration. Attachment of neighboring coated drug particles will take place due to the sticking tendency of polymer-formed liquid bridges.

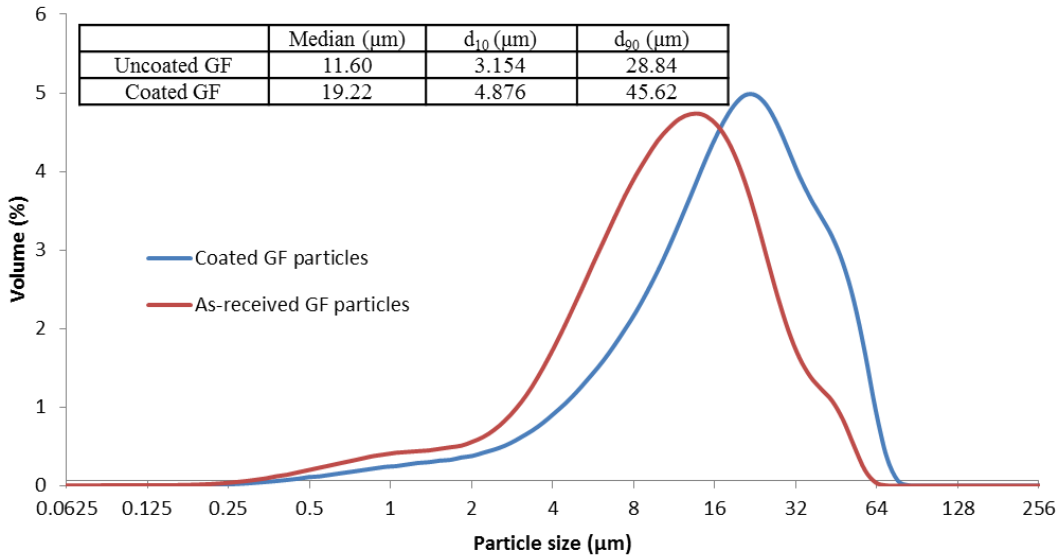

Figure 5.2 Particle size distribution for uncoated GF and coated GF under PHFAC.

5.3.5 TGA Characterization of Polymer Coated Drug Particles

TGA analysis was used to determine the percent weight loss of the sample as a function of increasing temperature. In order to measure the weight of the polymer coating (and thus the thickness of the coating) for polymer coated drug particles, it is necessary to identify the different temperature ranges over which weight loss is caused by both drug decomposition and polymer decomposition as the sample is heated in the TGA.

A small amount of pure GF particles was placed in a hang down pan inside the TGA analyzer and the temperature was increased from 25 ^{o}C to 550 ^{o}C at a rate of 10 ^{o}C/min. In Figure 5.3 (a), the blue line shows the TGA result for an as-received GF sample. The drug will start decomposing when heated up with all of the weight loss occurring between 150 and 270 ^{o}C suggesting that this is the temperature range over which GF decomposes.

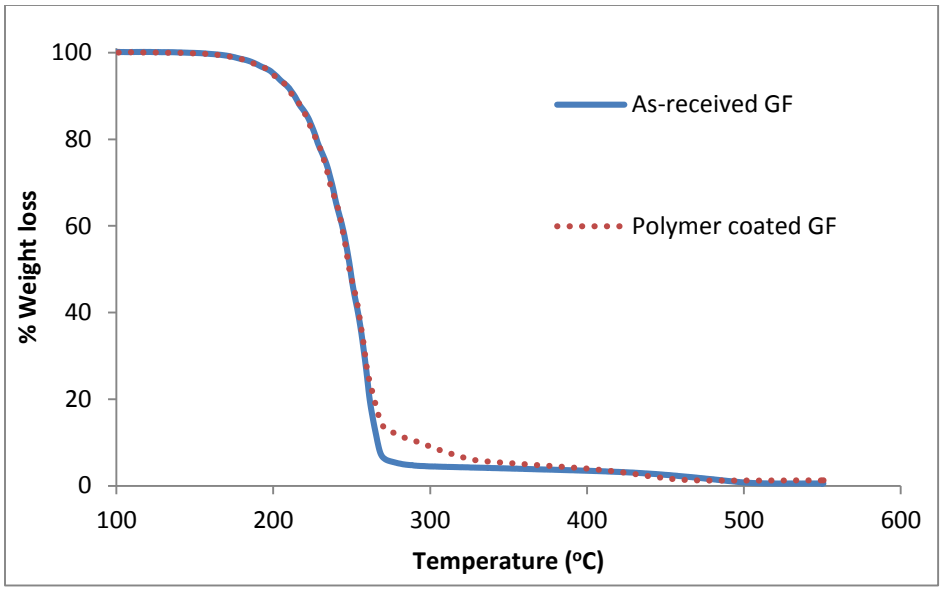

(a)

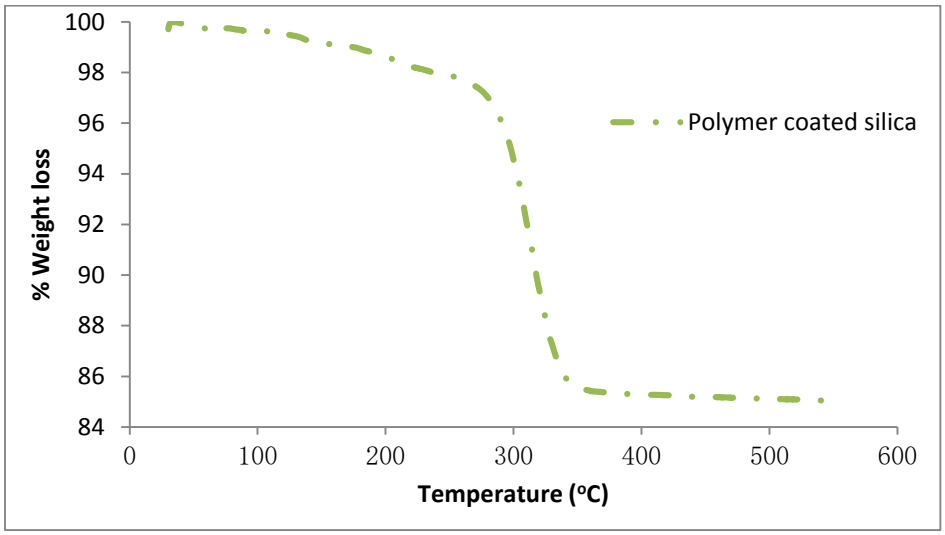

(b)

Figure 5.3 TGA results of (a) as-received GF and coated GF particles; (b) polymer coated silica particles.

Figure 5.3 (b) is a typical TGA result for Eudragit RL 100 coated silica particles taken from Figure 2.13. Since silica particles do not decompose even when the temperature goes up to 550 °C, the percent weight loss is due to the loss of the polymer. Thus the temperature range of polymer decomposition is in the range from 150 to 550 °C.

Therefore, the overlapping temperature range of the drug and polymer decomposition is from about 150 to 270 ^{o}C. The total polymer weight loss can be divided into two parts: the weight loss in the range from 150 to 270 ^{o}C and the weight loss in the range from 270 to 550 ^{o}C. From Figure 5.3 (b) the polymer weight loss in the range of 150-270 ^{o}C is about 2 %, whereas the weight loss in the range of 270-550 ^{o}C is about 10 %.

For the polymer-coated drug (red-dot curve in Figure 5.3 (a)), one can assume that the polymer-based weight loss of the sample from 150 to 270 ^{o}C will be also be about 2%. From Figure 5.3 (a), the weight loss of the polymer coated sample between 270 to 550 ^{o}C is about 10%. Therefore, the total weight loss of the polymer over the entire temperature range can be estimated by adding the 2% weight loss of the polymer in the temperature range 150 to 270 ^{o}C to the 10% weight loss observed for the polymer coated drug shown by the red-dot curve in Figure 5.3 (a) in the temperature range of 270 to 550 ^{o}C. Thus it can be estimated that about 12% of the weight loss of the sample was due to the decomposition of the polymer coating over the drug particles.

To estimate the thickness of the polymer coating, one assumes that every drug crystal is a rectangular parallelepiped having dimensions H_{drug}, W_{drug} and L_{drug} with a polymer coating of uniform thickness h covering the entire drug crystal. The equation governing the relationship between the mass of the polymer coating and the mass of the drug particle is obtained from equation (3.1). The densities of the drug particles and polymer are ρ_{drug} (1.4 g/ml) and $\rho_{polymer}$ (1.1 g/ml), respectively. The length, width and height of the drug crystals are estimated to be 10 μm, 2 μm, and 2 μm based on SEM micrograph results (see Figure 5.1 (c)). Based on the TGA results discussed above, the

ratio $m_{drug}/m_{polymer}$ is equal to 8.34 (=1/0.12). Using equation 3.1, the polymer coating thickness, h, was estimated from the equation to be 0.075 μm or 75 nm.

The most likely reason why this estimate of the coating thickness is considerably higher than the observed thickness measured by STEM analysis in Figure 5.1 (h) is the following. It has been already observed from Figure 5.3 that there is a certain amount of agglomeration in the coated crystals with around two crystals joining together. The considerable amount of polymer present in the bridges between two crystals is not taken into account by equation (3.1) which is based on the total mass of polymer present as measured by the TGA. This essentially increases the estimated thickness around a single particle assumed to be uniformly coated around its perimeter. Further, there will be variations in thickness around a crystal whereas Figure 5.1 (h) shows only a particular location.

5.3.6 XRD and Raman Results

Flattened powder formats of the uncoated GF crystals and polymer coated GF crystals were prepared and analyzed by XRD to identify whether the coating of the drug crystals by the PHFAC process will damage the crystal structure of GF. As can be seen from the XRD results in Figure 5.4 (a), both uncoated and coated GF patterns show no alteration in the peak position. The characteristic peaks of both samples are identical. Figure 5.4 (b) illustrates the Raman spectra results for uncoated and coated GF crystals at the Raman shift range from 0 to 4000 cm^{-1}. Identical peaks for both uncoated GF and the polymer-coated GF proved that during the anti-solvent crystallization process, even though the GF drug has crystallized from a solution containing the dissolved polymer and has been coated by

the polymer, the molecular structure remained intact. Raman spectra were in accordance with the XRD results in Figure 5.4 (a).

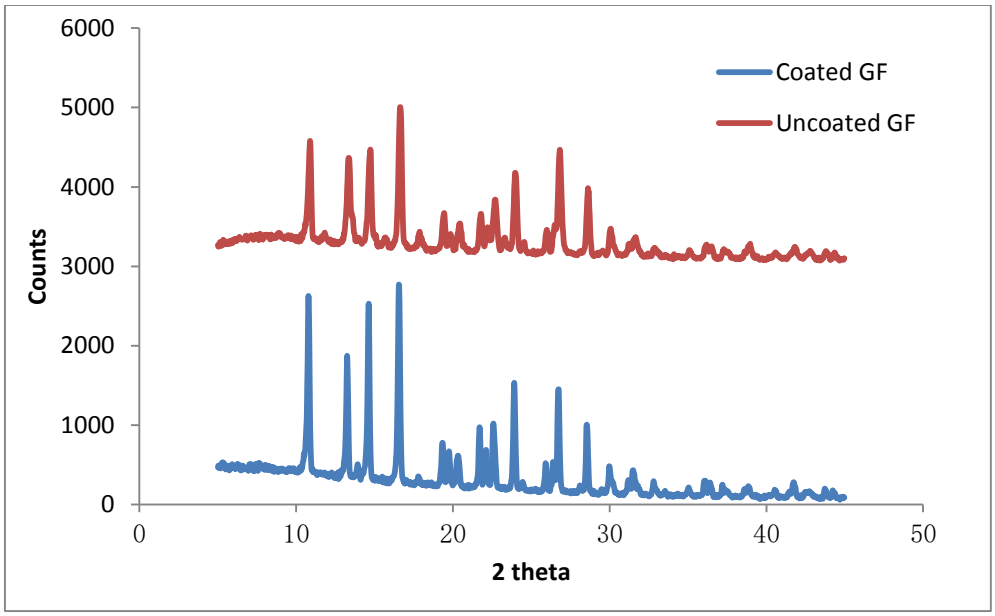

(a)

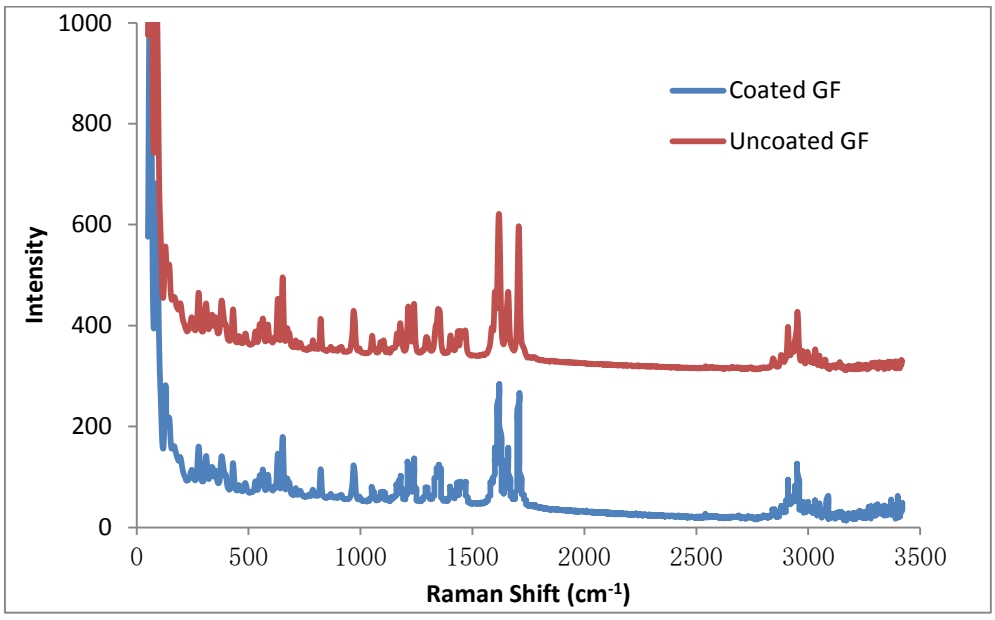

(b)

Figure 5.4 (a) X-ray diffractograms of uncoated GF and coated GF samples; (b). Raman spectra for uncoated GF and coated GF samples.

5.3.7 Differential Scanning Calorimetry

DSC patterns for as-received GF and the polymer-coated GF are shown in Figure 5.5. In the thermogram, the peak starting position implied that the melting point of as-received GF is 219.97 ^{o}C. This peak position is comparable to the pattern for polymer coated GF which has the value of 219.22 ^{o}C. The intensity difference may be attributed to the coating covering the drug particles; it is likely to attenuate the signal strength. The very close, almost identical, positions of the peaks in both the XRD and DSC diagrams suggest that the polymer coating by the anti-solvent crystallization process did not alter the crystallinity of the drug.

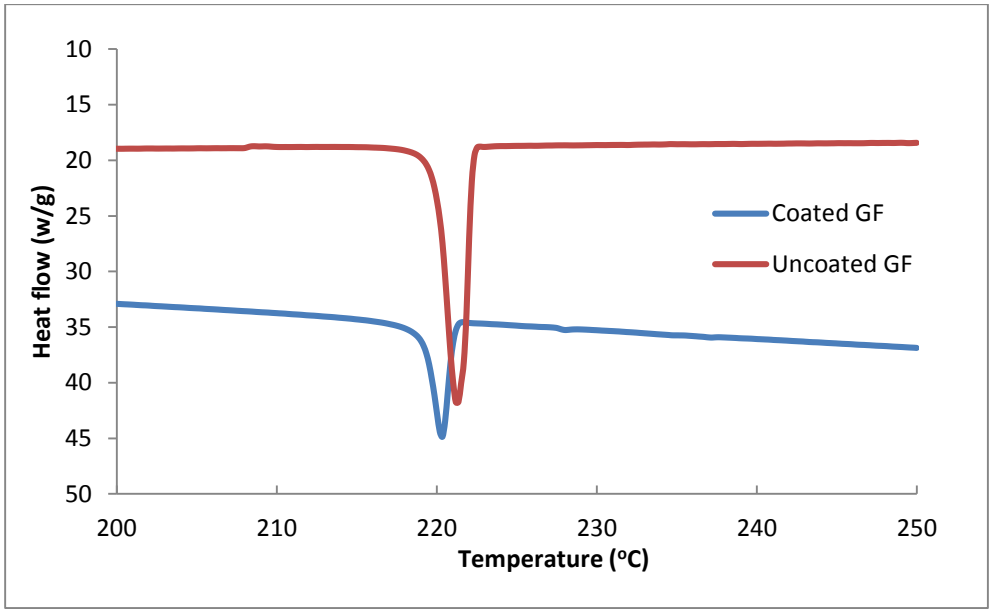

Figure 5.5 Differential scanning calorimetry patterns for uncoated GF and coated GF.

5.3.8 Dissolution Testing

To illustrate the advantages of a coated drug for controlled release, dissolution tests were performed on three samples: as-received drug, uncoated drug, and polymer coated drug. The dissolution studies were conducted in 900 mL of 0.27% SDS aqueous solution at

37 °C. GF has very limited solubility in water; it will take more than 2 hours to dissolve the drug particles. SDS was added to facilitate dissolution and the time needed to dissolve it. Figure 5.6 shows the dissolution profiles for the three samples up to 50 minutes. The as-received and uncoated GF show very similar dissolution curves indicating that even after being pumped through the PHFAC device and crystallized by the PHFAC process, uncoated GF crystals will still dissolve with time in almost the same manner as the as-received drug. On the other hand, the polymer coated GF dissolved only about 20% after 50 min which suggests that the coating will help achieve controlled release of GF.

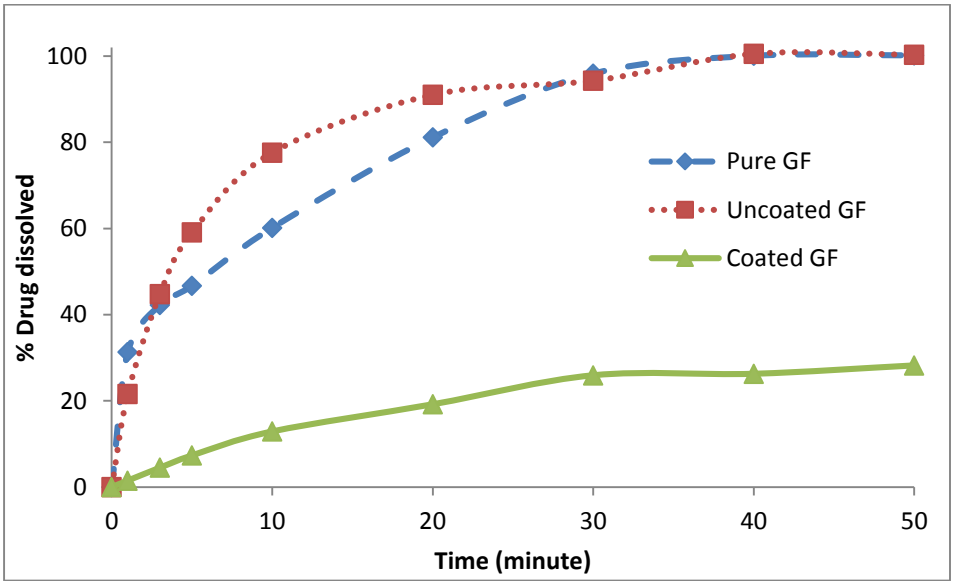

Figure 5.6 Dissolution profiles for crystals of as-received GF, uncoated GF, and polymer coated GF, the latter two obtained by the PHFAC technique.

CHAPTER 6

GENERAL CONCLUSIONS AND RECOMMENDATION FOR FUTURE STUDIES

6.1 Summary

Currently, no technique is available to continuously film coat nano-sized drug particles with a polymer to produce large amounts of free-flowing coated particles. Continuous polymer coating of nanoparticles is of interest in many industries such as, pharmaceuticals, cosmetics, food, and electronics. In this thesis, two novel crystallization methods, SHFCC and PHFAC, have been developed to coat the host particles in a continuous basis.

Chapters 2 and 3 introduced a novel SHFCC crystallizer/heat exchanger that was utilized to continuously coat silica particles with a polymer as well as continuously synthesize GF drug particles coated with polymers from a solution of the drug and the polymer which contained dissolved drug molecules. The cloud point of the polymer solution was determined by UV spectrophotometry for the polymer-solvent-nonsolvent systems of Eudragit RL100/acetone/water and PLGA/dioxane/water. After determining the cloud point of the polymer solutions, the solid hollow fiber cooling crystallization (SHFCC) technique was adapted to continuously coat host particles with the polymer. In this method the polymer solution containing a suspension of submicron particles or nanoparticles flow in the lumen of a solid polymeric hollow fiber. Controlled cooling of the polymer solution by a coolant on the shell side of the hollow fibers allows for polymer nucleation on the surface of the particles; the precipitated polymer forms a thin film around the particles, the thickness of which can be varied depending on the operating conditions. Scanning electron microscopy (SEM), transmission electron microscopy (TEM), energy dispersive X-ray

spectrometry (EDS), laser diffraction spectroscopy (LDS), thermogravimetric analysis (TGA), X-Ray Diffraction (XRD), Raman spectroscopy, and dissolution testing were all used to characterize the coatings. The results indicate that a uniformly coated and free-flowing product can be achieved under optimized conditions in the SHFCC and suitable post-treatments. This novel crystallization/coating method should be attractive for polymer coating of nanopharmaceuticals since scale-up is relatively simple and coated particles can be mass produced continuously.

Chapter 4 introduces a facile anti-solvent crystallization method to continuously coat submicron and nano-sized particles using a porous hollow fiber membrane (PHFAC) device. Submicron (550 nm) and nano-sized (12 nm) silica particles were selected as the host particles; Eudragit RL 100 and PLGA were used as coating polymers. A suspension of the silica particles in an acetone solution of the polymer used for coating was continuously pumped through the shell side of a hollow fiber membrane module. The anti-solvent (water) flowing in the hollow fiber lumen was forced through the membrane pores into the shell side liquid generating intense mixing with the flowing suspension. This led to rapid precipitation of the polymer and coating of the particles. Coated silica particles collected in a vacuum filtration device were analyzed after vacuum drying using a variety of characterization tools. These results indicate that a polymer coating of the silica particles can be developed by this novel PHFAC method. Further, two widely different polymers were used to coat silica-based submicron particles as well as nanoparticles. This continuous method based on the porous hollow fiber membrane containing modules appears to be amenable to convenient scale up.

Chapter 5 focuses on continuous synthesis of polymer coated GF drug particles by a PHFAC device. In such a device, the anti-solvent water flowing through the lumen of porous hollow fibers is introduced through the pores in the wall of the hollow fibers into the shell side where an acetone solution of the drug GF and the polymer Eudragit is flowing. The intense mixing created by the anti-solvent streaming jets into the feed acetone solution generates very high supersaturation throughout the solution flowing in the shell side. This causes drug crystals to appear very rapidly; subsequently each GF crystal is coated by a thin layer of the precipitating polymer undergoing nucleation around each GF crystal surface leading to polymer coated drug crystals.

A variety of analytical techniques were used to characterize the polymer coated drug particles obtained. It was demonstrated that by applying the PHFAC method one can obtain uniform and free-flowing coated drug particles. Results from XRD and Raman spectra and DSC measurements suggest that the polymer coating did not alter the molecular structure of the drug. Controlled release of the drug inside of the coating was demonstrated by drug dissolution tests which showed that less than 20% of the drug dissolved after 50 minutes. The process can be scaled up by increasing the number of porous hollow fibers and the shell-side diameter, while maintaining the shell-side residence time of the feed solution and the ratio of the feed flow rate to the anti-solvent flow rate so as to obtain coated drug particles having similar morphology and polymer coating thickness. Different variations of this technique may be implemented, including introducing the drug and the polymer through two different streams. Furthermore, by changing the material of the host particle and coating polymer, this novel PHFAC technique can be utilized in the production of cosmetics, personal care products, food, and pharmaceuticals.

The concentration of the drug in the feed will influence the level of supersaturation created by the antisolvent and therefore the rate and extent of drug nucleation/crystallization. Lower concentrations will lead to lower rates of supersaturation development and potentially lower rates of growth, and therefore smaller numbers of smaller crystals. If the polymer concentration is too low and/or the polymer precipitation rate is too slow, the coverage of the crystal surfaces may be compromised. The behavior of any drug-polymer-solvent-anti-solvent system will need to be evaluated on an individual basis. It is also necessary to study the stability of such coated crystals in physiological environment and over time.

Although the PHFAC technique has been illustrated using GF, a commonly studied antifungal drug, there does not appear to be any limitation to using other drugs. The drug particle sizes can be varied over a wide range by varying the residence time of the feed solution and the relative flow rates of the two streams.

In conclusion, with the novel SHFCC and PHFAC crystallization devices provide two different ways to continuous coat the drug particles with different polymers. SHFCC is extremely useful when the solubility of the coating polymer is sensitive to the temperature change, but the coating efficiency might be less than that of PHFAC since normally the polymer cannot precipitate entirely from the solution due to the temperature reduction. PHFAC can be used in those circumstances where the coating polymer is sensitive to the anti-solvent but the control over the precipitation might be weaker than that through SHFCC method. One can choose to apply either crystallization technique to coat the drug particles depending on different conditions and requirements. They are both economical, practical, easy to scale-up and do not require critical operating conditions

compared to conventional coating techniques; thus the possibility of applying these continuous polymer coating techniques in the production of polymer-coated cosmetics, food, fertilizers, agricultural seeds and pharmaceuticals look promising.

6.2 Suggested Future Work

Future efforts should first focus on the development of these two techniques to coat a variety of drug particles by different polymers in order to prove the universality of the methods and devices. By the modification of pre-treatments such as the host particles addition, temperature, ratio of solvent to anti-solvent, etc, one can precisely control the coating morphology and thickness. Systematic development of a model for both SHFCC and PHFAC process will also be helpful for a study of these two novel techniques. Using appropriate simulations, one can not only predict the coating thickness and distribution of the concentration, but also save considerable time for the development of polymer coated drug particles.

APPENDIX A

SAMPLE CALCULATIONS

A.1 Calculation of the Coating Thickness of the Submicron Silica Particles From TGA Analysis

Figure A.1 shows the process of uncoated silica particles to those being coated by polymer after the crystallization of polymer.

For single uncoated silica particles shown in Figure A.1 (a), the mass of silica particles can be written as

$$m_{Silica} = \rho_{Silica} \frac{4}{3} \pi r^3 ,$$

For polymer coated silica particles shown in Figure A. 1 (b), the mass of polymer that covered the silica particles can be written as

$$m_{Polymer} = \rho_{Polymer} \frac{4}{3} \pi \{(\mathrm{r}+\mathrm{h})^3 - r^3\},$$

where r is the radius of as-received silica (for submicron silica, r = 275 nm) and h is the polymer coating thickness. m_{Silica} and $m_{Polymer}$ are the mass of the particles and polymer, respectively. The densities of the host particles and polymer are ρ_{Sliica} (=2.65 g/ml) and $\rho_{Polymer}$ (=1.1 g/ml). Theoretically the ratio of silica to polymer can be interpreted as

$$\frac{m_{Silica}}{m_{Polymer}} = \frac{\rho_{Silica} \frac{4}{3} \pi r^3}{\rho_{Polymer} \frac{4}{3} \pi \{(r+h)^3 - r^3\}} \qquad (2.1)$$

To calculate the polymer coating thickness, the ratio of polymer to silica has to be first identified by TGA analysis listed in Figure 2.13. Since uncoated silica particles do not decompose during the heating up, the weight loss of 14.5% is primarily due to

decomposition of the polymer coated on the particles. The actual ratio of the mass of polymer to silica from TGA results should be equal to the theoretical ratio of polymer to silica calculated from the density and volume. Equation (2.1) can be thus re-written as

$$\frac{m_{Silica}}{m_{Polymer}} = \frac{\rho_{Silica}\frac{4}{3}\pi r^3}{\rho_{Polymer}\frac{4}{3}\pi\{(r+h)^3 - r^3\}} = \frac{85.5\%}{14.5\%},$$

Introducing the information provided above,

$$\frac{2.65\times\frac{4}{3}\pi\times 275^3}{1.1\times\frac{4}{3}\pi\{(275+h)^3 - 275^3\}} = \frac{85.5\%}{14.5\%},$$

the polymer coating thickness for the submicron particles h is found to be 33 nm.

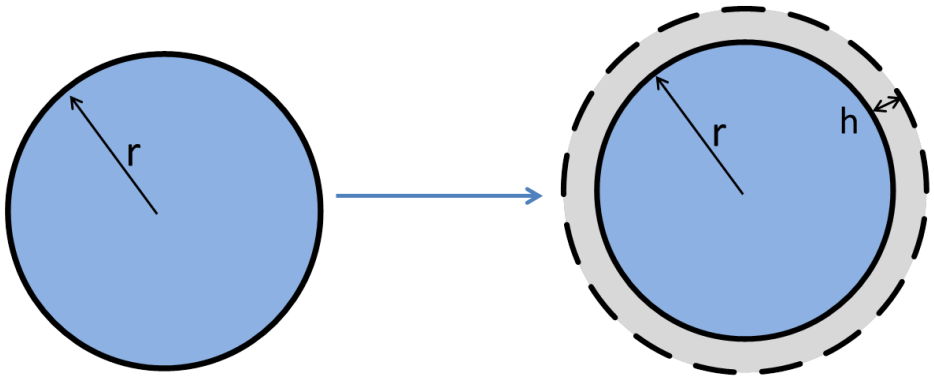

(a) (b)

Figure A.1 Schematic of coating process of silica particles: (a) uncoated silica particles; (b) polymer coated silica particles.

APPENDIX B

PRELIMINARTY MODELLING OF THE CRYSTALLIZATION PROCESS

B.1 Predication of Coating Thickness Along the Hollow Fiber Length in A SHFCC Module

In the SHFCC module, the polymer first precipitated from the solution due to the rapid temperature reduction of the shell side, and subsequently coated the silica particles in the tube side. The supersaturation is related to the kinetics of the system in which the solute mass balance can be written as:

$$-\frac{dC}{dt} = \frac{A}{M_{Solvent}} G + \frac{R_b}{M_{Solvent}} \tag{B.1}$$

Here A represent the total surface area of host particles, G is the growth kinetics and R_b is the nucleation rate. Since the nucleation rate is relatively small ($A*G>>R_b$[50]), $G=k_g \Delta C^g$, and equation B. 1 can be interpreted as follows:

$$-\frac{dC}{dt} = k_g \frac{A}{M_{Solvent}} \Delta C^g = k_g \frac{A}{M_{Solvent}} (C - C^*)^g \tag{B.2}$$

where $M_{Solvent}$ is the molar mass of the solvent, C is the polymer concentration in solution, C* is the solubility of the polymer, Since C* corresponds to the temperature T, and T has a essentially linear relationship with fiber length Z. So assume the relationship between C* and Z is C*= f (Z).

For the left side of the equation,

$$\frac{dC}{dt} = \frac{dC}{dZ} \times \frac{dZ}{dt} = \frac{dC}{dZ} \times v$$

Where Z is the length of the hollow fiber, v is the axial average velocity of the flow in the hollow fiber lumen side, equation (B.2) can then be simplified to the following equation,

$$-\frac{dC}{dZ} = k_g \frac{A}{M_{Solvent} v}\{C - f(\mathrm{Z})\}^g$$

Since all the coefficients (k_g, $M_{Solvent}$, v, A, g) can be calculated from the boundary conditions, thus one can predict the polymer coating thickness (using the polymer concentration C) as a function of various hollow fiber length (Z) from the equation.

B.2 Predication of Coating Thickness by the Variation of Silica Addition

The surface area of single silica ball can be written as

$$A_{Single} = 4\pi r^2$$

The number of silica particles can be assumes in the following if assuming m_{Silica} as the mass of silica added in the solution,

$$N_{Silica} = \frac{m_{Silica}}{\rho_{Silica} V_{Silica}} = \frac{m_{Silica}}{\rho_{Silica} \times \frac{4}{3}\pi r^3}$$

The total surface area of silica particles can be interpreted as

$$A = N_{Silica} \times A_{Single} = \frac{m_{Silica}}{\rho_{Silica} \times \frac{4}{3}\pi r^3} \times 4\pi r^2 = \frac{3m_{Silica}}{\rho_{Silica} r}$$

Equation B.2 can thus be re-written as

$$-\frac{dC}{dt} = \frac{3k_g m_{Silica}}{\rho_{Silica} r M_{Solvent}}(C - C^*)^g$$

Integration of the equation,

$$\frac{(C - C^*)^{1-g}}{g-1} = \frac{3k_g m_{Silica}}{\rho_{Silica} r M_{Solvent}} t + D = \frac{3k_g m_{Silica}}{\rho_{Silica} r M_{Solvent}} \times \frac{Z}{v} + D$$

Thus one can predict the polymer coating thickness (using polymer concentration C) since it's a function of silica addition m_{Silica} for a given hollow fiber length Z.

B.3 Predication of Coating Efficiency of SHFCC and PHFAC Processes

SHFCC

For polymer coating of silica submicron particles (550 nm) by SHFCC method, since the coating thickness h= 33 nm by TGA results and the actual silica addition is 2.4 g. So the actual polymer coated the silica particles at the outlet can be calculated by equation (2.1)

$$\frac{0.4\text{g}}{m_{Polymer}} = \frac{2.65 \times \frac{4}{3}\pi \times 275^3}{1.1 \times \frac{4}{3}\pi\{(275+33)^3 - 275^3\}}$$

$m_{Polymer}$= 0.07 g. Since the actual polymer addition is 2.4 g, the coating efficiency can then be calculated as 0.07/2.4= 3%.

PHFAC

For polymer coating of silica submicron particles (550 nm) by PHFAC method, since the coating thickness h= 33 nm by TGA results and the actual silica addition is 2.4 g. So the actual polymer coated the silica particles at the outlet can be calculated by equation (2.1)

$$\frac{0.4\text{g}}{m_{Polymer}} = \frac{2.65 \times \frac{4}{3}\pi \times 275^3}{1.1 \times \frac{4}{3}\pi\{(275+94)^3 - 275^3\}}$$

$m_{Polymer}$= 0.235 g. Since the actual polymer addition is 0.6 g, the coating efficiency can then be calculated as 0.235/0.6= 40%.

REFERENCES

[1] Langer, R. New Methods of Drug Delivery. Science. 1990, 249, 1527.

[2] Guiot, P. ; Couvreur, P. ; Eds. Polymeric Nanoparticles and Microspheres, CRC Press, Boca Raton, LA, 1986.

[3] Hrkach, J. S.; Peracchia, M. T.; Domb, A.; Lotan, N.; Langer, R. Nanotechnology for Biomaterials Engineering: Structural Characterization of Amphiphilic Polymeric Nanoparticles by 1H NMR Spectroscopy. Biomaterials. 1997, 18, 27-30.

[4] Ringe, K.; Walz, C.M.; Sabel, B. A. Nanoparticle Drug Delivery to the Brain. Encyclopedia of Nanoscience and Nanotechnology. 2004, 7, 91-104.

[5] Gelperina, S.; Kisich, K.; Iseman, M. D.; Heifets, L. The Potential Advantages of Nanoparticle Drug Delivery Systems in Chemotherapy of Tuberculosis. American Journal of Respiratory and Critical Care Medicine. 2005, 172, 1487.

[6] Leong, K. W.; Mao, H.-Q.; Truong-Le, V.L.; Roy, K.; Walsh, S.M.; August, J.T. DNA-polycation Nanospheres as Non-viral Gene Delivery Vehicles. J. Control. Rel. 1998, 53 (1-3), 183-193.

[7] Wang, X.; Yang, C.; Zhang, Y.; Zhen, X.; Wu, W.; Jiang, X. Delivery of Platinum (IV) Drug to Subcutaneous Tumor and Lung Metastasis Using Bradykinin-potentiating Peptide-Decorated Chitosan Nanoparticles. Biomaterials. 2014, 35 (24), 6439-6453.

[8] Nance, E. A.; Woodworth, G. F.; Sailor, K. A.; Shih, T. Y.; Xu, Q.; Swaminathan, G.; Xiang, D.; Eberhart, C.; Hanes, J. A Dense Poly (Ethylene Glycol) Coating Improves Penetration of Large Polymeric Nanoparticles Within Brain Tissue. Science Translational Medicine. 2012, 4 (149), 119-149.

[9] Kreuter, J. Drug Delivery to the Central Nervous System by Polymeric Nanoparticles: What Do We Know?. Advanced Drug Delivery Reviews 2014, 71, 2-14.

[10] Zhang, B.; Luo, Z.; Liu, J.; Ding, X.; Li, J.; Cai, K. Cytochrome c End-capped Mesoporous Silica Nanoparticles as Redox-responsive Drug Delivery Vehicles for Liver Tumor-targeted Triplex Therapy in Vitro and in Vivo. Journal of Controlled Release. 2014, 192, 192-201.

[11] Zheng, H.; Li, S.; Pu, Y.; Lai, Y.; He, B.; Gu, Z. Nanoparticles Generated by PEG-Chrysin Conjugates for Efficient Anticancer Drug Delivery. European Journal of Pharmaceutics and Biopharmaceutics. 2014, 87 (3), 454-460

[12] Du, J. Z.; Mao, C. Q.; Yuan, Y. Y.; Yang, X. Z.; Wang, J. Tumor Extracellular Acidity-activated Nanoparticles as Drug Delivery Systems for Enhanced Cancer Therapy. Biotechnology Advances. 2013, 32 (4), 789-803.

[13] Lai, S. K.; Wang, Y.Y.; Hanes, J. Mucus-penetrating Nanoparticles for Drug and Gene Delivery to Mucosal tissues. Adv. Drug Deliv. Rev. 2008, 61 (2), 158.

[14] Zahr, A.S.; Davis, C.A.; Pishko, M.V. Macrophage Uptake of Core-Shell Nanoparticles Surface Modified with Poly (ethylene glycol). Langmuir. 2006, 22 (19), 8178.

[15] Wang, Y.; Dave, R.N.; Pfeffer, R. Polymer Coating/encapsulation of Nanoparticles using a Supercritical Anti-solvent Process. J. Supercritical Fluids. 2004, 28, 84.

[16] Kim, J.H.; Paxton, T.E.; Tomasko, D.L. Microencapsulation of Naproxen using Rapid Expansion of Supercritical Solutions. Biotechnol. Prog. 1996, 12, 650-661.

[17] Tsutsumi, A.; Nakamoto, S.; Mineo, T.; Yoshida, K. A Novel Fuidized-bed Coating of Fine Particles by Rapid Expansion of Supercritical Fluid Solutions. Powder Technol. 1995, 85, 275-278.

[18] Pessey, V.; Mateos, D.; Weill, F.; Cansell, F.; Etourneau, J.; Chevalier, B. SmCO5/CU Particles Elaboration using a Supercritical Fluid Process. J. Alloys Compounds. 2001, 323, 412-416.

[19] Falk, R.; Randolph, T.W.; Meyer, J.D.; Kelly, R.M.; Manning, M.C. Controlled Release of Ionic Compounds from Poly (L-lactide) Microspheres Produced by Precipitation with a Compressed Antisolvent. J. Control. Release. 1997, 44, 77-85.

[20] Myerson, A.S. Handbook of Industrial Crystallization. 2nd Ed. Butterworth-Heinemann, Boston, MA, 2002.

[21] Tavare, N.S; Micromixing Limits in an MSMPR Crystallizer. Chemical Engineering Technology. 1989, 12, 1–12.

[22] Midler, M.; Paul, E. L.; Whittington, E. F.; Futran, M.; Liu, P. D.; Hsu, J.; Pan, S.H. 1994. Crystallization Method to Improve Crystal Structure and Size. US Patent 5,314,506.

[23] Zarkadas, D.M.; Sirkar, K.K. Solid Hollow Fiber Cooling Crystallization. Ind. Eng. Chem. Res. 2004, 43, 7163.

[24] Zarkadas, D.M.; K.K. Sirkar, Antisolvent Crystallization in Porous Hollow Fiber Devices, Chem. Eng. Sci., 2006, 61, 5030- 5048.

[25] Grön, H.; Borissova, A.; Roberts, K.J. In-Process ATR-FTIR Spectroscopy for Closed-loop Superaturation Control of a Batch Crystallizer Producing Monosodium Glutamate Crystals of Defined Size. Ind. Eng. Chem. Res. 2003, 42, 198.

[26] Togalidou, T.; Tung, H.H.; Sun, Y.; Andrews, A.; Braatz, R.D. Solution Concentration Prediction of Pharmaceutical Crystallization Processes using Robust Chemometrics and ATR-FTIR Spectroscopy. Org. Proc. Res. Dev. 2002, 6 (3), 313.

[27] http://en.wikipedia.org/wiki/Scanning_electron_microscope#mediaviewer/File: Schema_MEB_(en).svg (accessed on date 11.5.2014).

[28] http://qub.ac.uk/schools/SchoolofChemistryandChemicalEngineering/FileStore/InternalForms/ASEPAnalyticalServicesandEnvironmentalProjects/TGA/Filetoupload,404697,en.pdf (accessed on date 11.5.2014).

[29] http://centers.njit.edu/mclab/instruments/particle-size-analyzer.php (accessed on date 11.5.2014).

[30] https://www.sympatec.com/EN/LaserDiffraction/LaserDiffraction.html (accessed on date 11.5.2014).

[31] http://www.azomining.com/article.aspx?ArticleID=160 (accessed on date 11.5.2014)

[32] http://www.chem.umd.edu/wp-content/uploads/2014/01/RamanSpectroscopy.jpg (accessed on date 11.5.2014).

[33] http://pslc.ws/macrog/dsc.htm (accessed on date 11.5.2014).

[34] Zarkadas, D.M.; Sirkar, K.K. Polymeric Hollow Fiber Heat Exchangers: an Alternative for Lower Temperature Applications. Ind. Eng. Chem. Res. 2004, 43, 8093.

[35] Lee, H.; He, F.; Song, L.; Gilron, J.; Sirkar, K.K. Desalination with a Cascade of Crossflow Hollow Fiber Membrane Distillation Devices Integrated with a Hollow Fiber Heat Exchanger. AIChE J. 2011, 57 (7), 1780.

[36] Zarkadas, D.M.; Sirkar, K.K. Cooling Crystallization of Paracetamol in Hollow Fiber Devices. Ind. Eng. Chem. Res. 2007, 46, 2928.

[37] http://eudragit.evonik.com/product/eudragit/en/products-services/eudragit-products/sustained-release-formulations/rl-100/pages/default.aspx (accessed on date 11.5.2014).

[38] Hua, F. J.; Park, T. G.; Lee, D. S. A facile preparation of highly interconnected macroporous poly (D , L –lactic acid-co -glycolic acid) (PLGA) scaffolds by liquid – liquid phase separation of a PLGA – dioxane – water ternary system. Polymer. 2003, 44, 1911.

[39] Tang, L.; Fan, T.M.; Borst, L.B.; Cheng, J. Synthesis and Biological Response of Size-Specific, Monodisperse Drug-Silica Nanoconjugates. ACS Nano. 2012, 6 (5), 3954-3966.

[40] Meng, H.; Xue, M.; Xia, T.; Ji, Z.; Tarn, D.Y.; Zink, J.I.; Nel, A.E. Use of Size and a Copolymer Design Feature To Improve the Biodistribution and the Enhanced Permeability and Retention Effect of Doxorubicin-Loaded Mesoporous Silica Nanoparticles in a Murine Xenograft Tumor Model. ACS Nano. 2011, 5 (5), 4131-4144.

[41] Oh, K. S.; Lee, K. E.; Han, S.S.; Cho, S.H.; Kim, D. Yuk, S. H. Formation of Core/Shell Nanoparticles with a Lipid Core and Their Application as a Drug Delivery System. Biomacromolecules. 2005, 6 (2), 1062-1067.

[42] Stejskal, J.; Trchová, M.; Brodinová, J.; Kalenda, P.; Fedorova, S.V.; Prokeš, J.; Zemek, J. Coating of zinc ferrite particles with a conducting polymer, polyaniline, Journal of Colloid and Interface Science. 2006, 298 (1), 87-93.

[43] Parveen, S.; Sanjeeb, K. S. Long circulating chitosan/PEG blended PLGA nanoparticle for tumor drug delivery. European Journal of Pharmacology. 2011, 670 (2-3), 372-383.

[44] Estephan, Z. A.; Jaber, J. A.; Schlenoff, J. B. Zwitterion-Stabilized Silica Nanoparticles: Toward Nonstick Nano. Langmuir. 2010, 26 (22), 16884-16889.

[45] Korin, N.; Kanpathipillai, M. B.; Matthews, D.; Crescente, M.; Brill, A.;Mammoto, T.; Ghosh, K.; Jurek, S.; Bencherif, S. A.; Bhatta, D.; Coskun, A.U.; Feldman, C.L.; Wagner, D.D.; Ingber, D.E. Shear-Activated Nanotherapeutics for Drug Targeting to Obstructed Blood Vessels. Science. 2012, 337, 738-742.

[46] Botequim, D.; Maia, J.; Lino, M.M.F.; Lopes, L.M.F.; Simeos, P.N.; Ilharco, L.M.; Ferreira, L. Nanoparticles and Surfaces Presenting Antifungal, Antibacterial and Antiviral Properties. Langmuir. 2012, 28 (20), 7646-7656.

[47] Zahran, F.; Cabanas, A.; Cheda, J.; Renuncio, J.; Pando, C. Dissolution Rate Enhancement of the Anti-inflammatory Drug Diflunisal by Coprecipitation with a Biocompatible Polymer Using Carbon Dioxide as a Supercritical Fluid Antisolvent. J. Supercritical Fluids. 2014, 88, 56-65.

[48] Ambrogio, Michael W.; Frasconi, Marco.; Yilmaz, M. Deniz.; Chen, Xinqi New Methods for Improved Characterization of Silica Nanoparticle-Based Drug Delivery Systems. Langmuir. 2013, 29, 15386-15393.

[49] Joscelyne, S.M.; Trägard, G. Membrane Emulsification—A Literature Review. J. of Membrane Science. 2000, 169, 107–117.

[50] Barthe, S.C. Investigation and Modeling of the Mechanisms Involved in Batch Cooling Crystallization and Polymorphism Through Efficient Use of the FBRM. Georgia Institute of Technology. Atlanta, GA. 2008.